

HEAT TRANSFER TO PACKED BEDS

by

CHONG YONG YOON

B. S., Oregon State College
(1956)

S. M., Massachusetts Institute of Technology
(1958)


SUBMITTED IN PARTIAL FULFILLMENT
OF THE REQUIREMENTS FOR THE
DEGREE OF DOCTOR OF SCIENCE

from the

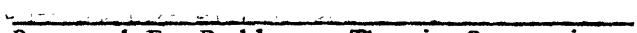
MASSACHUSETTS INSTITUTE OF TECHNOLOGY

September, 1959

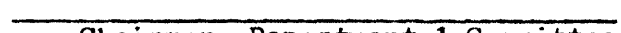
Signature of Author


Department of Chemical Engineering
August 24, 1959

Approved by


Raymond F. Baddour, Thesis Supervisor

Accepted by


Chairman, Departmental Committee
on Graduate Students

ABSTRACT

HEAT TRANSFER TO PACKED BEDS

by

Chong Yong Yoon

Submitted to the Department of Chemical Engineering
on August 24, 1959 in partial fulfillment of the
requirements for the degree of Doctor of Science.

The heat transfer properties of a packed bed are customarily described by so-called effective conductivities or apparent conductivities. The previous investigations on this subject were carried out by a number of different methods. Among them are the postulations of a mean heat transfer coefficient; an average apparent conductivity; an average effective conductivity plus a wall coefficient; and the measurement of local effective conductivity. In addition to these experiments under flow conditions, studies were made in the past on the static-bed conductivities. As the result, considerable amount of information is now available. However, various uncertainties still exist in connection with individual contributing mechanisms, and among them are the behavior of the modified Peclet number based on the local effective conductivities; the physical picture of the so-called wall effect; the relation between the particle Reynolds number and the solid-fluid-solid series conduction mechanism; the effects of solid conductivity and temperature gradient on the radiation mechanism; and the question of proper effective conductivities to be used in a system where the solid and fluid temperatures are significantly different from each other.

The measurement of local effective conductivity was carried out in the present study using 6-inch-diameter annular beds packed with total 6 different kinds of spherical pellets. Air was used as the fluid and the particle Reynolds number was varied up to 1300. The experimental results indicated that the modified Peclet number was constant at about 11, regardless of the radial position in the bed; the effective conductivity in the region within a 1/2-particle-diameter distance from the wall was found to be significantly different from that in the interior of the bed; the solid-fluid-solid series conduction mechanism was essentially independent of the Reynolds number; the radiation mechanism was practically a function of the local conditions only and was found to be affected by the solid conductivity of packing material. Theoretical and empirical correlations were proposed for an estimation of the static-bed conductivity, and theoretical treatment was given to the cases of significantly different solid temperature from that of fluid.

Thesis Supervisor:
Title:

Raymond F. Baddour
Associate Professor
of Chemical Engineering

Department of Chemical Engineering
Massachusetts Institute of Technology
Cambridge 39, Massachusetts
August 24, 1959

Professor L. F. Hamilton
Secretary of the Faculty
Massachusetts Institute of Technology
Cambridge 39, Massachusetts

Dear Professor Hamilton:

In partial fulfillment of the requirements for the degree of Doctor of Science in Chemical Engineering, I hereby submit the thesis entitled "Heat Transfer to Packed Beds."

Respectfully submitted,

Chong Yong Yoon

ACKNOWLEDGEMENTS

The author wishes to gratefully acknowledge the guidance of Professor R. F. Baddour, whose interest and encouragement made the initiation of this work possible, and whose patient supervision was essential during the course of this investigation.

The advice and friendly criticisms from the members of the thesis committee, Professors E. R. Gilliland, H. S. Mickley, and D. F. Fairbanks were most useful in the design of the experiments.

The guidance of Professor H. C. Hottel on the matters of thermal radiation was particularly helpful.

A special acknowledgement is due to Mr. W. Paul Jensen, Research Associate at the Fuels Research Laboratory, who benefited the author greatly with a grant of free access to the facilities of the Fuels Research Laboratory, and with helpful advice on many technical matters.

The friendly discussions with many fellow Sc. D. candidates in the Department were fruitful, and a special mention is due to W. C. Behrmann, N. Y. Chen, and D. A. Sama.

The patient assistance of Messrs. H. A. Chasen, H. Passler, and R. Fulton in the construction of the apparatus was indispensable.

The author was financially supported during the course of this study by Scientific Design Fellowship, without which the work would have been much more difficult.

The generous contributions of Aluminum Company of America and New Departure, Bristol, Connecticut in the procurement of packing materials were deeply appreciated.

TO THE MEMORY OF MY PARENTS

TABLE OF CONTENTS

	page
SUMMARY	1
(1) Definition of Basic Concept	1
(2) Previous Investigations	2
(3) The Scope of This Thesis	5
(4) Experimental Appatus and Procedures...	7
(5) Results.....	9
(6) Conclusions.....	15
CHAPTER I. INTRODUCTION	16
(1) Definition of Basic Concept.....	16
(2) Previous Investigations.....	25
(A) Heat Transfer through Both Fluid and Solid Phases under Flow Conditions	25
(B) Heat Transfer through the Solid Phase and the Static-bed Conductivity.....	44
(C) Summary of Previous Investigations	51
(3) The Scope of This Thesis.....	55
CHAPTER II. EXPERIMENTAL APPARATUS	58
(1) Theory.....	58
(2) Heat Transfer Column	60
(3) Calrod Heater	62
(4) Thermocouples.....	63
(5) Air Supply and Flow Meters.....	66
(6) Preheaters.....	68
(7) Potentiometer.....	69
(8) Watt-meter.....	69
(9) Heat Transfer Column for Static Runs..	69
(10) Packing Materials.....	71
CHAPTER III. EXPERIMENTAL PROCEDURES	73
(1) Packing the Column.....	73
(2) Actual Run	75
(3) Calculation of Effective Conductivity.	77
(4) Determination of Flow Profiles.....	80
(5) Determination of Static-bed Conductivity.....	85

TABLE OF CONTENTS (Cont'd)

	page
CHAPTER IV. RESULTS	88
(1) The Local Effective Conductivity under Flow Conditions	88
(2) The Modified Peclet Number.....	89
(3) Wall Effective Conductivity.....	90
(4) The Static-bed Conductivity.....	92
CHAPTER V. DISCUSSION OF RESULTS	104
(1) Radial Heat Transfer Peclet Number...	104
(2) Solid-fluid-solid Series Conduction Mechanism.....	106
(3) The Wall Effect.....	110
(4) Comparison with Previous Expressions of Wall Effect.....	116
(5) Static-bed Conductivity.....	123
(6) General Correlations for Mechanisms No. 4 and No. 5.....	126
(7) The Static-bed Conductivity near the Wall.....	140
(8) Cases Where Solid and Fluid Temperatures Are Significantly Different from Each Other.....	143
CHAPTER VI. CONCLUSIONS	149
CHAPTER VII. RECOMMENDATIONS.....	153
(1) Cases Where Fluid and Solid Temper- atures Are Nearly Equal at Every Position in the Bed.....	153
(2) Cases Where the Fluid and Solid Temperatures Are Significantly Different from Each Other.....	154

TABLE OF CONTENTS (Cont'd)

	page
APPENDIX I. SUMMARY OF DATA AND CALCULATED VALUES.....	157
APPENDIX II. SAMPLE CALCULATIONS.....	185
APPENDIX III. ERROR ANALYSES.....	192
APPENDIX IV. CONDUCTION CONTRIBUTION TO THE STATIC BED CONDUCTIVITY (Fig. V-9).....	197
APPENDIX V. MATHEMATICAL DERIVATIONS.....	206
APPENDIX VI. CALCULATIONS OF EQUIVALENT WALL COEFFICIENT, AVERAGE EFFECTIVE CONDUCTIVITY, & MEAN HEAT TRANSFER COEFFICIENT.....	212
APPENDIX VII. PHYSICAL PROPERTIES OF PACKING MATERIALS AND AIR.....	220
APPENDIX VIII. FILM COEFFICIENT BETWEEN FLUID AND PACKED SOLIDS & AXIAL EFFECTIVE CONDUCTIVITY.....	224
APPENDIX IX. FLUID PULSATION TO IMPROVE THE HEAT TRANSFER RATE.....	228
APPENDIX X. TABLE OF NOMENCLATURE.....	231
APPENDIX XI. BIBLIOGRAPHY.....	236
APPENDIX XII. BIOGRAPHICAL NOTE.....	241

LIST OF FIGURES

	page
Fig. (I-1) Modified Peclet Number vs. Particle Reynolds Number for a Packed Bed	29
Fig. (II-1) Large Experimental Column	72
Fig. (II-2) Flow Sheet for Experimental Apparatus...	72
Fig. (III-1) A Typical Bed Temperature Profile.....	87
Fig. (III-2) A Typical Velocity Profile	87
Fig. (IV-1) Effective Conductivity of 0.165" Alumina.....	94
Fig. (IV-2) Effective Conductivity of 0.312" Alumina.....	94
Fig. (IV-3) Effective Conductivity of 0.141" Steel.....	95
Fig. (IV-4) Effective Conductivity of 0.282" Steel.....	95
Fig. (IV-5) Modified Peclet Number of 0.165" Alumina.....	96
Fig. (IV-6) Modified Peclet Number of 0.312" Alumina.....	96
Fig. (IV-7) Modified Peclet Number of 0.141" Steel.....	97
Fig. (IV-8) Modified Peclet Number of 0.282" Steel.....	97
Fig. (IV-9) Modified Peclet Number of All Materials Used.....	98
Fig. (IV-10) Wall Effective Conductivity of 0.165" Alumina.....	99
Fig. (IV-11) Wall Effective Conductivity of 0.312" Alumina.....	99

LIST OF FIGURES (Cont'd)

	page
Fig. (IV-12) Wall Effective Conductivity of 0.141" Steel.....	100
Fig. (IV-13) Wall Effective Conductivity of 0.282" Steel.....	100
Fig. (IV-14) Static Bed Conductivity of 0.165" Alumina.....	101
Fig. (IV-15) Static Bed Conductivity of 0.312" Alumina.....	101
Fig. (IV-16) Static Bed Conductivity of 0.282" Steel.....	102
Fig. (IV-17) Static Bed Conductivity of 0.141" Steel	102
Fig. (IV-18) Static Bed Conductivity of 0.236" Soft Glass.....	103
Fig. (IV-19) Static Bed Conductivity of 0.25" Aluminum.....	103
Fig. (V-1) Packing Configuration near the Wall.....	113
Fig. (V-2) Comparison with Previous Work, (A)..	121
Fig. (V-3) Comparison with Previous Work, (B)..	121
Fig. (V-4) Comparison with Previous Work, (C)..	122
Fig. (V-5) Comparison with Previous Work, (D)..	122
Fig. (V-6) Magnified View of Packed Bed.....	127
Fig. (V-7) Electric Analog of Static Bed Conductivity.....	127
Fig. (V-8) Theoretical Model of Packing Arrange- ment.....	130
Fig. (V-9) Conduction Contribution to Static Bed Conductivity.....	136

LIST OF FIGURES (Cont'd)

	page
Fig. (V-10) Radiation Contribution to Static Bed Conductivity.....	137
Fig. (V-11) Comparison with Previous Work, (E)..	138
Fig. (V-12) Comparison with Previous Work, (F)..	138
Fig. (V-13) Comparison with Previous Work, (G)..	139
Fig. (V-14) Solid-, and Fluid-temperature Profiles under Various Circumstances.	146
Fig. (A4-1) Unit Structure of Rectangular Model (Side View).....	197
Fig. (A4-2) Unit Structure of Tetrahedral Model.	201
Fig. (A7-1) Thermal Conductivity of Air & Alumina.....	222
Fig. (A7-2) Thermal Conductivity of Steel and Aluminum.....	222
Fig. (A7-3) Air Viscosity.....	223
Fig. (A7-4) Total Emissivity of Materials Used.	223

SUMMARY

(1) Definition of Basic Concept

Packed columns of granular materials are widely applied in the chemical industry, and the heat transfer problem has received considerable attention.

To describe the heat transfer properties of a fixed bed, so-called effective conductivities (or apparent conductivities) have been in use. Depending on specific needs, either a single effective conductivity is used for the combined body of the fluid and solid phases in a bed, or a separate effective conductivity is assigned to each of the two phases. When the temperatures of the solid and fluid phases are significantly different from each other, the amount of heat flow through each of the two phases must be separately accounted for. For this reason, it is necessary to postulate separately the solid phase effective conductivity, K_s and the fluid phase effective conductivity, K_g .

Both K_s and K_g may be functions of the direction of heat flow as well as the position in the bed. In a system where the fluid flow is essentially unidirectional with negligible net radial component, both K_s and K_g may be divided into two different kinds, namely the axial effective conductivity and

the radial effective conductivity. Ordinarily, the axial conduction is negligible in comparison with the heat flux due to the bulk flow, and only the radial effective conductivity is important. For this reason, only the radial effective conductivity is considered hereafter.

The fluid phase effective conductivity is believed to depend on the following two mechanisms:

- a) Mechanism No. 1. Turbulent-diffusion in the fluid.
- b) Mechanism No. 2. Molecular conduction in the fluid.

The solid phase effective conductivity, on the other hand, is believed to depend on the following three mechanisms:

- c) Mechanism No. 3. Solid-solid conduction through the points of contact.
- d) Mechanism No. 4. Solid-fluid-solid series conduction.
- e) Mechanism No. 5. Thermal radiation

When the solid and fluid temperatures are nearly equal throughout the bed, all the above 5 mechanisms may be incorporated into a single term, or "combined" radial effective conductivity, k_e or k_a , where k_e refers to a local value while k_a is used for an average value for the whole bed.

(2) Previous Investigations

Most of the previous investigations were carried out to

determine the "combined" radial effective conductivity, k_e or k_a . The large number of authors who have studied this subject may be classified into four different major categories according to their methods of analyses.

Group No. 1 treated the packed column in a manner similar to the treatment of ordinary tubular heat exchangers. Thus, these authors determined experimentally an overall or mean heat transfer coefficient based on the area of the wall of the tube and the logarithmic mean of the terminal temperature differences. The results of this group indicated that the mean heat transfer coefficient, h_o was strongly affected by particle-to-tube diameter ratio, and at a fixed particle Reynolds number, h_o decreased exponentially with increasing d_p/D_t .

Group No. 2 used in their analyses the concept of effective conductivity and experimentally determined an average k_a for an entire column. The general result of this group was that the modified Peclet number defined as $Pe = C G_o d_p / k_{td}$, where k_{td} is the turbulent diffusion contribution to k_a , generally increased with increasing Reynolds number and d_p/D_t , and departed widely from the mass transfer Peclet number of about 11. This means that the effect of flow velocity on the overall heat transfer rate became proportionally smaller as the velocity increased, and more so with larger particles. This phenomenon was attributed to the wall effect, but its physical meaning was not established, and instead, a family of curves were usually

employed to correlate the data over a range of variables.

Group No. 3 assumed that a separate resistance existed at zero distance from the column wall but otherwise a single value of k_a applied to an entire bed. Thus, they postulated a wall coefficient, h_w and used it with k_a . The average effective conductivity defined in this manner was generally found to be correlated linearly with the Reynolds number, and the modified Peclet number so calculated ranged from approximately 6.5 to 13. Although there is a 2-fold difference between them, the above range of values is approximately equivalent to the mass transfer counterpart of about 11. Therefore, it is generally assumed that the Peclet number based on this type of k_a is approximately equal to about 11. The experimental values of h_w , however, varied rather widely from one author to another, and its relation with the Reynolds number was often found to be quite irregular. This is probably because h_w accommodates not only the wall effect but also any other factors which contribute to make k_a variable in a bed.

Group No. 4 determined the point-to-point variations of k_e and reported that the Peclet number so calculated varied significantly across the bed and was generally much lower than the value of 11 predicted from the "random walk" analogy. These authors suspected that the uncertain assumptions on the flow velocities in the bed might have affected their results.

In addition to the above experiments under flow conditions,

a number of authors studied the static-bed conductivities. The overall results indicated that: (1) Mechanism No. 2 was found to be given by $k_g(\delta)^{1.3}$ where k_g and δ are the thermal conductivity of the fluid and the volume fraction void in the bed, respectively; (2) Mechanism No. 3 was generally believed to be negligible in comparison with the other contributions; (3) Mechanism No. 4 was found by a few authors to be significantly affected by the Reynolds number, but several other authors did not find such effect; (4) Mechanism No. 5 has been almost exclusively estimated through Damköhler's equation,⁽¹⁴⁾ but the effects of solid conductivity and the temperature gradient on this mechanism were not adequately studied; and (5) Neither theoretical nor experimental treatment has been given to the cases where a significant difference existed between the temperatures of the solid and fluid phases.

(3) The Scope of This Thesis

In handling various practical problems not restricted to idealized simple cases, it is often necessary to evaluate various individual contributions to heat transfer under various circumstances and assemble them suitably to best fit the true aspects of a given problem. To help complete such a technique was the general aim of this thesis, and in particular, studies were made to clarify the various uncertainties mentioned above

in connection with the individual transfer mechanisms.

Included in this study were: Construction and operation of an experimental apparatus with which the true local values of the "combined" radial effective conductivity, k_e can be obtained with minimum amount of mathematical manipulations;

(2) Clarification of the physical picture of the so-called wall effect through the measurement of local effective conductivity, and subsequent derivation of a single rule with which the wide variety of previous data can be generalized and coordinated; (3) Determination of the modified Peclet number based on the local effective conductivity to clarify how it varies across the radius of a bed, and how it is related to the result of theoretical studies based on the "random walk" analogy; (4) Determination of the effect of the Reynolds number on the solid-fluid-solid series conduction mechanism, and derivation of a theoretical correlation with which the contribution of this mechanism can be predicted under various circumstances; (5) Determination of the effects of the solid conductivity and temperature gradient on the radiation mechanism, and development of an empirical correlation to be used for an estimation of this contribution; (6) Theoretical treatment of the cases where the temperatures of the solid and fluid phases are significantly different from each other.

(4) Experimental Apparatus and Procedures

The basic requirement of the present investigation was the measurement of the local effective conductivity. With an ordinary packed column where the flowing fluid acts as the heat sink, it is necessary to account for the flow velocity variations from one position of the bed to another, and the mathematical complexity is almost prohibitive. Therefore, for the purpose of this investigation, it was essential to design a column where the fluid is not a heat sink and the velocity and temperature profiles remain constant along the height of the column.

In order to meet the above requirement, an annular heat transfer column made of a 65-inch-long, 6-inch-diameter, standard steel pipe was employed, and the heat supplied with an 1-inch-O.D. calrod inserted along the axis of the column was withdrawn by the cooling-water around the column. The column was equipped with a 12-inch-long bottom section which was compartmentized into 3 concentric annuli for its entire length with 3- and 5-inch-diameter galvanized chimney pipes. Properly preheated air was introduced separately into each of these compartments at an appropriate rate, so that the inlet temperature and velocity profiles were approximately equal to those in the test section which lay between 1.5 and 3 feet from the top of the column. Under such conditions, heat was transferred in the radial

direction only and practically none was lost to the flowing fluid. The bed temperature traverses were measured at 5 different bed heights around the test section at about 6-inch interval, at 6 different radial positions on each of the 5 levels. Total 30 thermocouples were placed in the bed, 18 of them radially and the rest axially.

The air supply was drawn from the "oil-free air line" in the Fuels Research Laboratory, Building 31, M.I.T., and commercial close-tolerance sharp-edge orifice meters were used to measure the flow rates of various air streams.

Air was preheated with a multiple-unit electric furnace consisting of 3 heating units and 2 single-unit electric furnaces, all of which were passed through in series by a section of the air line.

The power input was measured with a watt-meter.

For the static runs, a small column made of a 6-inch-diameter, 8-inch-long galvanized sheet metal cylinder was used. Heat was supplied with a 0.6-inch-O.D. calrod inserted along the axis of the column and was withdrawn by the cooling-water around the column. Total 12 axial thermocouples were used to measure the temperature traverses at 2 different bed heights around the middle of the column height at about 2-inch interval, at 6 different radial positions on each level.

The packing materials used in the flow runs were 0.165- and 0.312-inch-diameter alumina balls, and 0.141- and 0.282-inch-dia.

steel balls. In the static runs, 0.250-inch-diameter aluminum balls, and 0.236-inch-diameter glass beads were used in addition to the other 4 materials.

The value of local effective conductivity was calculated through the basic Fourier equation for heat flow, by substituting the amount of heat input as measured with the watt-meter, the radial position in the bed, and the graphically obtained temperature gradient at the particular radial position of the bed.

The velocity profile in the bed was estimated by calculation based on the assumption that the pressure drop between 2 bed heights must be identical at every radial position in the bed.

The particle Reynolds number was varied up to 1300, and the maximum temperature used in the flow runs was about 450 °F, while the same for the static runs was over 1000 °F.

(5) Results

Local values of the "combined" radial effective conductivity, k_e were measured at various radial positions of the bed both with and without flow, and the following results were obtained:

1. In the interior of the bed outside a 1/2-particle-diameter distance from the confining walls, Mechanism No. 1,

or the turbulent-diffusion in the fluid phase was found to be characterized by the modified Peclet number of 11, regardless of the radial position, the Reynolds number, solid conductivity, particle diameter, or the temperature level. Or,

$$k_{td} = k_e - k_B = (1/11)(C_p \mu)(Re) \dots\dots\dots (1)$$

This is believed to indicate that the random displacement of fluid parcels is the principal mode of heat transfer in the fluid phase at everywhere in the bed outside a 1/2-particle-diameter distance from the column wall.

The same mechanism, however was found to be expressed by

$$k_{td}' = k_e' - k_B' = (0.01)(C_p \mu)(Re) \dots\dots\dots (2)$$

for the region inside a 1/2-particle-diameter distance from the column wall. The heat transfer process within this interval is believed to be distinctly different from the interior of the bed because (1) owing to the sudden increase in the fraction void, the radial displacement of fluid parcels is sharply decreased, (2) the column wall poses as a permanent barrier to fluid movement, and the radial displacement of fluid parcels toward the wall is thereby discouraged, and (3) due to the skin friction at the column wall, a laminar boundary layer may develop on the surface. For these reasons, the heat transfer process within this interval is believed to resemble

more an ordinary tubular heat exchanger than the interior of a packed bed. Since the turbulence intensity in a packed bed relative to that in an ordinary tube is considered to be about 10 to 1, the above result seems reasonable.

The above difference in the effective conductivities between the two regions, within and without a 1/2-particle-diameter interval from the column wall, is believed to be what constitutes the phenomenon generally known as the wall effect. The above two correlations were tested on various types of previous data covering d_p/D_t as large as 0.3, and as a whole an excellent agreement was obtained.

2. The fact that the modified Peclet number in the interior of the bed was found to be identical with the mass transfer value of 11, and that no significant difference was observed between the Peclet numbers of various packing materials of different solid conductivities, was considered to indicate that Mechanism No. 4, or the solid-fluid-solid series conduction was essentially independent of the Reynolds number. This means that the fluid in the channel between pellets is essentially in a laminar state, regardless of the superficial mass flow rate, at least within the range covered in this study. Further, it indicates that Mechanism No. 1 is essentially additive to Mechanism No. 4. If the fluid channel between pellets is pictured as a capillary tube, it may be shown that the Reynolds

number based on the actual flow velocity in the capillary and the capillary diameter was at most 3200 within the range covered in the present study. For this reason, the above experimental result is believed reasonable.

3. The static-bed conductivities of aluminum and glass at 100 °F showed less than a 3-fold difference while their solid conductivities differed by more than a 300-fold. This result is considered to be in agreement with the general conclusions obtained in the previous investigations that the contribution of solid-solid conduction through the points of contact was negligible.

4. The static-bed conductivities observed at a fixed local bed temperature but at several bed temperature gradients differing up to 4 fold were found to coincide in most cases, indicating that the radiation mechanism is practically independent of the temperature gradient and is a function of the local conditions only.

5. The tetrahedral, and rectangular close-packing models were found to be the closest approximations for the packing configurations in the interior of the bed and in the vicinity of the wall, respectively. Heat was assumed to travel through these models in one direction only, or these packing models were hypothetically divided into numerous parallel heat transfer paths, each having a differential quantity of heat transfer area

and a series of solid and fluid segments occurring in a particular proportion. By summing the amount of heat flowing in each of these differential paths over a unit area of a packed bed, the conduction contribution to the static-bed conductivity was theoretically established. The result was expressed in terms of dimensionless groups, $(k_B)_c/k_s$ vs. k_g/k_s , where $(k_B)_c$ represents the contribution by Mechanisms No. 2 and No. 4 inclusive. The theoretical curve based on the tetrahedral model is for the interior of the bed, while the one based on the rectangular model is for the region within a 1/2-particle-diameter distance from the column wall.

The theoretical curve based on the tetrahedral model was found to be in good agreement with the empirical curve of Polack⁽⁴⁵⁾ within 15%. Further, the results of the present experiments showed that as the temperature level became lower, that is, as the radiation contribution became smaller, the experimental values of k_B approached closely to the theoretical value of $(k_B)_c$. For these reasons, the derived correlation is considered a satisfactory expression of Mechanisms No. 2 and No. 4 inclusive.

6. Assuming the additivity between Mechanisms No. 4 and No. 5, the radiation contribution to the static-bed conductivity was obtained by taking the difference between an observed k_B and the theoretical value of $(k_B)_c$ based on the tetrahedral model.

The results were plotted in terms of $(k_B)_r/k_s$ vs. k_r/k_s , where $(k_B)_r$ represents the contribution by thermal radiation, and k_r was obtained from Damköhler's equation (see Equation I-30), where the proportionality constant, s was taken as 1. The experimental points covering a 300-fold difference in the solid conductivity and the local bed temperature of up to 1100 °F were found to be correlated by

$$(k_B)_r/k_s = (1.3)(k_r/k_s)^{0.70} \dots\dots\dots (3)$$

The above result is an indication that Mechanism No. 5 is not independent of the solid conductivity as was assumed by Damköhler⁽¹⁴⁾ and many other previous investigators. The above equation on the radiation contribution was found to apply approximately also to the region inside a 1/2-particle-diameter distance from the column wall, if the fraction void, δ is taken as 1 in the calculation of k_r .

7. The above various correlations were tested on a variety of previous data, and a good agreement was obtained. This indicates that the theoretical correlations of $(k_B)_c$ as well as the empirical correlation of $(k_B)_r$ are satisfactory for their purpose.

8. As the result of a theoretical consideration, it was shown that the fluid phase effective conductivity, K_g is merely the sum of Mechanisms No. 1 and No. 2, while the solid phase effective conductivity, K_s is essentially equal to $(k_B)_r$.

(6) Conclusions

1. The local values of the "combined" radial effective conductivity in a packed bed are satisfactorily represented by Equations (1) and (2). These equations have been found adequate not only for a rigorous estimation of the local effective conductivity, but also for an estimation of various types of average effective conductivities, if appropriate values of mean physical properties are used with them.

2. It has been found that the static-bed conductivities, k_B and k_B^* appearing in these equations are obtainable by taking the sum of appropriate values of $(k_B)_c$ and $(k_B)_r$, where the conduction contribution, $(k_B)_c$ is represented by the theoretical correlations based on the tetrahedral, and rectangular close-packing models for the interior of the bed and the vicinity of the wall, respectively. The radiation contribution, $(k_B)_r$ may be estimated through Equation (3) for both the interior of the bed and the vicinity of the wall.

3. The above basic equations have been found adequate to generalize and coordinate a wide variety of previous data covering most of the practical ranges of variables.

CHAPTER I. INTRODUCTION

(1) Definition of Basic Concept

Packed columns of granular materials are widely applied in the chemical industry as preheaters, heat regenerators, catalytic reactors, adsorption columns and so on. Many of these applications involve a heat exchange between the bed and surroundings, and consequently, the heat transfer problem has received considerable attention.

As a convenient method of describing the heat transfer characteristics of a fixed bed, so-called effective conductivity (or apparent conductivity) has been in use. By definition, the effective conductivity, k_e is the conductivity of a hypothetical solid mass which is considered to be completely equivalent to at least a portion of the packed bed in question, as far as the heat transfer properties are concerned. With an effective conductivity, k_e so defined, the heat transfer across an imaginary boundary in a fixed bed may be expressed by Fourier's equation as follows:

$$\frac{dq}{d\theta} = (-k_e)(A) \frac{dt}{dx} \dots\dots\dots(I-1)$$

Depending on specific needs, either a single effective conductivity is used for the combined body of the fluid and solid phases in a bed, or a separate effective conductivity is assigned to each of the two phases.

Using the effective conductivities defined as above, the complete energy balance of a packed bed may be rigorously expressed by the following two equations:

$$\begin{aligned} & \frac{\partial}{\partial x} \left(k_{gx} \frac{\partial t_g}{\partial x} \right) + \frac{\partial}{\partial y} \left(k_{gy} \frac{\partial t_g}{\partial y} \right) + \frac{\partial}{\partial z} \left(k_{gz} \frac{\partial t_g}{\partial z} \right) \\ & - \frac{\partial}{\partial x} \left((C_p)_g \rho_g u_x t_g \right) + \frac{\partial}{\partial y} \left((C_p)_g \rho_g u_y t_g \right) + \frac{\partial}{\partial z} \left((C_p)_g \rho_g u_z t_g \right) \\ & + \frac{\partial}{\partial x} \left(k_{sx} \frac{\partial t_s}{\partial x} \right) + \frac{\partial}{\partial y} \left(k_{sy} \frac{\partial t_s}{\partial y} \right) + \frac{\partial}{\partial z} \left(k_{sz} \frac{\partial t_s}{\partial z} \right) - \Delta H \\ & = \left[(C_p)_s \rho_s (1-\delta) \frac{\partial t_s}{\partial \theta} \right] + \left[(C_p)_g \rho_g (\delta) \frac{\partial t_g}{\partial \theta} \right] \dots (I-2) \end{aligned}$$

$$\begin{aligned} & \frac{\partial}{\partial x} \left(k_{sx} \frac{\partial t_s}{\partial x} \right) + \frac{\partial}{\partial y} \left(k_{sy} \frac{\partial t_s}{\partial y} \right) + \frac{\partial}{\partial z} \left(k_{sz} \frac{\partial t_s}{\partial z} \right) - \Delta H \\ & = (h)(a)(t_s - t_g) + (C_p)_s \rho_s (1 - \delta) \frac{\partial t_s}{\partial \theta} \dots (I-3) \end{aligned}$$

Equation (I-2) represents an energy balance for both fluid and solid phases, while Equation (I-3) is for the solid phase only. ΔH in these equations is equivalent to the

enthalpy increase of the reactants in the bed, or the amount of energy absorbed by the reactants in the bed. t_g and t_s are the temperatures of the fluid and solid phases, respectively.

In the above equations, for the sake of perfect generality, separate effective conductivities were assigned to the fluid and solid phases, and each of these effective conductivities was considered as a function of the direction of heat flow as well as the position in the bed. Thus, K_{gx} , K_{gy} , and K_{gz} are the effective conductivities of the fluid phase in the x-, y-, and z-directions, respectively. Likewise, K_{sx} , K_{sy} , and K_{sz} are the effective conductivities of the solid phase in the x-, y-, and z-directions, respectively.

In the above two equations, for the purpose of generality, the fluid velocity was also considered as a function of the direction of fluid flow as well as the position in the bed. Thus, the fluid velocity was expressed in terms of its x-, y-, and z-components.

If a system can be safely assumed to have a unidirectional fluid flow, such as in the z-direction, with negligible net radial components, then, the above equations are considerably simplified. In such cases, K_{gz} and K_{sz} represent the axial effective conductivities of the fluid and solid phases, respectively. Further, if the system is symmetric with respect to the direction of flow, i. e. the z-direction, then, K_{gx}

and K_{gy} represent the radial effective conductivities of the fluid phase, and they should be identical in magnitude. Likewise, K_{sx} and K_{sy} should be equal in magnitude and together represent the radial effective conductivity of the solid phase. In many practical instances, the axial conduction is negligible in comparison with the energy flux due to the bulk flow. Therefore, the axial effective conductivities are generally less important than the radial effective conductivities. For this reason, the subject concerning the axial effective conductivities was excluded from the scope of this thesis, and instead, they are briefly discussed in APPENDIX VIII.

The reason for the separate postulation of fluid phase effective conductivity and solid phase effective conductivity is rather obvious. Many of the practical applications of packed beds involve either absorption or liberation of heat in the bed due to chemical reactions or otherwise, and the temperatures of the solid and fluid phases can be significantly different. If this is the case, the temperature gradients of the two phases would not coincide, and hence the amount of heat flow through each of the two phases must be separately accounted for.

The radial effective conductivity of the fluid phase probably depends on two different mechanisms, namely molecular conduction and turbulent diffusion in the fluid phase.

The radial effective conductivity of the solid phase, on the other hand, is much more complex and is believed to depend on at least three different mechanisms, namely solid-to-solid conduction through the points of contact, transfer of energy through the solid-fluid-solid series paths, and finally thermal radiation.

If the temperatures of the solid and fluid phases are significantly different from each other, there is still another mechanism which belongs to neither the solid phase effective conductivity nor the fluid phase counterpart. This is the mechanism which represents the net heat transfer between the two phases. Since this mechanism does not belong to any of the effective conductivities, it is separately taken care of by the solid-fluid heat-transfer film coefficient, h , in Equations (I-2) and (I-3).

Summing up the above discussion, the overall heat-transfer process in a packed bed may be attributed to the following six different mechanisms:

- Mechanism No. 1. Turbulent diffusion in the fluid phase
- Mechanism No. 2. Molecular conduction in the fluid phase
- Mechanism No. 3. Solid-solid conduction through the points of contact

- Mechanism No. 4. Solid-fluid-solid series conduction
- Mechanism No. 5. Thermal radiation from solid to solid
- Mechanism No. 6. Net heat exchange between fluid and solid phases by conduction, convection, and radiation.

Mechanisms No. 1 and No. 2 are able to transfer heat because of the presence of a fluid phase temperature gradient, and they together constitute the fluid phase effective conductivity, K_g . Once the fluid phase temperature gradient is fixed, the same amount of heat should be transferred by these mechanisms, regardless of the conditions in the solid phase.

Mechanisms No. 3, No. 4, and No. 5 are effective by the virtue of the solid phase temperature gradient, and therefore, they constitute the solid phase effective conductivity, K_s . All these three mechanisms involve the solid phase as a section of the heat transfer path, and therefore, these three mechanisms are considered interdependent on one another. In addition, Mechanism No. 4 is expected to depend also on the fluid phase conditions, because it involves the fluid phase in its transfer path. The fluid between two adjacent particles serves as a medium to transmit heat from one particle to the other. This "ferry-boat service" is provided by Mechanisms No. 1 and No. 2, and therefore, the amount of energy transported by Mechanism No. 4

may partially overlap with what is transferred by Mechanisms No. 1 and No. 2.

Mechanism No. 5 does not involve the fluid phase directly, but, like in any other radiant transfer, it is a function of the heat source and heat sink. The conditions of these heat terminals may well be dependent on the conditions of the fluid as well as the solid phase, and therefore, Mechanism No. 5 may also be dependent on the fluid phase conditions.

Mechanism No. 6, which represents the net heat transfer between phases, involves to a large extent the same various physical processes which constitute Mechanism No. 4, because both of them are concerned with the heat transfer between phases. In a case where the fluid temperature gradient coincides with the inter-particle temperature gradient, the fluid between two adjacent particles takes heat from one particle and gives it to the next particle with little or no net gain for itself. Such a process involves primarily the solid surfaces which are parallel with the direction of fluid flow. Since the fluid merely serves as a bridge in this case, and there is no net heat transfer from one phase to another, it is mathematically convenient to include the transfer process in a radial effective conductivity, rather than accounting for each transaction which takes place between phases. Mechanism No. 4 is the one which represents this type of inter-phase transfer.

When the fluid and solid temperatures are significantly different, on the other hand, the heat transfer between phases is essentially a one-way affair, and the fluid no longer serves as a bridge between two solid particles. In this case, the heat transfer between phases would primarily involve the solid surfaces which are perpendicular to the direction of fluid flow. This type of transfer process must be accounted for through a film coefficient between phases. Mechanism No. 6 is the one which represents this case. It is seen, therefore, the distinction between Mechanisms No. 4 and No. 6 stems not so much from the difference in the physical aspects as from the convenience of "book-keeping." As for the details of the "book-keeping," further discussion is given in CHAPTER V.

When it is necessary to handle the solid and fluid temperatures separately, two simultaneous equations, such as Equations (I-2) and (I-3) must be used with separate effective conductivities for the two phases. If the temperatures of the two phases are nearly equal at every position in the bed, however, Mechanisms No. 1 through No. 5 may be incorporated into "combined" effective conductivities, and the energy balance of a packed bed may be expressed by the following equation:

$$\begin{aligned} & \frac{\partial}{\partial x} \left[k_x \frac{\partial t}{\partial x} \right] + \frac{\partial}{\partial y} \left[k_y \frac{\partial t}{\partial y} \right] + \frac{\partial}{\partial z} \left[k_z \frac{\partial t}{\partial z} \right] \\ & - \frac{\partial}{\partial x} \left[(C_p)_g \rho_g u_x t \right] + \frac{\partial}{\partial y} \left[(C_p)_g \rho_g u_y t \right] + \frac{\partial}{\partial z} \left[(C_p)_g \rho_g u_z t \right] \\ & - \Delta H = (C_p)_s \rho_s (1-\delta) + (C_p)_g \rho_g (\delta) \frac{\partial t}{\partial \theta} \dots\dots\dots(I-4) \end{aligned}$$

where t is the temperature common to both phases, and k_x , k_y , and k_z are the "combined" effective conductivities in the x-, y-, and z-directions, respectively. If the flow of fluid is unidirectional, such as along the z-direction, with negligible net radial component, k_z represents the "combined" axial effective conductivity, and k_x and k_y are the "combined" radial effective conductivities. If the system is symmetric with respect to the direction of fluid flow, k_x and k_y should be equal in magnitude.

The "combined" radial effective conductivity described above has been the principal objective of most of the previous investigations, and it is what is normally known as effective conductivity or apparent conductivity. In the present study, the experimental work was carried out for the determination of the "combined" effective conductivity, but in subsequent analyses, the relations between the "combined" effective conductivity and "separate" effective conductivities were clarified. However, most of the discussion for the rest of this thesis is concerned with the "combined" radial effective conductivity, and therefore, henceforth it is referred to merely as effective conductivity, k_e or k_a , where k_e refers to the local value while k_a is used for an average value for the entire bed.

(2) Previous Investigations

(A) Heat Transfer through Both Fluid and Solid Phases under Flow Conditions

Because of the extensive applications of packed beds in the industry, a considerable amount of previous work has been devoted to the study of the heat transfer properties. The large number of authors who have studied this subject may be classified into four different major categories according to their methods of analyses.

In the earliest method of analyses, the packed column was treated in a manner similar to the treatment of ordinary tubular heat exchangers. Thus, a group of authors expressed their experimental results in terms of an overall or mean heat transfer coefficient, h_o based on the area of the wall of the tube and the logarithmic mean of the terminal temperature differences. Colburn,^(12, 13) Furnas,⁽²⁰⁾ and Leva and coworkers^(32, 33, 34) belong to this category. In the most recent one among the investigations done by this group, Leva and coworkers heated or cooled air flowing downward through a jacketed tube (1/2-, 3/4-, and 2-inch standard size) filled with a wide variety of packings. The results were correlated by

$$\frac{h_o D_t}{k_g} = 0.813 \left(\frac{d_p G_o}{\mu} \right)^{0.9} e^{-\frac{6d_p}{D_t}} \quad \text{Heating} \quad \dots \quad (I-5)$$

$$\frac{h_o D_t}{k_g} = 3.50 \left(\frac{d_p G_o}{\mu} \right)^{0.7} e^{-\frac{4.6d_p}{D_t}} \quad \text{Cooling} \quad \dots \quad (I-6)$$

which were claimed to be valid for d_p/D_t ratios less than 0.35. When tube diameter and the particle Reynolds number are fixed, these equations show that h_o should decrease with increasing particle size.

A different group of authors (Group No. 2) used in their analyses the concept of effective conductivity or apparent conductivity. Neglecting axial conduction, and assuming constant k_a , C_p , and G_o , Equation (I-4) may be reduced to the following equation for a steady-state conduction in a cylindrical bed with no chemical reactions:

$$\frac{\partial t}{\partial x} = \frac{k_a}{C_p G_o} \left(\frac{1}{r} \frac{\partial t}{\partial r} + \frac{\partial^2 t}{\partial x^2} \right) \quad \dots \dots \dots (I-7)$$

Equation (I-7) was integrated for constant wall temperature and uniform mass velocity, and the integrated result was used to calculate k_a from the measured terminal temperature differences. Hougen and Piret,⁽²⁶⁾ Singer and Wilhelm,⁽⁵¹⁾ and Vershoor and Schuit⁽⁵⁴⁾ followed this procedure.

Hougen and Piret⁽²⁶⁾ cooled air flowing downward in tubes

containing Celite packing. The values of k_a computed in the above manner were correlated by

$$\frac{k_a}{k_g} = \frac{2.74}{\delta} \left(\frac{G_o \sqrt{A_p}}{\mu} \right)^{1/3} \dots\dots\dots (I-8)$$

where A_p is the surface area of one piece of packing.

Vershoor and Schuit⁽⁵⁴⁾ collected data for heating of air in tubes containing glass beads, lead and steel balls, crushed pumice, and terrana tablets. They correlated their results by

$$\frac{k_a}{k_g} = 1.72 \left(\frac{k_s}{k_g} \right)^{0.26} + 0.1 (aD_t)^{0.5} \left(\frac{G_o}{\mu a} \right)^{0.69} \dots\dots(I-9)$$

a: surface area of packing per unit volume of packed bed

within 16 per cent. For spherical particles, this gives

$$\frac{k_a}{k_g} = 1.72 \left(\frac{k_s}{k_g} \right)^{0.26} + \frac{0.071 \left(\frac{d_p G_o}{\mu} \right)^{0.69}}{(d_p/D_t)^{0.5} (1-\delta)^{0.19}} \dots\dots (I-10)$$

Singer and Wilhelm⁽⁵¹⁾ postulated the various heat-flow mechanisms which contributed to the value of k_a as follows:

1. Heat flow through the solid phase
 - a. With transfer of heat between particles

- through the flowing fluid, with allowance for film resistance at the particle surface.
- b. With transfer of heat between particles through the points of contact and adjoining fillets of stagnant fluid.
2. Heat flow through the continuous phase
- a. By molecular conduction
 - b. By turbulent eddy diffusion.

Recalling the discussion in the previous section, the various contributing mechanisms therein described are approximately in parallel with the above postulation of Singer and Wilhelm, except that no mention was made in the latter of the radiation contribution.

Neglecting mechanism 1-a in the above, Singer and Wilhelm subsequently derived

$$\frac{k_a}{k_g} = \frac{K_s}{k_g} + \delta + \frac{E}{d} \quad \dots\dots (I-11)$$
$$d = \frac{k_g}{c_p \rho}$$

in which the terms represent mechanisms 1-b, 2-a, and 2-b, respectively. Neglecting the effective conductivity of the solid phase for low-conductive materials, and assuming the

molecular conduction represented by δ , the fraction void in the bed, negligible, Singer and Wilhelm determined the turbulent diffusivity, E and plotted a modified Peclet number

$$\begin{aligned}
 Pe &= \left(\frac{d_p G_o}{\mu} \right) \left(\frac{C_p \mu}{k_g} \right) \left(\frac{\delta}{E} \right) \\
 &= \frac{C_p G_o d_p}{k_{td}} \dots\dots\dots (I-12)
 \end{aligned}$$

against the particle Reynolds number for heating of gas while flowing downward, as shown in Fig. (I-1).

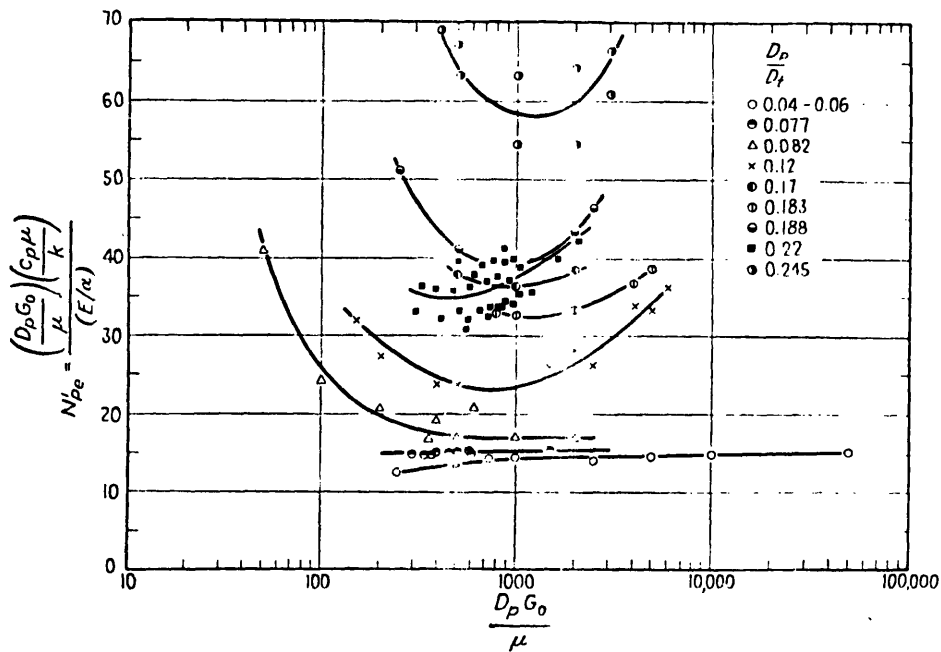


Fig. (I-1)

Modified Peclet Number vs. Particle Reynolds Number for a Packed Bed⁽⁵¹⁾

A close parallelism is noticeable between the results of Singer and Wilhelm and those of Vershoor and Schuit. Equation

(I-10) by the latter authors indicates that k_a should decrease with increasing particle-to-tube diameter ratio. This is in agreement with Singer and Wilhelm's results where the Peclet number increased with increasing particle-to-tube diameter ratio. Further, both Equations (I-8) and (I-10) obtained by Hougen and Piret, and Vershoor and Schuit, respectively show that k_a is proportional to a fractional power of particle Reynolds number, meaning that the effect of fluid flow on k_a becomes proportionally smaller as it increases. This trend is in agreement with Singer and Wilhelm's results where the Peclet number increased with increasing Reynolds number in the region of Reynolds number larger than approximately 1000. In the region of smaller values of Reynolds number, however, Fig. (I-1) shows the reverse trend, in contradiction with the results of Hougen and Piret, and Vershoor and Schuit. This contradiction is particularly conspicuous at large values of d_p/D_t . Remembering that Fig. (I-1) was based on the data obtained for heating of air while flowing downward, a possible presence of natural convection in the opposite direction to the fluid flow may have given apparently too low a value of k_a and hence too large a value of Peclet number. Since the effect of such natural convection would be larger for smaller bulk flow rate and larger pellet size, the above contradiction

between the results of Singer and Wilhelm and other two pairs of authors seems reasonable. If these differences are disregarded, the results of all these authors agree in that the modified Peclet number increases with increasing particle Reynolds number and increasing particle-to-tube diameter ratio.

The turbulent eddy diffusion in packed beds was alternately studied by injecting a tracer material in the inlet fluid and observing the dispersion of the tracer at a downstream side. By this technique, Bernard and Wilhelm⁽⁶⁾ arrived at a conclusion that the modified Peclet number for radial mass transfer should be constant at about 11. Baron⁽⁴⁾ treated the problem statistically and applied a one-dimensional "random walk" analogy to the process of turbulent diffusion. As the result of his analysis, he showed that the modified Peclet number for radial diffusion should be between 5 and 13, regardless of the particle Reynolds number. Ranz⁽⁴⁶⁾ studied the same problem geometrically and concluded that the modified Peclet number should be 11.2.

Comparing the results of Singer and Wilhelm given in Fig. (I-1) with the above theoretical analyses, the trend is evident that the radial heat transfer Peclet number approaches the theoretical value of 11 at low values of particle-to-tube diameter ratio. As d_p/D_t increases, however, the departure

from the theoretical results is striking, and the differences are further enhanced as the Reynolds number increases beyond 1000. This was explained by the authors as an indication of increasing wall effect with increasing d_p/D_t , but what the wall effect actually was, and how it could be predicted under various circumstances were not explained.

Belonging in a broad sense to Group No. 2 is Polack.⁽⁴⁵⁾ Like other authors in the group, Polack used the concept of effective conductivity, but unlike others, he employed an annular bed for the experiments. Heat was supplied with an electric calrod inserted along the axis of a column and was withdrawn from the column wall. Inlet gas was preheated to the mean temperature of the exit gas, and therefore, there was no net heat loss to the flowing gas. The amount of heat input measured with a watt-meter, the temperature drop across the annular space, and the logarithmic mean heat-transfer area were substituted into the following equation to compute the values of k_a :

$$q = - (k_a) (A)_{lm} \frac{\Delta t}{\Delta r} \dots\dots\dots (I-13)$$

Recognizing that the packing around the calrod was not representative of the entire bed, he used as Δt the difference between the column wall temperature and the temperature at approximately one-particle-diameter away from the calrod, and $(A)_{lm}$ and Δr were accordingly evaluated. The effective

conductivity so calculated was attributed to the arithmetic mean bed temperature and the overall flow rate, G_o . By this method, Polack found that k_a varied as the 0.7 power of the Reynolds number in what was considered as the turbulent region ($Re > 350$). He subtracted static bed conductivity, k_B from k_a and considered the difference, which he called k_f , equal to the turbulent diffusion contribution. He correlated $k_f/C_p \mu$ with the Reynolds number through a band of curves, each of which was approximately characterized by a particular value of particle-to-tube diameter ratio. The correlation showed a trend of decreasing k_f with increasing d_p/D_t .

Polack's results that k_a varied as the 0.7 power of Reynolds number, and that the turbulent conductivity, k_f decreased with increasing d_p/D_t , are in general agreement with the results of other authors in Group No. 2. As in the cases of other authors in the same group, this trend of increasing Peclet number with increasing d_p/D_t and increasing Reynolds number is believed due to the column wall effect, on which Polack gave no analysis.

Still another group of authors (Group No. 3) used a method of analyses which was different from anyone so far discussed.

Like Polack, the authors of this group experimentally measured temperature traverses across a packed bed, but unlike Polack, they used externally heated or cooled cylindrical columns in their experiments.

Recognizing that a constant value of k_a alone did not reproduce experimental temperature profiles, and suspecting that this was due to an additional resistance at the wall, the authors of this group postulated a wall coefficient, h_w . Thus, they assumed that there was a finite resistance at zero distance from the column wall but otherwise a single value of k_a applied to the entire column. This assumption gave a new boundary condition to Equation (I-7) (see APPENDIX V):

$$k_a \left(\frac{\partial t}{\partial r} \right)_{r=R} = h_w (t_w - t_{r=R}) \quad \dots\dots (I-14)$$

From the experimental temperature profiles, these authors computed k_a and h_w through Equations (I-7) and (I-14). Coberly and Marshall,⁽¹¹⁾ Felix and Neill,⁽¹⁹⁾ Phillips et al.,⁽⁴³⁾ Plautz and Johnstone,⁽⁴⁴⁾ Yagi and Kunii,^(60, 61, 62) and Yagi and Wakao^(63, 64) belong to this group.

The physical meaning of the wall coefficient, h_w defined as above is rather ambiguous. Unlike the inner-wall film coefficient of ordinary tubular heat exchangers, h_w does not account for the total resistance inside a column. Rather, by definition, h_w accounts only for the resistance which is supposed to exist at zero distance from the column wall. Thus, h_w is somewhat analogous to the contact conductance (reciprocal of resistance) between two solid surfaces which are

in an imperfect contact. However, when a heterogeneous body like a packed bed is in contact with a wall, this interpretation seems to have little significance. This is because at least the fluid phase is considered to be in a perfect contact with the wall, and if h_w were to represent the possible imperfectness of the pellet-wall contact, it would be almost a trivial parameter because the conduction through the points of contact between solids is believed to be extremely small anyway. (29, 30) Therefore, it seems most appropriate to consider h_w merely as a convenient hypothetical parameter which accommodates in itself all the discrepancies which arise from using a single value of k_a for the entire bed. Therefore, h_w may be a function not only of the wall effect but also of all other factors which make the effective conductivity variable within a bed. Perhaps this is an explanation why the experimental values of h_w often showed a gross irregularity. Coberly and Marshall⁽¹¹⁾ computed the values of h_w through the integrated form (see APPENDIX V) of Equations (I-7) and (I-14) and obtained widely scattered points when plotted against G_o . They, however, managed to draw a straight line among them and correlated h_w by

$$h_w = 2.95 G_o^{0.33} \dots\dots\dots (I-15)$$

Phillips et al.⁽⁴³⁾ computed h_w by the same technique as Coberly and Marshall's and found no general correlation.

Plautz and Johnstone,⁽⁴⁴⁾ instead of using the integrated form of Equations (I-7) and (I-14), extrapolated their experimental temperature profiles to the wall and calculated h_w from the average difference between the wall temperature and the extrapolated values, and the overall heat balance based on the terminal temperature differences of the flowing fluid. By this technique, they correlated h_w by

$$h_w = 0.09 G_o^{0.75} \dots\dots\dots (I-16)$$

Yagi and Wakao^(63,64) interpreted wall coefficient, h_w as a film coefficient corresponding to the laminar boundary layer which they assumed to exist at the column wall. Thus, they correlated their data as in the case of a turbulent heat-transfer coefficient for ordinary tubular heat exchangers:

$$j = \left(\frac{h_w}{C_p G_o} \right) \left(\frac{C_p \mu}{k_g} \right)^{2/3} = 0.20 \left(\frac{d_p G_o}{\mu} \right)^{-0.2} \dots (I-17)$$

They claimed the above correlation was valid for the values of Reynolds number larger than 20.

Yagi and Wakao's interpretation, which considers h_w as a film coefficient, seems to be in disagreement with the original definition of h_w . As pointed out earlier, h_w was not

designated to be a measure of the total resistance in the column, because the resistance in the bed proper was to be separately accounted for by the effective conductivity. Rather, h_w is merely something which compensates the discrepancies which arise from using a single value of k_a for the entire bed. When the Reynolds number is sufficiently large, and the resistance in the interior of the bed is much smaller than in the vicinity of the column wall, h_w may superficially behave like a film coefficient of ordinary tubular heat exchangers. However, as the Reynolds number decreases, the resistance to heat transfer would be more evenly distributed throughout the bed, and consequently, less discrepancy would be caused by using a single value of effective conductivity for the entire bed. This means that the wall coefficient, h_w should approach infinite as the Reynolds number approaches zero, whereas a film coefficient which represents the total resistance in the bed should keep on decreasing toward zero. Phillips et al.⁽⁴³⁾ reported that h_w sometimes did indeed turn out to be infinite at zero Reynolds number. For this reason, it is difficult to see how Yagi and Wakao's experimental data of h_w at low Reynolds number such as 20 were correlated by Equation (I-17). Recalling that h_w may accommodate in itself any other factors which make the effective conductivity variable within a bed, the near-zero values of h_w which Yagi and Wakao

observed at low Reynolds number might be due to some other reasons than the wall effect.

From the above discussion, it is seen that the wall coefficient, h_w as postulated by the 3rd group of authors does not provide a true physical picture of the wall effect.

Coupled with the wall coefficient, h_w , the authors of Group No. 3 computed the effective conductivity from the integrated form of Equations (I-7) and (I-14). Their results were generally correlated linearly with respect to the particle Reynolds number.

Coberly and Marshall⁽¹¹⁾ used 1/4-inch x 1/4-inch, and 3/8-inch x 1/2-inch Celite cylinders as packing materials in a 5-inch tube heated externally from the wall while air flowed upward, and the experimental results were correlated by

$$k_a = 0.18 + 0.00098 \frac{G_o \sqrt{A_p}}{\mu} \dots\dots (I-18)$$

where A_p is the surface area of a pellet.

Felix and Neill⁽¹⁹⁾ employed a variety of packing materials having thermal conductivities from 0.1 to 100 in 3- and 5-inch tubes and flowed heated and cooled air upward through voids.

They obtained a dimensional correlation:

$$\frac{k_a}{k_g} = \frac{1}{D_t} \left(\frac{k_s}{k_g} \right)^{0.12} (C_1 + C_2 \frac{d_p G_o}{\delta \mu}) \dots\dots (I-19)$$

The values of C_1 and C_2 were 3.65 and 0.0106 for cylindrical packings and 3.4 and 0.00584 for spherical packings.

Phillips and coworkers⁽⁴³⁾ used Molecular Sieve Type 5A standard 1/8-inch pellets as packing material in 4- and 8-inch tubes heated externally from the wall. They used air, argon, helium, hydrogen, methane, and propane to flow the column upward. Their experimental results were correlated by

$$k_a = 0.080 + 0.65k_g + \frac{d_p G_o C_p}{9.1} \dots\dots\dots (I-20)$$

Plautz and Johnstone⁽⁴⁴⁾ employed 1/2- and 3/4-inch glass spheres packed in an 8-inch tube heated externally while air flowed upward. They found a dimensional correlation:

$$k_a = 0.439 + 0.00129 \left(\frac{d_p G_o}{\mu} \right) \dots\dots\dots (I-21)$$

Yagi and Wakao^(63,64) used a variety of packing materials in a 36-mm I.D., steam-jacketed column purged with air. Their data on glass and cement clinkers were correlated by

$$\frac{k_a}{k_g} = 6.0 + 0.11 \left(\frac{C_p \mu}{k_g} \right) \left(\frac{d_p G_o}{\mu} \right) \dots\dots\dots (I-22)$$

for $d_p/D_t = 0.021\text{---}0.072$

$$\frac{k_a}{k_g} = 6.0 + 0.09 \left(\frac{C_p \mu}{k_g} \right) \left(\frac{d_p G_o}{\mu} \right) \dots\dots\dots (I-23)$$

for $d_p/D_t = 0.12\text{---}0.17$

while the data on steel balls were correlated by

$$\frac{k_a}{k_g} = 13 + 0.01 \left(\frac{C_p \mu}{k_g} \right) \left(\frac{d_p G_o}{\mu} \right) \dots\dots\dots (I-24)$$

for $d_p/D_t = 0.021\text{---}0.086$

Assuming that the difference between an observed value of k_a and the value of the static bed conductivity, k_B represents the turbulent-diffusion contribution to heat transfer, the modified Peclet number may be calculated from Equations (I-18) through (I-24). The modified Peclet number so calculated differed from one equation to another, ranging between approximately 6.5 and 13. If it is remembered that the theoretical and mass transfer Peclet numbers were about 11, the above range of numbers is in much closer agreement with the theoretical value than the ones shown in Fig. (I-1). This is probably because the postulation of h_w in the analyses of this group of authors helped reduce the influence of the wall effect on the heat transfer Peclet number. Nevertheless, there still exists up to a 2-fold difference between them, and this may be due to one or more of the following causes:

- i. The presence of temperature gradients in heat transfer experiments may affect the equivalence of heat- and mass-transfer Peclet numbers.

- ii. The presence of fluid-solid interaction as represented by Mechanism No. 4 described in the preceding section may make the heat transfer Peclet number apparently smaller than the mass transfer counterpart.
- iii. The Peclet number based on an average value of k_a for the entire bed, as is the case in the above, may be influenced by the geometry of the apparatus or the experimental conditions.

In view of the various uncertainties inherent in an average effective conductivity, k_a , a group of authors (Group No. 4) have attempted to measure the local or point values of k_e . Bunnell and coworkers,⁽⁷⁾ Schuler and coworkers,⁽⁴⁸⁾ Kwong and Smith⁽³¹⁾ belong to this category.

Bunnell et al.⁽⁷⁾ measured radial temperature profile at several depths in a 2-inch-diameter vertical tower packed with 1/8-inch cylinders of alumina. Hot air flowed upward, and heat was removed at the wall by water boiling in an external jacket. The values of k_e calculated by their results were correlated by

$$\frac{k_e}{k_g} = 5 + 0.061 \frac{d_p G_o}{\mu} \dots\dots\dots(I-25)$$

for the Reynolds number ranging from 30 to 110.

In the calculation of k_e , these authors did not use the integrated form of Equation (I-7), but instead they graphically evaluated the partial derivatives from the experimental temperature profiles and obtained k_e directly from Equation (I-7). This technique involved second-order graphical differentiations, and the results were subject to a considerable error. Furthermore, Equation (I-7) was originally set up on the assumption of constant k_e . Therefore, the above method of calculation would not have given them the true values of local effective conductivity.

Schuler and coworkers⁽⁴⁸⁾ experimented with 1/8-, 3/16-, and 1/4-inch cylindrical pellets in a 2-inch I.D. externally heated tube in which air flowed upward. This authors removed the assumption of constant k_e from Equation (I-7) and replaced it by

$$k_e \left\{ \frac{\partial^2 t}{\partial r^2} + \frac{1}{r} \frac{\partial t}{\partial r} \right\} + \frac{\partial k_e}{\partial r} \frac{\partial t}{\partial r} - C_p G \frac{\partial t}{\partial x} = 0 \dots (I-26)$$

They calculated k_e from Equation (I-26) by substituting graphically obtained various partial derivatives into the above equation. In addition to the hazardous second-order graphical differentiations, this technique required an extensive trial-and-error procedure, because Equation(I-26)

involved a partial derivative of k_e . The calculated results, therefore, were subject to even larger errors than those of Bunnell and Smith.⁽⁷⁾ Further uncertainties were introduced in their results by substituting Morale's isothermal velocity data⁽⁴¹⁾ for the unknown true flow profiles. They made some corrections to the isothermal data to account for the density differences across a bed, but they did not consider the presence of net radial velocity components, which would have occurred because of the variation of temperature profile along the height of the bed. Their calculated modified Peclet number ranged from 0 to 9 between Reynolds number of 0 and 400. Why the Peclet number should be so low was not explained, and no correlation was obtained to generalize the data.

Kwong and Smith⁽³¹⁾ used a variety of pellets in 2-, and 4-inch tubes heated externally and flowed with air or ammonia. They calculated k_e through Equation (I-26) by a numerical technique which assumed that the solution was represented as the product of two functions each of which was a function of respectively r and x only. Like Schuler and coworkers, these authors could not use the true local mass flow rate, G in Equation (I-26), and Schwartz and Smith's data⁽⁵⁰⁾ of isothermal velocity profiles were used instead. They presented the results so obtained in terms of a modified Peclet number,

which they defined as $Pe = d_p G C_p / k_e$ apparently because they considered the values of k_B were negligible. Their results showed that the modified Peclet number defined as above ranged approximately from 0.9 to 5.0 around the center of the bed but varied significantly across the radius, being generally higher near the column wall. No general correlation was obtained between the Peclet number and the radial position in the bed, however. Why the Peclet number should be so low was not explained, either. They suspected that the use of isothermal velocity profiles may have influenced their results.

Argo and Smith⁽²⁾ proposed a method by which an average effective conductivity was to be estimated. They assumed the equivalence of heat- and mass-transfer Peclet numbers, but they pointed out this was only for an estimation of an average effective conductivity. They suspected the turbulent-diffusion contribution to heat transfer might vary significantly across the radius of a bed, but no method was proposed for an estimation of the local effective conductivity.

(B) Heat Transfer through the Solid Phase
and the Static-bed Conductivity

It was pointed out earlier that in a packed bed part of the heat must travel through the solid phase, and three

different transfer mechanisms were involved in the process. These were Mechanism No. 3, or solid-solid conduction through the points of contact; Mechanism No. 4, or solid-fluid-solid series conduction; and Mechanism No. 5, or thermal radiation.

Because Mechanism No. 4 involves the fluid phase as a section of its transfer path, the total heat transfer through the solid phase is expected to be a function of the Reynolds number. It is impossible, however, to determine experimentally the solid phase effective conductivity alone under a flow condition, and an indirect method must be used for its determination.

Singer and Wilhelm⁽⁵¹⁾ calculated the solid phase effective conductivity, K_s on the assumption that heat- and mass-transfer Peclet numbers were identical. Thus, they experimentally measured an average effective conductivity, k_a and subtracted from it the turbulent-diffusion contribution calculated from the above assumption. The difference was assumed to be equal to K_s , the solid phase effective conductivity. As the result, they found that K_s was negligible for low-conductive ($k_s < 1.0$ Btu/hr.ft.^{°F}) materials but not for high-conductive particles. They reported that K_s for steel balls and lead shots increased approximately from 0.01 to 0.7 Btu/hr.ft.^{°F} between the

Reynolds number of 60 and 1000. They did not obtain any general correlation, however.

Plautz and Johnstone⁽⁴⁴⁾ reversed the procedure of Singer and Wilhelm and calculated the heat transfer Peclet number from the difference between k_a and the static-bed conductivity, k_B . As the result, they found that the heat transfer Peclet number was generally lower than the mass transfer counterpart by about 25%, that is, the effect of fluid turbulence on the heat transfer rate was so much larger than the similar effect on the mass transfer rate. They believed this was because the solid-fluid-solid series conduction was increased as the fluid turbulence grew larger. If this is true, i. e. if the solid-fluid-solid series conduction is affected by the Reynolds number to such an extent, then the Peclet number as calculated by them should be a function of the thermal conductivity of particles, being smaller for higher-conductive pellets. They used only glass beads in their experiments, and therefore, the possible effect of the solid conductivity on the Peclet number was not examined.

The results of Polack⁽⁴⁵⁾ and Yagi and Wakao^(63,64) indicated no significant difference between the Peclet numbers of high- and low-conductive materials. Their results, therefore, seem

to oppose the conclusions of Singer and Wilhelm, and Plautz and Johnstone, concerning the solid-fluid-solid series conduction mechanism as a function of the Reynolds number.

Regardless of whether the solid-fluid-solid conduction mechanism is affected appreciably by the Reynolds number, or not, the solid phase effective conductivity, K_s is largely based on the static-bed conductivity, k_B . At static conditions, the effective conductivity should depend on the same three mechanisms as were involved in K_s , plus Mechanism No. 2, or molecular conduction in the fluid phase. As for the solid-fluid-solid series conduction mechanism in this case, the effect of the Reynolds number should not be a problem, because there is no flow in a static bed.

Mechanism No. 2, or molecular conduction in the fluid phase was separately determined through a mass transfer experiment. Kimura and coworkers^(29, 30) reported that the ratio of the effective diffusivity in a static packed bed to the molecular diffusivity in the solvent alone was found to be related by the following equation for a variety of solvent and solute combinations:

$$\frac{D_e}{D_f} = \delta^{1.3} \dots\dots\dots (I-27)$$

δ : volumn fraction void

Alternately, Wyllie⁽⁵⁹⁾ studied the same problem with an electric analog. He used a packed bed of non-conductive pellets filled with an electrolytic liquid, and the electric conductance of the bed was compared with that of liquid alone. The ratio was given by

$$\frac{\lambda_e}{\lambda} = \delta^{1.3} \dots\dots\dots (I-28)$$

δ : volume fraction void

in agreement with Equation (I-27). Therefore, it seems reasonable to assume that the heat transfer contribution by Mechanism No. 2 is given by

$$(k_g)(\delta)^{1.3} \dots\dots\dots (I-29)$$

Mechanism No. 3, or solid-solid conduction through the points of contact was similarly measured with an electric analog. Kimura^(29,30) measured the electric conductances of packed beds of a variety of conductive pellets and compared them with the electric conductances of pellets alone. The ratio was found to be in the range of (0.74 ---15)(10⁻⁴). Assuming the similar ratio should also apply to the analogous heat transfer process, the point contact transfer mechanism is believed to be quite insignificant.

Neglecting the contribution of Mechanism No. 3 for the above reason, and considering the insignificant magnitude of

Mechanism No. 2 as given by Equation (I-29), the static-bed conductivity is believed to depend primarily on Mechanisms No. 4 and No. 5 only. Various correlations have been proposed by a number of authors with regard to the static-bed conductivity, k_B .

Schumann and Voss⁽⁴⁹⁾ correlated their data through a family of curves by plotting k_B/k_g against k_s/k_g at various values of fraction void, δ . Wilhelm and coworkers⁽⁵⁶⁾ subsequently found that the correlation of Schumann and Voss consistently underestimated experimental values of k_B . They believed this was because the contact-point conduction between solids was more important than was accounted for by the correlation, and proposed an empirical correction term to be added to the correlation. This view, however, seems to contradict Kimura's results.^(29,30)

Damköhler⁽¹⁴⁾ applied the basic Stefan-Boltzmann law to a simplified model of packed bed and derived the following equation for an estimation of radiation contribution:

$$k_r = (0.173)(\epsilon)(\delta)(s)(d_p)(4T^3/10^8) \dots \dots \dots \text{(I-30)}$$

s: proportionality constant

which was supposed to be evaluated at the average bed temperature.

Deissler and coworkers^(15,16) measured static-bed conductivities of MgO, steel, and Uranium Oxide powders ($d_p = 0.016$ --- 0.0017 inch) in air, argon, nitrogen and neon. They found a

fair agreement between the experimental results and calculated values based on a simplified model of packing configuration.

Polack⁽⁴⁵⁾ measured the static-bed conductivities of glass, steel, and alumina balls in a variety of gases, and with alumina balls he varied the pressure and temperature levels over a wide range. He found the static-bed conductivity was essentially independent of pressure variations around the one-atmosphere level, and he concluded that natural convection was almost absent. The results of his high-temperature runs with alumina balls showed a fair agreement with Danköbler's formula, Equation (I-30), and he concluded in agreement with Danköbler's⁽¹⁴⁾ assumption that the radiation contribution was additive to other mechanisms irrespective of the solid conductivity. However, the effect of solid conductivity on the radiation contribution was not experimentally checked with high-conductive pellets. Polack measured an average bed conductivity based on the arithmetic mean bed temperature, and therefore, the effect of temperature gradient on the local bed conductivity was not examined.

Hill and Wilhelm⁽²⁵⁾ measured local bed conductivity of alumina balls in air over a wide temperature range, and on the basis of an arbitrary assumption that the radiation mechanism was negligible at 0 °C, they reached a conclusion

that the ratio of heat transfer by radiation to that by conduction was 0.1 and 1.2 at 100 °C and 1000 °C, respectively. They proposed a theoretical model of radiation transfer in a packed bed, but its practical applicability has not been fully developed.

A number of authors, such as Kimura,^(29,30) Yagi and Kunii,^(60,61,62) and Argo and Smith⁽²⁾ derived theoretical equations for an estimation of the static-bed conductivity. These were based on various simplified models of packing configuration, and they either require characteristic constants to be evaluated from system to system,^(30,62) or are inclined to be oversimplified.⁽²⁾ Little or no experimental support has been reported for these theoretical equations, except a few cases at low temperature levels.

(C) Summary of Previous Investigations

The results of previous investigations discussed in the preceding pages may be summarized as follows:

1. The wall effect in a packed bed has been observed in a number of different ways and is believed to be strongly affected by the Reynolds number and particle-to-tube diameter ratio. However, its quantitative physical picture has not been established, but instead,

it has been treated empirically by one of the following various methods:

- a) The wall effect was incorporated into an average effective conductivity or mean heat transfer coefficient, and these quantities were correlated through a family of curves or a group of equations, each of which represented only a particular range of variables, such as d_p/D_t .
- b) A hypothetical resistance at zero distance from the column wall was assumed, and the wall effect was partially absorbed into the wall coefficient, h_w . Because h_w may be affected by various factors other than the wall effect, however, the experimental values of h_w often showed a gross irregularity.
- c) Attempts were made to clarify the wall effect through the measurement of local effective conductivity. The results, however, involved a number of uncertainties inherent in the experimental technique, and no general quantitative conclusions have been obtained.

2. Mechanism No. 1, or the turbulent-diffusion contribution to heat transfer has been customarily expressed by a modified Peclet number. The modified Peclet number calculated from an average effective conductivity has been found to approach the theoretical or the analogous mass transfer Peclet number of 11 at low d_p/D_t . This type of Peclet number, therefore, is generally assumed to be approximately equivalent to its mass transfer counterpart of about 11. On the other hand, the modified Peclet number calculated from the local effective conductivity has been reported to vary significantly across the radius of a column, and to be usually much smaller (0.9---5.0) than the theoretical value of 11. Because of experimental uncertainties, however, no general rule has been found as to its behavior, and why the value should be so low has not been adequately answered.

3. Mechanism No. 2, or the molecular conduction in the fluid phase, if existing alone, is believed to be expressed adequately by

$$(k_g)(\delta)^{1.3} \dots\dots\dots (I-30)$$

4. Mechanism No. 3, or the solid-solid conduction through the points of contact has been shown to be usually negligible.

5. Mechanism No. 4, or the solid-fluid-solid series conduction still remains uncertain as to its relation to the Reynolds number. Up to about 25% of the total effect of fluid turbulence on heat transfer rate has been attributed to this mechanism, but a conclusive support of this assumption is not available. Mechanism No. 4 for a static bed has been treated both empirically and theoretically, and a number of correlations are available.
6. Mechanism No. 5, or the contribution to heat transfer by thermal radiation has been estimated almost exclusively through Damköhler's formula, Equation (I-30), on the assumption that this contribution is additive to others in an equal amount, regardless of the solid conductivity or the temperature gradient. Little or no work has been reported involving both high-conductive pellets and high temperature levels, and consequently, the effects of solid conductivity and the temperature gradient on the coefficient of radiation contribution have not been adequately studied.
7. Neither theoretical nor experimental treatment has been given to the question of how the effective conductivities should be modified when the temperatures of the solid and fluid phases are significantly different from each other.

(3) The Scope of This Thesis

From the discussions in (1) Definition of Basic Concept, it is seen that a reasonably rigorous treatment of a packed bed heat transfer problem requires sound quantitative knowledge on the individual transfer mechanisms and their mode of interactions. In handling various practical problems not restricted to idealized simple cases, it is often necessary to evaluate various individual contributions under various circumstances and assemble them suitably to best fit the true aspects of a given problem. However, the discussions in (2) Previous Investigations indicate that considerable uncertainties still exist with the majority of individual mechanisms, and especially little is known about the behavior of the local effective conductivity. For this reason, the "cook-book technique", or the technique of estimating the proper value of effective conductivity through an appropriate assembly of ingredient mechanisms, has not been fully developed.

To help complete such a technique was the general aim of this thesis, and with this in mind, studies were made in the following particular areas:

- (A) Construction and operation of an experimental apparatus with which the true local values of the "combined" radial effective conductivity, k_e can be obtained with minimum amount of mathematical manipulations.
- (B) Clarification of the physical picture of so-called wall effect through the measurement of local effective conductivity, and subsequent derivation of a single rule with which the wide variety of previous data can be generalized and coordinated.
- (C) Determination of the modified Peclet number based on the local effective conductivity to clarify how it varies across the radius of a bed, and how it is related to the theoretical value of the Peclet number.
- (D) Determination of the effect of the Reynolds number on the solid-fluid-solid series conduction mechanism, and derivation of a theoretical correlation with which the contribution of this mechanism can be predicted under various circumstances.
- (E) Determination of the effects of the solid conductivity of pellets and temperature gradient on the radiation mechanism, and development of an empirical correlation to be used for the evaluation.

- (F) Theoretical treatment of the cases where the temperatures of the solid and fluid phases are significantly different from each other to determine what are the proper values of the effective conductivity to be used for such cases.
- (G) Comparison of the present results with a wide variety of previous data to test the generality and versatility of the former.

CHAPTER II. EXPERIMENTAL APPARATUS

(1) Theory

As mentioned in the preceding chapter, the basic requirement of the present investigation was the measurement of the local effective conductivity. The enormous experimental and analytical difficulties which encounter the similar requirement have been the cause of considerable uncertainties associated with the results of many previous attempts.

With an ordinary packed column where the flowing gas acts as the heat sink, the evaluation of the local effective conductivity requires the knowledge of accurate velocity profiles. First of all, no such knowledge is yet available especially for non-isothermal beds, and secondly, the temperature profile which varies along the height of the column would cause the velocity profile to vary also. Consequently, net radial velocity components would be expected in the system, and the ordinary analytical methods which assume no radial velocity components would not produce correct results. If this assumption is to be removed, both thermodynamic and hydrodynamic considerations are required in the analyses, and the ensuing mathematical difficulties are truly insurmountable.

In order to avoid the above difficulties, it is essential to design a column where (1) the fluid phase is not a heat sink, and (2) the velocity and temperature profiles remain constant along the height of the column. With such a system, the velocity data need not enter the calculations of k_e , and the computations are extremely simple with relatively small chance of error.

In an annular column where one of the two confining walls acts as the heat source and the other as the heat sink, the fluid introduced at the bottom would initially exchange heat with the walls, and thus the temperature and velocity profiles would vary as the fluid proceeds through the column. After the fluid has traveled a sufficient distance through the column, however, it would reach a point from where on the profiles of the temperature and velocity no longer change for the rest of the way. Therefore, if the column height were infinite, constant temperature and velocity profiles would be automatically established near the exit, regardless of the inlet conditions. The "calming distance" which the fluid must travel before it establishes constant temperature and velocity profiles would be shortened considerably, if the inlet temperature and velocity profiles were approximated to those in the interior of the bed. In an ideal case where the inlet profiles are

identical with those at the exit, the "calming distance" is zero. It is impossible to achieve this ideal situation, but nevertheless, it can be approximated if the inlet section is divided into several compartments, and properly preheated air is introduced into each of them at a proper rate. On the above principle was based the design of the apparatus of the present investigation.

(2) Heat Transfer Column

The main body of the column was made of a standard 6-inch-diameter, 65-inch-long Schedule 40 steel pipe. The top of the column was left open into the atmosphere. For the purpose of making the inlet temperature and velocity profiles approximately equal to those in the test section, the heat transfer column was equipped with a specially designed bottom section, which was hooked onto the bottom of the column with a set of cast-iron flanges. The outer shell of the bottom section was made of a 6-inch-diameter, 12-inch-long steel pipe of the same type as the main column. The inside of the bottom section was compartmentized into three concentric annuli for its entire length with 3- and 5-inch-diameter galvanized chimney pipes. These were concentrically silver-soldered onto a 1/4-inch-thick

steel disc, which was in turn welded on the bottom end of the bottom section. To ensure an even distribution of inlet air, a ring-shape distributor made of standard, 1/2-inch copper tubing with small perforations all around was fitted at the bottom of each annular compartment except the center one. These ring-shape distributors were silver-soldered onto the inlet-air taps which were also made of standard, 1/2-inch copper tubings. No distributor was used for the center compartment, and an inlet tap was directly connected to the center of the compartment. All three inlet-air taps pierced through the bottom disc of the bottom section and were connected to an air supply. The bottom section was then filled with many pieces of wire screens for the rest of its entire height.

At about 2 inches above the top of the bottom section, a perforated steel plate was fitted inside the main column and was held with a set of screws to support the packing materials. The size of the perforations was approximately 1/16 inch in diameter. A concentric 1-inch-diameter hole was punched through the disc in order to hold the calrod heater in place.

Starting at 18 inches from the bottom of the main column, (excluding the bottom section), 6 equally spaced thermocouple-holes tapped with 1/8-inch pipe-threads were installed at a

6-inch interval along a vertical line on one side of the main body of the column. On the opposite side of the column, an equal number of thermocouple-holes were symmetrically installed.

Around the outside of the column, a removable cooling-water jacket made of a 10-inch-diameter galvanized chimney pipe was installed. Cooling-water was introduced from both sides of the column at an approximately equal rate to ensure an even wall temperature around the column.

(3) Calrod Heater

An electric calrod heater rated for 3 KW at 220 V was order-made by Acme Electric Heating Company, Boston. It was made of 4 separate bundles of carefully wound nichrome wire coils housed in an 1-inch-diameter stainless steel sheath. The heating length was 61-inches with a 2-inch cold tip on each end. Both power terminals were installed on one end. The uniformity of heat liberation throughout the calrod surface was checked by measuring its surface temperature in the quiescent air at various positions of the surface.

The calrod was inserted axially in the center of the main column and was held in place at the bottom by the perforated-steel bed-support which was equipped with a concentric

1-inch-diameter hole in the center. After the column was packed, a perforated-steel disc was securely placed on the top of the packings to prevent the bed from floating at high flow velocities of the fluid. This disc had a 1-inch-diameter concentric hole and served to hold the calorod in place near its top. The calorod was connected to a 220 V AC source through an induction regulator, and the power input was measured with a calibrated watt-meter.

(4) Thermocouples

Temperature measurement was carried out with thermocouples made of 30-gauge, iron-constantan duplex wires. The 1.5-foot-long section of the bed which lay between 1.5 and 3 feet from the top of the column was chosen as the test section. There were total 6 thermocouple-holes in the test section, 3 on the front side of the column at a 6-inch interval, and 3 similarly placed holes on the back side of the column. Through each of the 3 holes on the front side of the column, 3 thermocouples were horizontally inserted into the bed. These 3 thermocouples were spaced approximately at 1-inch interval starting at the calorod surface. Through each of the 3 holes on the back side, similarly 3 thermocouples were inserted horizontally. These three thermocouples were placed approximately 1, 2, and 2.75

inches from the center of the column, respectively. The correct radial positions of the thermocouples were determined at the time of each packing by measuring the distances between the reference points on the thermocouple wires outside the column and the column wall surface. Thus, the radial temperatures at each of the 3 bed heights in the test section were measured at 6 different radial positions. In all cases, no thermocouple wells were used, and the flow disturbance due to the radially inserted wires was considered negligible. To minimize the error due to the conduction through the thermocouple wires, the tips were made relatively large with a lump of silver-solder. The 3 thermocouples inserted through each hole were held together by a brass male-connector screwed into the thermocouple-hole. The column was packed up to the bottom level of the test section, and 2 groups of 3 thermocouples were carefully inserted, one from each side of the column, and the bed was packed above them for another 6 inches, and the whole procedure was repeated thereafter. The thermocouple wires were led out of the cooling-water around the column through rubber tubings.

In addition to the above-mentioned radial thermocouples, two groups of 6 thermocouples were axially inserted from the top of the column. The 6 thermocouples in each of these groups were placed at 0.75, 1.0, 1.5, 2.0, 2.5, and 2.75 inches

from the center of the column. The first group of 6 axial thermocouples were aligned along a single radius of the bed forming approximately a 90-degree-angle with either of the radii along which the radial thermocouples were aligned. The depth at which the first group of thermocouples were placed varied from one packing to another but was about 5 inches above the top of the test section.

The second group of 6 thermocouples were similarly inserted axially, but these were aligned along a radius approximately 180 degrees apart from the first group of the axial thermocouples. The spacing of the second group was identical with that of the first group. The depth at which the second group of axial thermocouples were inserted also varied but was approximately 5 inches above the level of the first group. The 6 thermocouples in each of these 2 axially inserted groups were held in place along a radius of the bed by a horizontal spacer which was made of a 1/8-inch-diameter porcelain tubing.

The purpose of these axial thermocouples was to check the symmetry of the bed and to check the accuracy of the radially placed thermocouples.

In addition to these thermocouples placed inside the column, shielded thermocouples were used to measure the

temperatures of the inlet-air streams at about 1 inch from the bottom of the column. The outer wall temperature of the column was measured with thermocouples located on two opposite sides of the column at about 3 inches above the bottom of the test section. These thermocouples were silver-soldered into the small dents prepared on the outer wall.

The cold junction of the thermocouples was maintained in a Dewar flask at 32 °F. A Rubicon precision potentiometer was used to measure the EMF of the thermocouples.

(5) Air Supply and Flow Meters

The air supply was drawn from the "oil-free air line" in the Fuels Research Laboratory, Building 31, M. I. T. Its average moisture content has been reported to be approximately 0.0017 lb. H₂O/lb. air.

The air was drawn from a 3-inch supply line and was metered with Orifice No. 1. (Fig. II-2). Then, it was split into two streams, one of which was metered with Orifice No. 2 and was introduced into the outer compartment of the bottom section. The other stream was led through a preheater and was again split into 2 streams. Different amounts of cold air were by-passed into these 2 streams to obtain a desired temperature difference between them.

The colder stream of the two was metered with Orifice No.3 to be introduced into the middle compartment of the column. The hotter one was introduced into the center compartment without metering. The flow rate of this stream was, therefore, calculated by difference from the measurements of the other streams.

The temperature of the coldest stream was measured with a thermometer inserted in the line. (Fig. II-2). The temperatures of the other two streams were measured with shielded thermocouples inserted in the inlet-air taps near the bottom of the column.

Orifice No. 1 was a purchased standard sharp-edge orifice of 0.620-inch orifice diameter. It was installed in a standard 2-inch line which had a 6-foot upstream and a 2-foot downstream section.

Orifices No. 2 and No. 3 were also purchased standard sharp-edge orifices with orifice diameters of 0.589 and 0.434 inch, respectively. They were installed in 3/4-inch-diameter pipe lines.

Flange-taps were used for all these orifice meters, and each set of pressure taps were connected to a mercury and a water manometer with polyethylene tubings. Mercury manometers

were used for large P, and water manometers for small P. Flow rates were calculated by the procedures described in an ASTM manual.⁽³⁾

(6) Preheaters

A multiple-unit electric furnace consisting of 3 heating units, and 2 single-unit electric furnaces were used to preheat the air. The multiple-unit furnace (Chem. Eng. Dept. Equip. No. 244) drew total 6.65 Amps at 220 V, and each single-unit furnace (Chem. Eng. Dept. Equip. No. 400 and 324) drew 5 Amps at 110 V.

A section of air line made of 1-inch-diameter brass pipes was passed through these 5 heating units in series. The total heated length was about 6 feet including the space between units.

The electric furnaces were equipped with rheostats to regulate the amount of heat input.

The air lines leading from the preheaters to the column were carefully covered with asbestos pipe insulators.

(7) Potentiometer

A precision potentiometer (Chem. Eng. Dept. Equip. No. 1556) manufactured by Rubicon Company, Philadelphia was used to measure the EMF of the thermocouples.

(8) Watt-meter

A Weston wall-meter (M.I.T. Elec. Eng. Dept. No. D2699) was used to measure the amount of energy input into the calrod.

(9) Heat Transfer Column for Static Runs

For the purpose of investigating wider variety of packing materials over wider range of temperature levels than in the flow runs, a special smaller column was employed for static runs. This was because some packing materials such as glass and aluminum balls were not available in sufficient quantity, and any possible damage to the expensive metallic packing materials from an accidental overheating in static runs was expected to be more costly with the large column which uses larger quantity of packing materials.

The structure of this column is similar to the large one described earlier. It consists of a 6-inch-diameter, 8-inch-long, galvanized sheet metal cylinder jacketed on the outside for the cooling-water. The annular space for the cooling-water was about 1 inch.

A 0.6-inch-O.D., 6.5-inch-long electric calrod rated for 0.95 KW at 115 V AC was tightly fitted into an equal length, 1-inch-O.D. copper sleeve, and the combination was inserted

along the axis of the column to be held at the bottom by a trancite disc with an 1-inch-diameter concentric hole in the center. The purpose of the copper sleeve was to obtain the maximum uniformity of heat liberation throughout the calrod surface.

Two groups of 6 thermocouples were inserted axially into the bed by exactly the same technique as was used for the large column. The locations of the 6 thermocouples in each of the two groups were 0.75, 1.0, 1.5, 2.0, 2.5, and 2.75 inches from the center of the column, respectively. One group of thermocouples were placed in the middle of the bed height along a radius of the bed. The other group of thermocouples were placed about 180 degrees apart from the first group, and at about 2 inches above them. By comparing the temperature measurements of these two groups, the symmetry of the column and the extent of heat loss from the top of the column were checked. Both the top and bottom of the column were carefully covered with asbestos insulating materials and glass wool.

The same watt-meter and potentiometer which were used for the large column were employed for this column also.

(10) Packing Materials

Alumina Balls

Tabular alumina balls

Grade T-164, 1/4-inch nominal size, actual
average size = 0.312 inch in diameter

Grade T-162, 1/8-inch nominal size, actual
average size = 0.165 inch in diameter

These were supplied by ALCOA, Pittsburgh, Pa., and
were reported to be 99.5+ % pure Al_2O_3 .

Steel Balls

0.282-inch-diameter, and 0.141-inch-diameter,
close-tolerance ball bearings were supplied by
New Departure Company, Bristol, Connecticut.

These were reportedly made of SAE 51100 steel.

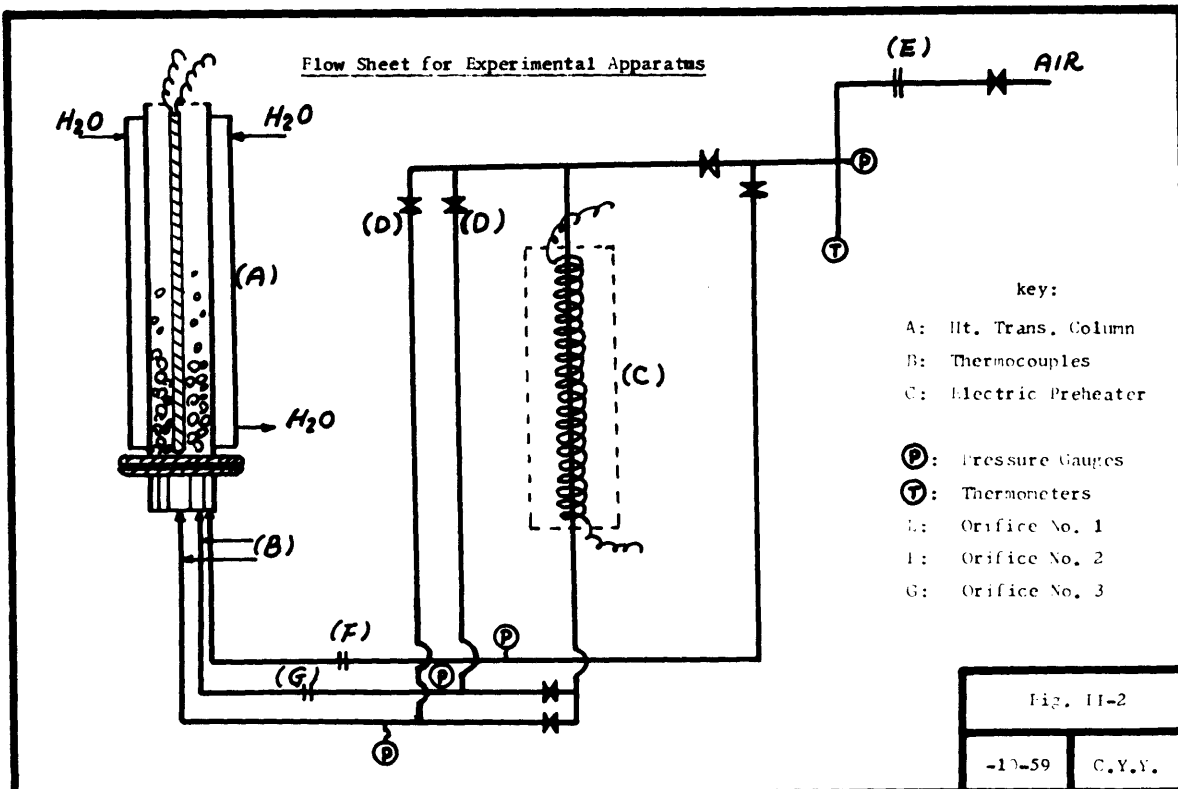
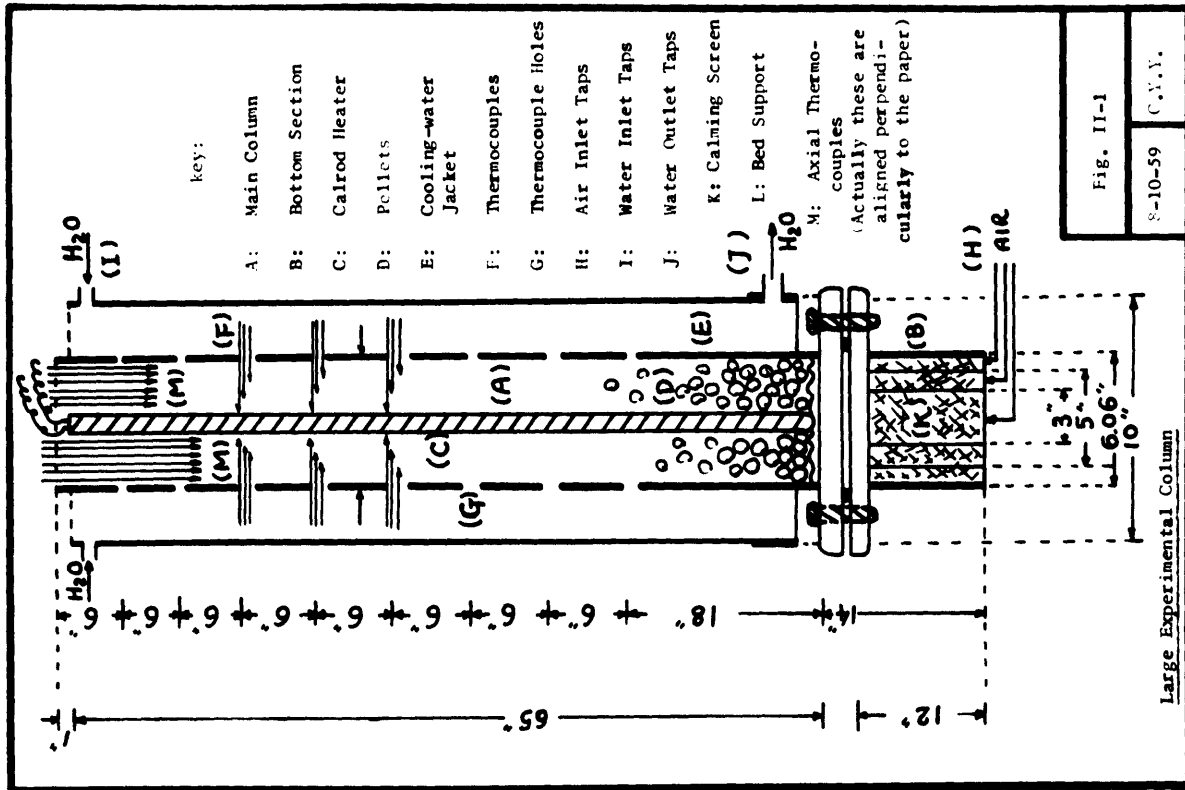
Aluminum Balls

0.250-inch-diameter aluminum balls were supplied
by Hartford Steel Ball Company. These were re-
ported to be about 0.005-inch oversize.

Glass Beads

0.236-inch-diameter soft glass beads were available
from the stockroom of the Chem. Engr. Dept., M.I.T.

The physical properties of the above various packing
materials are tabulated in APPENDIX VII.



CHAPTER III. EXPERIMENTAL PROCEDURES

(1) Packing the Column

First, the bottom section was connected to the bottom of the main body of the column by coupling the flanges with nuts and bolts. Then, the electric calrod heater was lowered into the column until its bottom end was fitted into the center hole of the perforated-steel bed-support. Holding the calrod exactly in the axis of the column, preweighed packing material was slowly dumped into the column to form a random packing. No tamping or any other artificial means of packing were used in the present study. The column was slowly packed as above until the packing height was even with the bottom level of the test section. Then, an 1/8-inch brass male-connector holding 3 thermocouples was screwed into a thermocouple-hole located immediately above the packed level. After the connector was securely tightened so that the thermocouples would not slip, the distances between the column wall and the reference points on the thermocouple wires outside the column were measured within $\pm 1/32$ inch. This measurement permitted the determination of the exact locations of the thermocouple tips in the bed. Similarly, three more thermocouples were inserted into the bed from the

opposite side of the column using the same technique.

The packing material was then slowly placed over the thermocouples, taking cautions not to disrupt them. The column was then packed for another 6 inches and the thermocouples for the next level were placed by the same technique as above. The whole process was repeated until total 18 thermocouples were placed radially in the bed, 3 in a group, 2 groups on each level, 3 levels in the test section.

When this was done, the packing level was even with the top of the test section. The bed was packed for about 5 more inches, and a group of 6 thermocouples held together by a porcelain spacer was lowered from the top of the column until the tips of the thermocouples were barely touching the packing. The porcelain spacer which held the thermocouples at fixed relative distances was made to touch the calrod surface and be perpendicular to it. The exact locations of the thermocouples were therefore known. The bed was cautiously packed for another 5 inches, and another group of 6 thermocouples were axially placed by exactly the same technique as above. These were aligned along a radius about 180 degrees apart from the other.

Under the present experimental conditions, the temperatures of the gas and solid at a given location of the bed were considered approximately equal, and therefore, no particular care

was taken to make separate measurements. After the column was packed to about 1 inch from the top edge, a perforated-steel disc was placed on the packings, and it was held with a set of screws.

From the overall bed volume and the weight of the packing material used, the packing density was calculated. From the actual density of the packing material and the above packing density, the volume fraction void was calculated.

After the column was completely packed, the removable water jacket was fitted around the column, and the joint was sealed with sealing-wax.

The above process was followed by connecting the electric leads to the calrod, water hoses to the cooling-jacket, and thermocouple wires to the multiple switches. The column was then ready for an operation.

(2) Actual Run

The amount of energy input into the calrod was adjusted to a desired level with the induction regulator, and the watt-meter reading was recorded. Cooling-water was turned on, and the flow rate was maintained sufficiently high, so that the inlet and outlet temperatures did not differ from each other

by more than 3 °F. This way, the outer wall temperature of the column was maintained essentially uniform for its entire length.

Then, the air was turned on to obtain a desired amount of overall flow rate, which was metered with Orifice No. 1.(Fig. II-2). Initially, the mass flow rates, G of inlet air into all three compartments of the bottom section were maintained equal.

Then, the electric furnaces were turned on to preheat the air streams entering the center and middle compartments. The bed thermocouple readings were obtained every 15 minutes to determine the temperature profiles in the test section. Then, the rheostats of the preheater and the cold air by-pass valves were adjusted, so that the inlet air temperatures would match the temperature profile at the bottom level of the test section. This was done by adjusting the inlet temperatures of the center and middle compartments approximately equal to the bed temperatures at $r=1.0$ and 2.0 inches, respectively. The air temperature in the supply line was usually close enough (within 10 °F) to the bed temperature at $r=2.75$ inches, and therefore, no preheating was performed for the stream entering the outer compartment, but instead, a small adjustment was made to the inlet temperature of the middle compartment, so that the total heat content of all the inlet streams was equal to that of the exit stream. The flow rates, G of the three air streams,

which were equal initially, were also readjusted so that they matched the velocity profile in the bed. The latter was determined by calculation, using the pressure drop correlation proposed by Baumeister and Bennett⁽⁵⁾ and the measured bed temperature data. (see Determination of Flow Profiles.)

The above procedures of adjusting the inlet-air temperatures and flow rates were repeated as long as the bed temperature profile varied with time. It was repeated every 15 minutes for the first 1 to 2 hours, but as a steady state was approached, once in every 30 minutes was adequate.

When the bed finally reached a point where (1) the bed temperature profiles no longer varied with time, (2) the inlet-air temperatures approximately matched the measured bed temperature profiles, (3) the inlet-air flow rates approximately matched the calculated velocity profile in the bed, and (4) the three radial temperature profiles in the test section coincided, then, the bed was assumed to have reached a steady state, and the run was concluded with final readings of the instruments.

Typical temperature and velocity profiles determined in this manner appear in Fig. (III-1) and (III-2), respectively.

(3) Calculation of Effective Conductivity

The method of calculation of the effective conductivity can be best shown with an illustration.

Referring to Fig. (III-1), the bed temperature of 100, 150, 200, 250, and 300 °F occurred in this particular run at the radial positions of $r = 2.77, 2.10, 1.57, 1.18, \text{ and } 0.89$ inches, respectively, where r is the distance out from the center of the column. Graphically differentiating the curve at these positions, the temperature gradients were found to be 64, 86, 112, 144, and 198 (-°F/inch), respectively.

The bed temperature profile remained constant within the test section indicating that the heat was transferred in the radial direction only and practically none was lost to the flowing fluid. The amount of power input in this run was 1.99 KW.

Using the basic Fourier equation for heat flow, k_e is given by

$$k_e = \frac{q}{(2\pi r)(L)(-dt/dr)} \dots\dots\dots \text{(III-1)}$$

Equation (III-1) permitted the calculation of k_e at any desired radial position in the bed by substituting appropriate local values of r and $(-dt/dr)$ into it.

Thus, the values of the local effective conductivity at these various radial positions were found to be, in this particular run, 1.12, 1.10, 1.12, 1.15, and 1.13 Btu/hr.ft.°F, respectively. These values were then attributed to the

observed local bed temperatures and the Reynolds numbers determined as illustrated in Determination of Flow Profiles.

The local effective conductivity in the immediate vicinity of the column wall was obtained as follows:

The bed temperature at 1/2-particle-diameter distance from the column wall was obtained from the experimental temperature profile. Depending on the size of the packing material and the exact location of the nearest thermocouple to the wall, a small extrapolation of the profile was necessary for this purpose. The thickness of the column wall and the amount of heat input into the calorod permitted the calculation of the inner wall temperature from the observed outer wall temperature. Usually, the difference between the outer and inner wall temperatures was less than 1 °F.

The total temperature drop within 1/2-particle-diameter distance from the column wall was thus evaluated, and the average temperature gradient within the interval was calculated by dividing the temperature drop by the radius of a pellet. The temperature gradient so calculated was substituted into Equation (III-1) together with the mean value of r (the radius of the column minus 1/4-particle-diameter) to obtain the effective conductivity within the interval.

In Run 109, the average outer wall temperature was 65 °F, and the inner wall temperature was calculated to be 65.7 °F.

The temperature profile in Fig. (III-1) gave $t=93^{\circ}\text{F}$ at $1/2$ -particle-diameter distance from the column wall, or $r=2.87$ inches. The average gradient within this interval was 175 ($=^{\circ}\text{F}/\text{inch}$), and the value of r at the midpoint of this interval was 2.96 inches. Substituting these values into Equation (III-1), the wall effective conductivity, k'_e was found to be, in this run, 0.39 Btu/hr.ft. $^{\circ}\text{F}$. This value was attributed to the arithmetic mean of the boundary temperatures of this interval and to the Reynolds number determined by the same technique as in the interior of the bed.

(4) Determination of Flow Profiles

When the radial temperature profile in the bed is constant with respect to the bed height, the radial velocity profile must also be constant. The presence of a temperature gradient in the bed makes the flow profile different from flat, and the mass flow rate, G varies across the radius.

The ratio of the mass flow rates at any two different radial positions may be estimated from the following equations,⁽⁵⁾ remembering that the amount of pressure drop, ΔP between any two bed levels must be equal at all radial positions:

$$f = \frac{g_c d_p \rho (-\Delta P)}{2 G^2 L} \dots\dots\dots \text{(III-2)}$$

and $f = 30.7 \left(\frac{\mu}{d_p G} \right)^{0.2} \dots\dots\dots \text{(III-3)}$

for Re= 40 -----50,000

The above equation were developed for the purpose of calculating the overall pressure drop in a packed column, but these were assumed to be approximately applicable to the local conditions of the bed.

From Equations (III-2) and (III-3), it follows that

$$\begin{aligned} (G_2/G_1) &= (\mu_1/\mu_2)^{1/9} (\rho_2/\rho_1)^{1/1.8} \\ &= (T_1/T_2)^{1/1.8} \dots\dots\dots \text{(III-4)} \end{aligned}$$

Using Equation (III-4), the velocity profile across the radius was calculated as follows:

The cross-sectional area of the bed was hypothetically divided into 5 incremental concentric annular areas, each having a 0.5-inch annular distance. (The annular area next to the column wall had an annular distance of 0.53 inch.) If the average mass flow rates in these 5 annular areas are expressed by G_1, G_2, \dots, G_5 , starting from the one next to the calrod, then the overall mass flow rate, G_o is related to them by

$$G_1 \left(\frac{\pi}{4} \times 3 \right) + G_2 \left(\frac{\pi}{4} \times 5 \right) + G_3 \left(\frac{\pi}{4} \times 7 \right) + G_4 \left(\frac{\pi}{4} \times 9 \right) + G_5 \left(\frac{\pi}{4} \times 11.8 \right) = G_0 \left(\frac{\pi}{4} \times 35.8 \right) \dots\dots\dots \text{(III-5)}$$

Substituting Equation (III-4) into Equation (III-5), and rearranging,

$$G_1 = \frac{G_0 (35.8)}{3 + 5 \left(\frac{T_1}{T_2} \right)^{1/1.8} + 7 \left(\frac{T_1}{T_3} \right)^{1/1.8} + 9 \left(\frac{T_1}{T_4} \right)^{1/1.8} + 11.8 \left(\frac{T_1}{T_5} \right)^{1/1.8}} \dots\dots\dots \text{(III-6)}$$

$$G_2 = G_1 \left(\frac{T_1}{T_2} \right)^{1/1.8}, G_3 = G_1 \left(\frac{T_1}{T_3} \right)^{1/1.8} \text{ etc.} \dots\dots\dots \text{(III-7)}$$

where T_1, T_2, \dots, T_5 are the average absolute temperatures of the 5 incremental annular areas and were assumed to be equal to the bed temperatures at $r=0.75, 1.25, 1.75, 2.25,$ and 2.75 inches, respectively.

Thus, from the measured temperature data and the overall flow rate, G_0 , the velocity profile in the bed was established through Equations (III-6) and (III-7). This permitted the calculation of the Reynolds number at any desired radial position in the bed. Typical examples of the velocity and Reynolds number profiles in the bed determined in this manner appear in Fig. (III-2).

The above method of velocity profile determination took into consideration only the temperature effect on the velocity and disregarded any possible presence of channeling. This is equivalent to assuming that the velocity profile would be flat, if the bed were isothermal. Schwartz and Smith⁽⁵⁰⁾ studied flow profiles in isothermal beds by measuring the velocity traverses at about 2 inches above the packing level with a hot wire anemometer. They assumed that the flow profile in that level represented the flow profile in the interior of the bed, and proposed the "hump profile" theory. According to them, when d_p/D_t was less than 0.033, the flow profile was essentially flat with only a small velocity hump near the column wall which was greater than the velocity at the center by less than 20%. When d_p/D_t was larger than 0.033, however, they found that the velocity hump near the column wall was 30% or more greater than at the center, reaching 100% at d_p/D_t of 0.125. They also found that the results of their experiments were affected appreciably by the distance above the packing level at which the velocity traverses were measured. The 2-inch distance was used only because the results were most reproducible at that height. For this reason, how closely their experimental data truly represented the velocity in the interior of the bed is uncertain.

The d_p/D_t ratios involved in the present work were, disregarding the presence of the calrod, 0.023, 0.028, 0.046, and 0.052 for 0.141-inch steel, 0.165-inch alumina, 0.282-inch steel, and 0.312-inch alumina balls, respectively. If Schwartz and Smith's data⁽⁵⁰⁾ are assumed to be the true representation of the flow profile in the interior of the bed, the velocity profile in the present study would have been essentially flat for the first two packing materials, but the "hump" for the latter two may have been appreciable. In view of this possibility, the significance of the present method of velocity determination needs to be discussed.

The present method of velocity determination which assumes a flat profile in an isothermal bed was chosen in preference to the "hump profile" theory for the following various reasons:

- a) The present experimental technique permitted the calculation of local effective conductivity without involving the velocity profile in any manner. Therefore, the question of velocity profile is raised only for the purpose of correlating the data.
- b) The values of the local effective conductivity determined experimentally in the present work were correlated by the flat profile assumption quite consistently and in complete agreement with the "random walk" analogy, whereas the "hump profile" theory would have produced irregular results.

- c) The correlations obtained in the present work based on the flat profile assumption were found to reproduce various previous data involving d_p/D_t as large as 0.3. This indicates that the present method of correlation is valid even in the cases where the "hump profile" theory would predict a difference of several hundred per cent between the velocities at the center of the bed and at the "hump."
- d) In practical applications of a correlation, one which is based on the flat profile assumption is much more convenient to use than the other, as long as the former produces equal or better results.

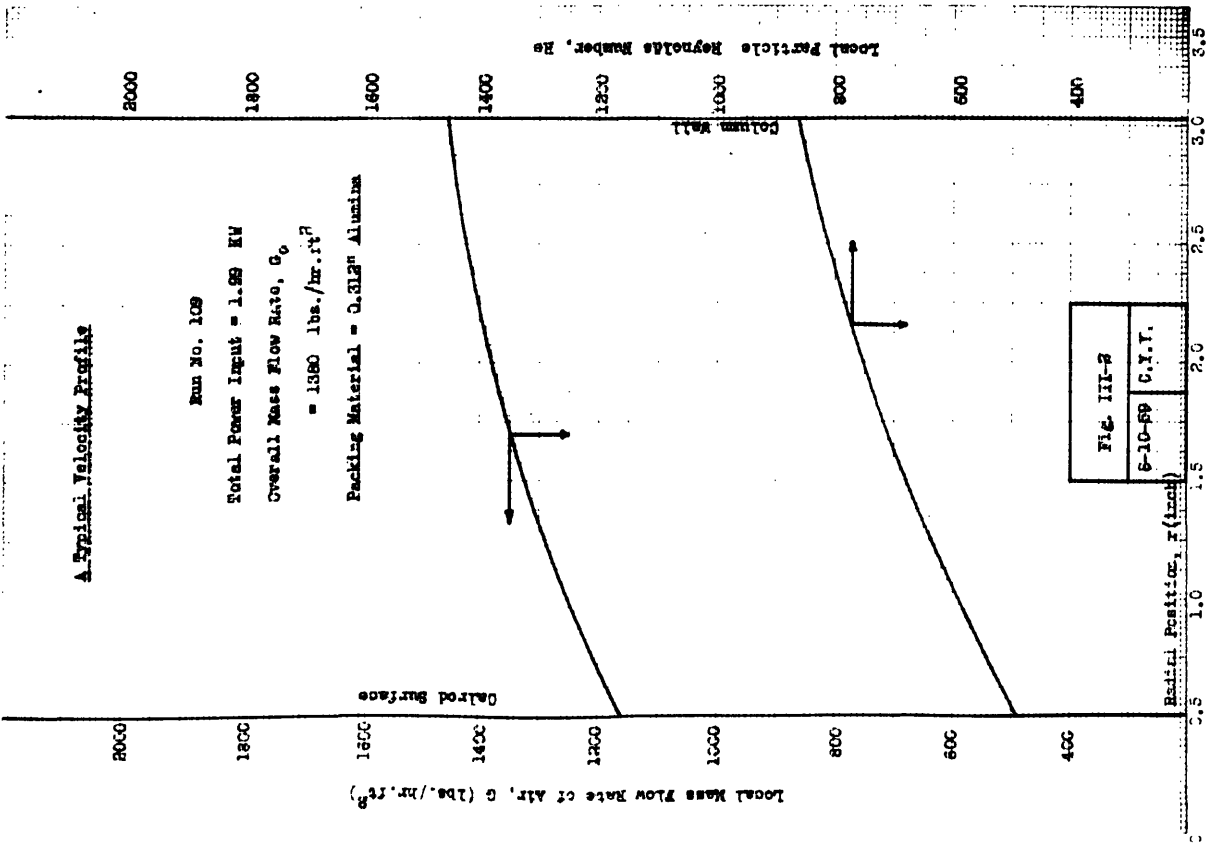
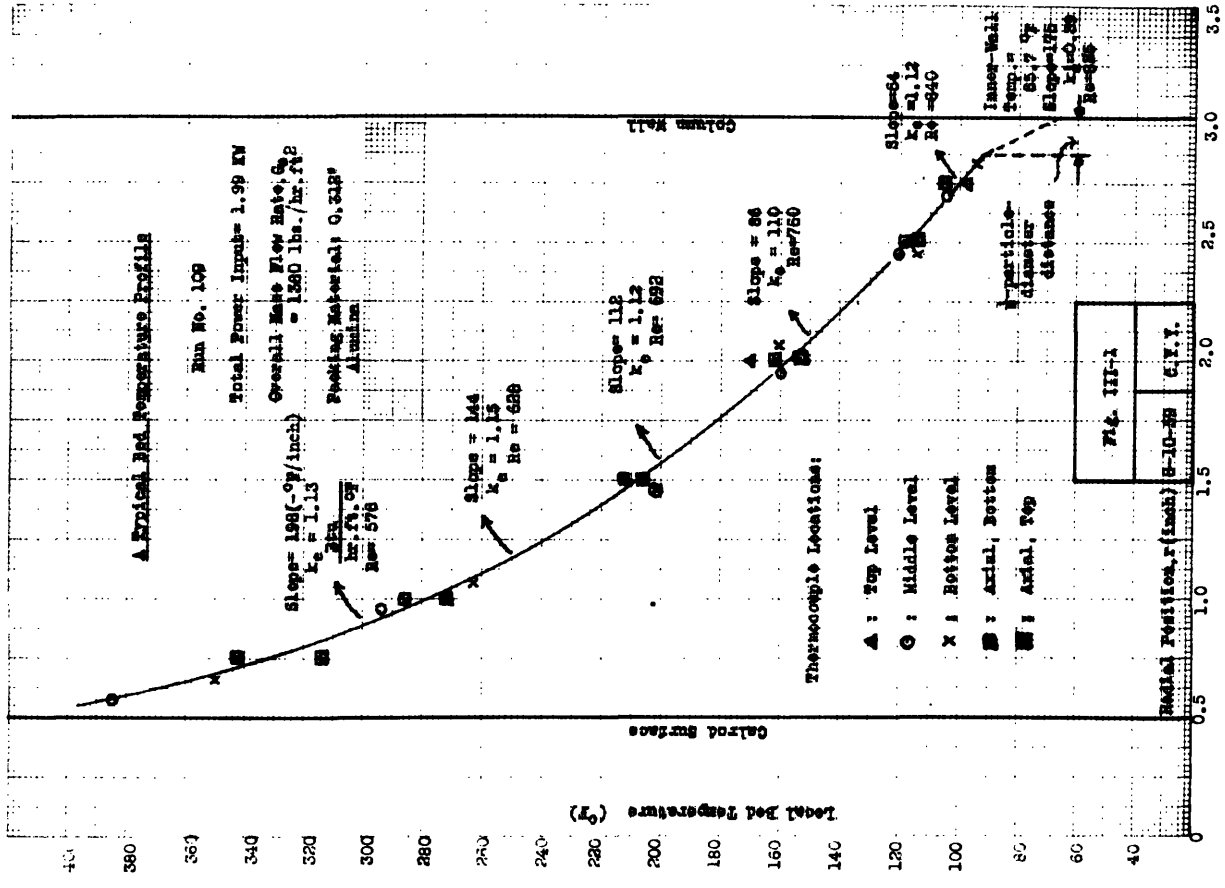
(5) Determination of Static-bed Conductivity

The local effective conductivity in a static bed, k_B was measured with both the large and small columns. With the large column, the packing material was limited to 0.141- and 0.282-inch steel balls, and 0.165- and 0.312-inch alumina balls. The maximum temperature used in the large column was around 450 °F. With the small column, on the other hand, two more packing materials, namely, 0.236-inch glass beads and 0.250-inch aluminum balls were used in addition to the others, and the maximum temperature was over 1000 °F.

The packing procedures for the large column were identical with those in the flow runs which were described earlier in this chapter. The small column was packed in exactly the same manner, except that no radially placed thermocouples were used in this case.

Since a static run did not involve any flow, all that was necessary was maintaining the energy input into the calorimeter constant and waiting for the steady state.

The calculations of k_B were performed by the identical technique as described earlier concerning the calculations of effective conductivity in the flow runs. The calculated value of k_B was attributed to the corresponding local bed temperature.



CHAPTER IV. RESULTS

The experimental results obtained in the present study are presented in this chapter in graphical forms. The original calculated values on which these graphs were based are included in APPENDIX I.

(1) The Local Effective Conductivity under Flow Conditions.

The local effective conductivity, k_e correlated in Figures (IV-1) through (IV-4) is the "combined" radial effective conductivity in the sense that it incorporates both the solid phase effective conductivity and fluid phase effective conductivity.

The values of k_e calculated as illustrated in the preceding chapter were grouped together in these figures by various common local bed temperatures, regardless of the radial positions at which they were observed. Thus, the experimental points connected by any one of the curves may have been observed at any radial position in the bed outside a 1/2-particle-diameter distance from either the calorod or column wall surface.

For an illustration, these figures show only those groups of experimental values which were observed at bed temperatures

of 150 and 250 °F. The experimental values obtained at other bed temperatures were also found to behave similarly, and this may be seen from Figures (IV-5) through (IV-8), and from the tables in APPENDIX I.

The values of k_e were correlated with the Reynolds number determined by the method described in the preceding chapter.

(2) The Modified Peclet Number

The turbulent-diffusion contribution to heat transfer, k_{td} was calculated by taking the difference between k_e and k_B at the same bed temperature. The values of static-bed conductivity, k_B used in the calculation were the mean values, which were obtained by averaging all the values of k_B observed at the same bed temperature in different static runs using the large column. As is shown in later pages, the values obtained with the large and small columns coincided in most cases.

The values of k_{td} calculated as above were correlated in terms of the modified Peclet number defined in Equation (I-12) as a function of the Reynolds number.

Figures (IV-5) through (IV-8) show the relation between the modified Peclet number and such variables as the Reynolds

number and temperature level for any one particular packing material. Figure (IV-9), which is the combination of all the above 4 figures, shows the relations between the modified Peclet number and such variables as particle size and solid conductivity in addition to the Reynolds number and temperature level.

(3) Wall Effective Conductivity

Correlated in Figures (IV-10) through (IV-13) are the values of the wall effective conductivity, k'_e , or the local effective conductivity within 1/2-particle-diameter distance from the column wall. How this particular quantity, i.e. 1/2-particle-diameter, was arrived at is as follows:

- a) The local effective conductivity evaluated at any radial position outside a 1/2-particle-diameter distance from the column wall or calorimeter surface behaved similarly, regardless of the radial position at which it was observed. When the values of k'_e were correlated as in Figures (IV-1) through (IV-4), the experimental points obtained as near as 1/2- to 1-particle-diameter distance from the column wall did not show any particular deviation. This result directed toward the possibility of

confining the wall effect within a distance from the wall which is not larger than 1/2-particle-diameter.

- b) However, the original concept of effective conductivity, itself ~~is~~ based on the macroscopic nature of a packed bed, and therefore, further smaller subdivisions of a 1/2-particle-diameter interval is both meaningless and incompatible with the concept of k_e .
- c) To be no larger and yet no smaller than a certain quantity is to be that quantity, itself, or in this case, 1/2-particle-diameter.
- d) Subsequent experimental results produced a consistent correlation which was reasonable from the theoretical point of view. (see CHAPTER V.)

The values of the wall effective conductivity were correlated in Figures (IV-10) through (IV-13) as a function of the product of $(C_p \mu)$ and the Reynolds number. The Reynolds number was determined by the same technique as was described in CHAPTER III.

The reason why the product of $(C_p \mu)$ and the Reynolds number was used in the correlation instead of the Reynolds

number alone was as follows: Being an expression of a heat transfer property on which the fluid turbulence may have an effect, the wall effective conductivity, k'_e was expected to be a function of the Prandtl number as well as the Reynolds number, and the functional form was assumed to be a dimensionless equation such as

$$\frac{k'_e - k'_B}{k_g} \propto \left(\frac{C_p \mu}{k_g} \right)^n \left(\frac{d_p G}{\mu} \right)^m \dots\dots\dots (IV-1)$$

The Prandtl number was varied only within a limited range in this study, and its exponent was not determined experimentally. However, the Prandtl numbers of most of the gaseous materials are close to unity, and it was considered reasonable to use the value of unity for the exponent. This assumption is believed to be particularly reasonable in this case, because, as shown in Figures (IV-10) through (IV-13), the slopes are quite small for all these curves, and a slight change in the exponent of Prandtl number would have caused only a negligible difference in the values of k'_e .

(4) The Static-bed Conductivity

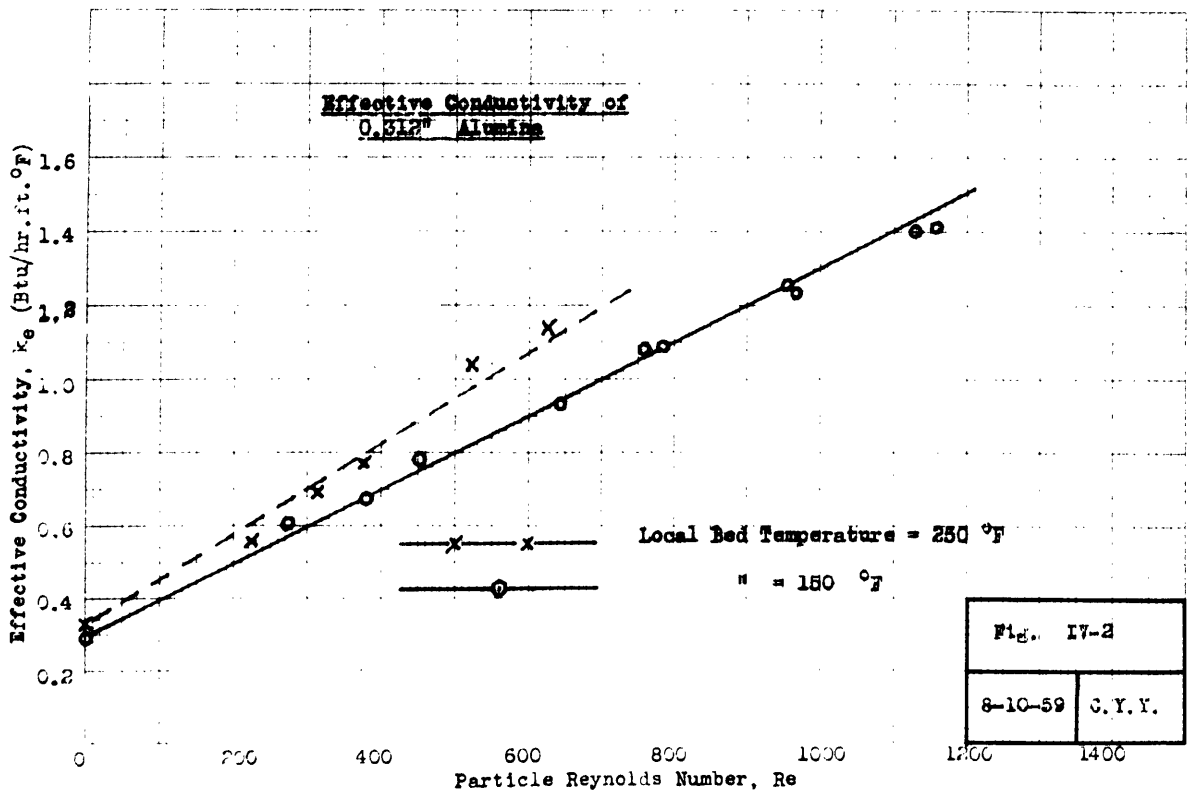
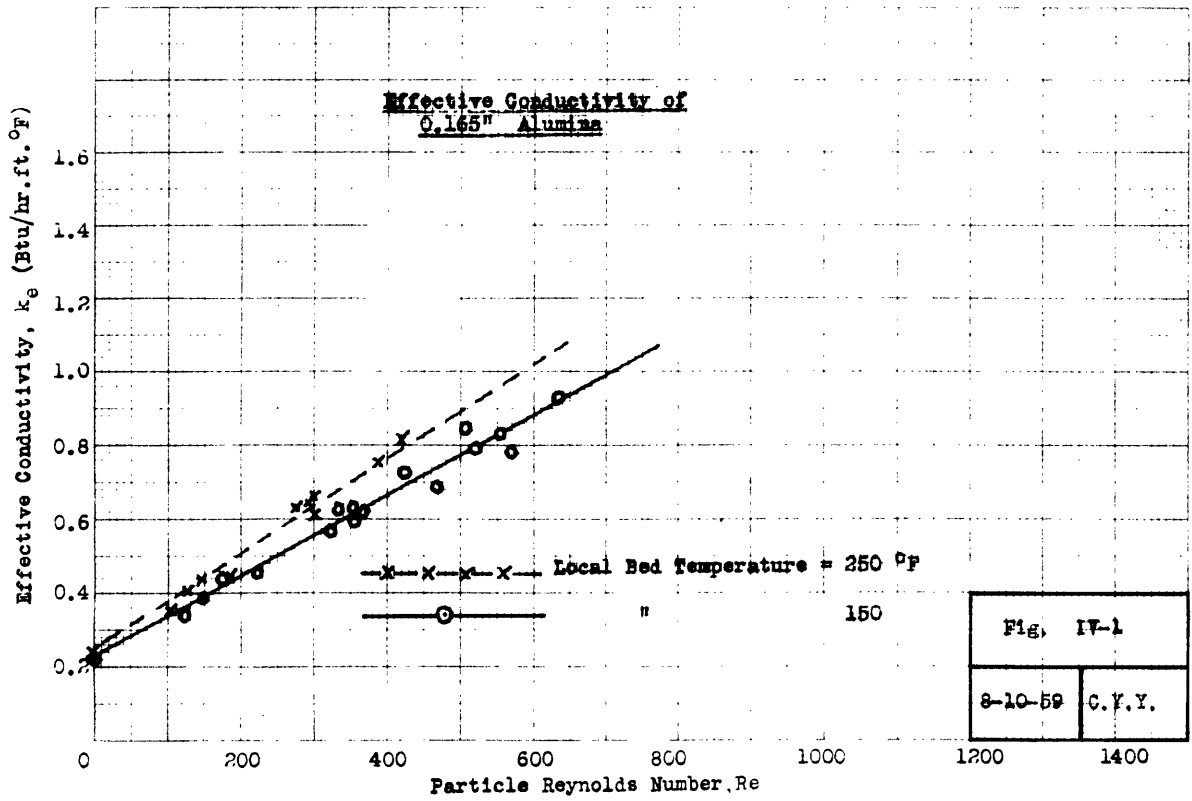
Figures (IV-14) through (IV-19) present the data on the static-bed conductivity as a function of the local bed

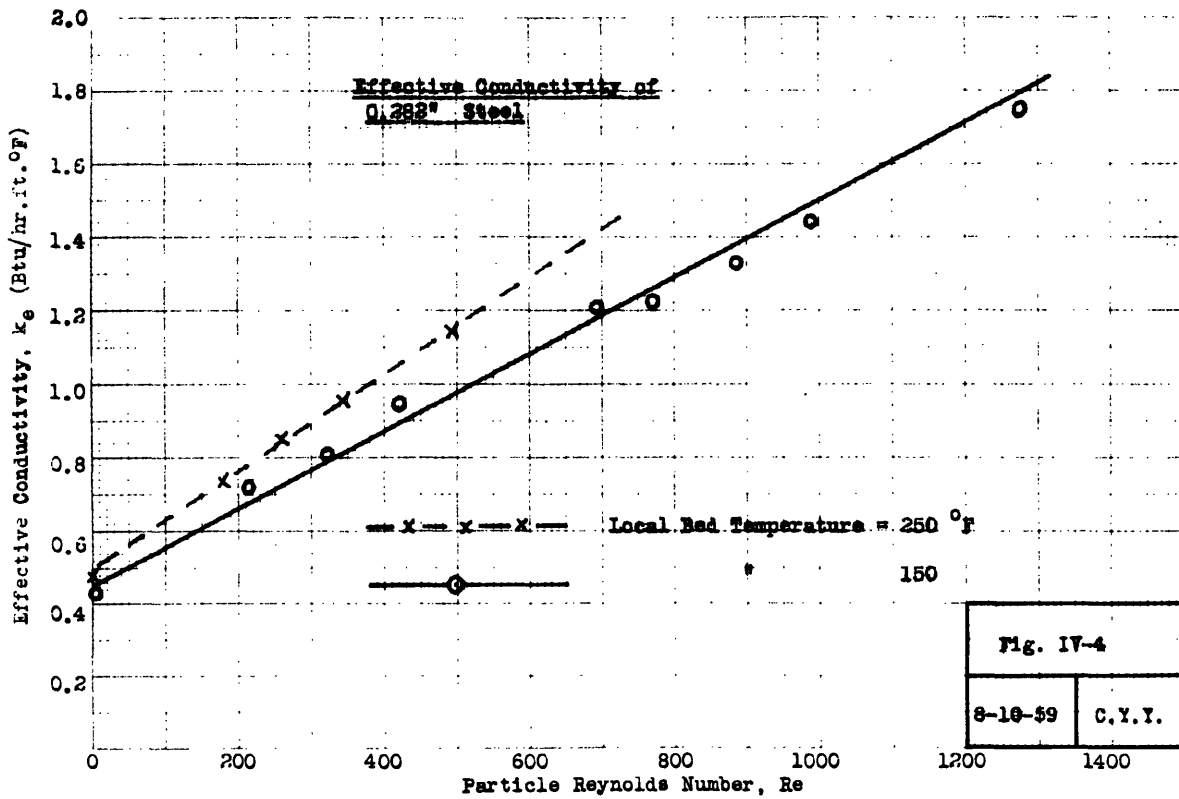
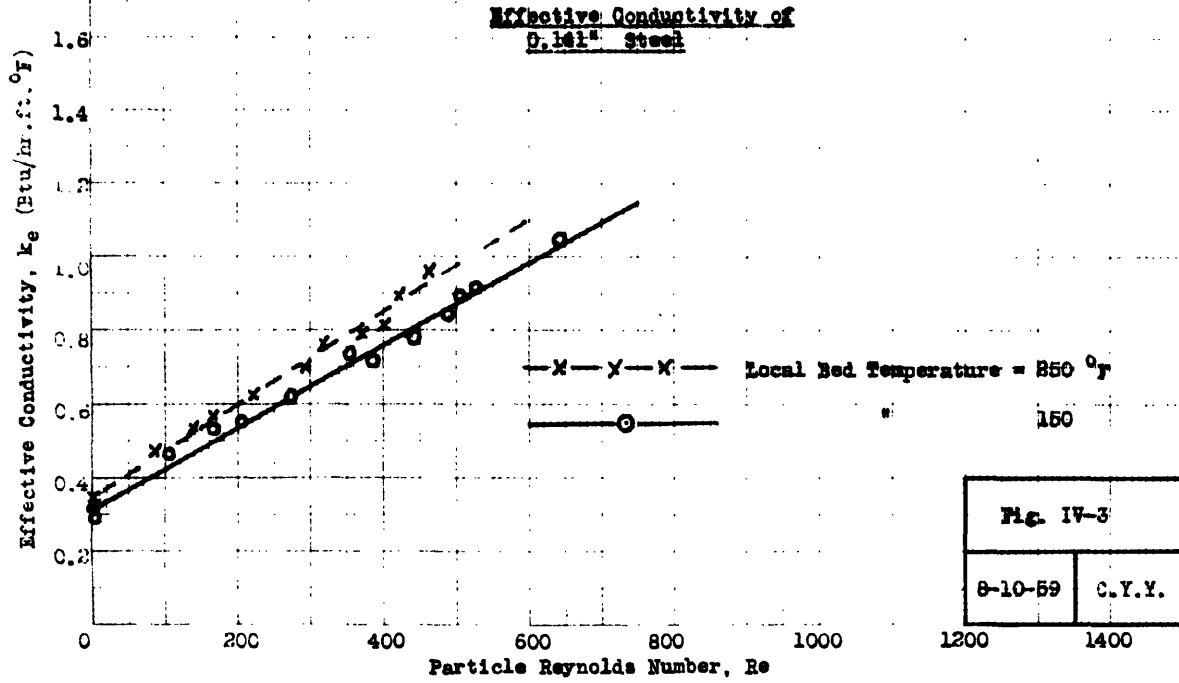
temperature for various packing materials. The indicated temperatures are not the average temperatures of the entire bed but ~~are~~ the local temperatures at which the corresponding values of the static-bed conductivity were observed.

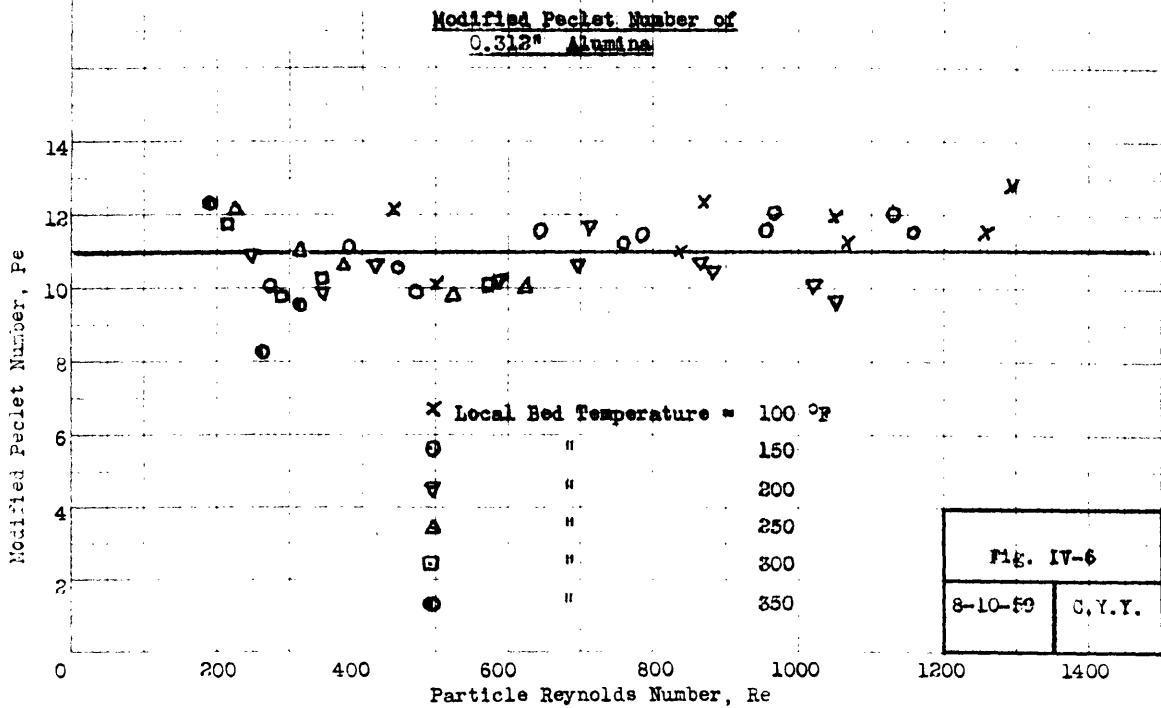
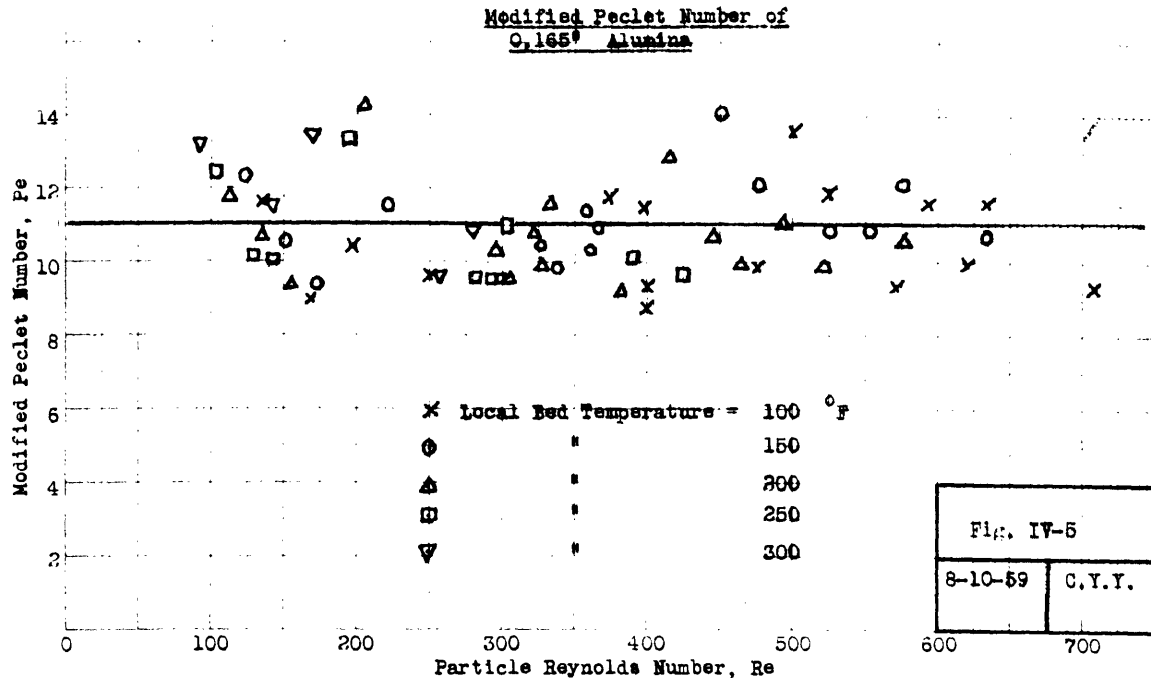
The approximate temperature gradient in the vicinity of where the conductivity was observed was indicated by symbols to show the effect of temperature gradient on the radiation contribution.

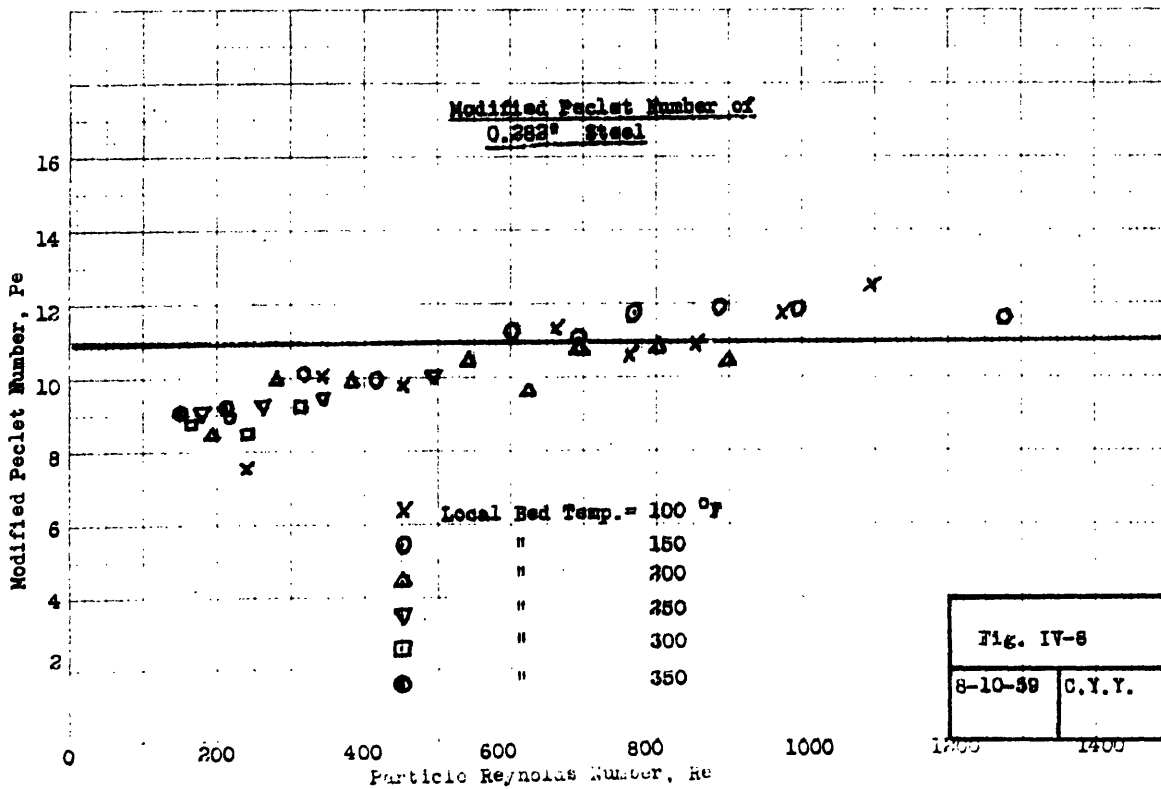
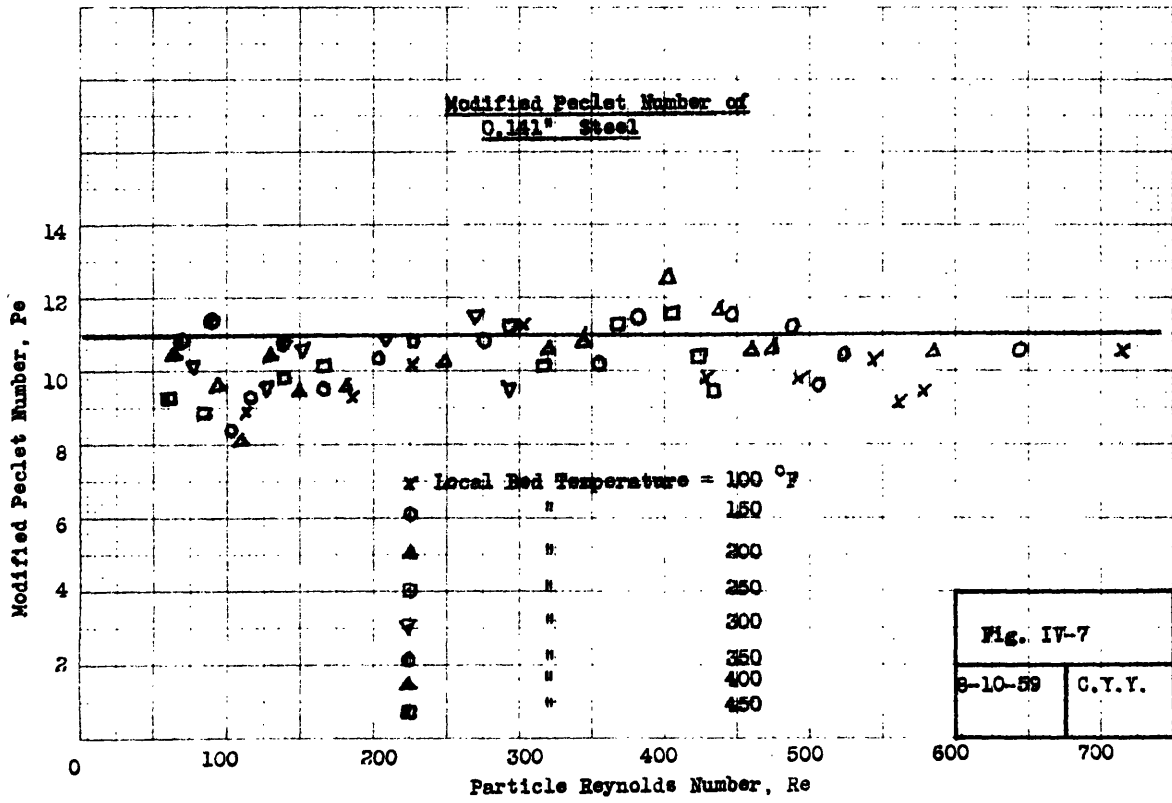
In the cases of alumina and steel balls, the data obtained with the large heat transfer column were shown with others.

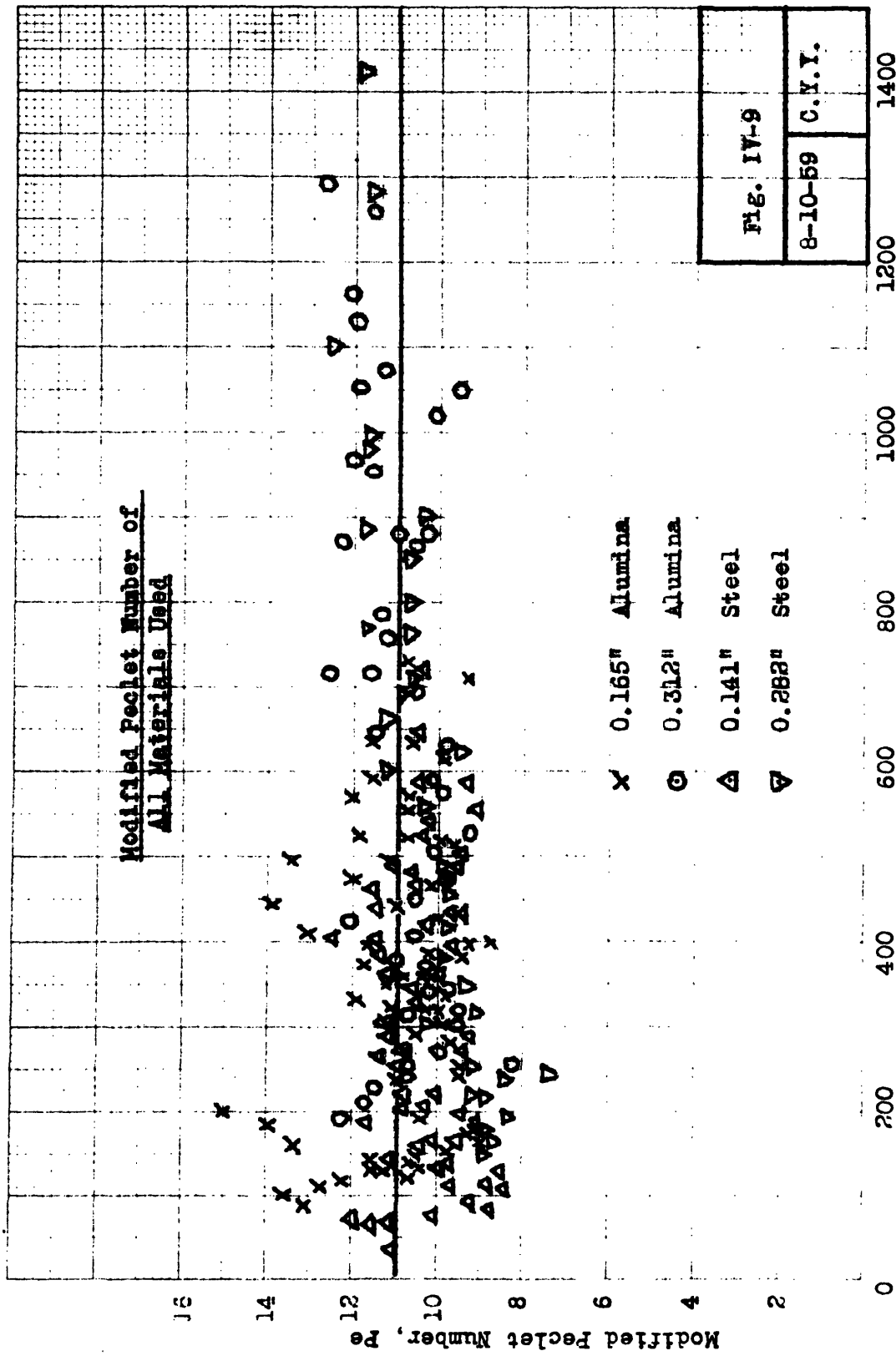
The dashed lines on the graphs indicate the calculated values obtained by the method to be discussed in CHAPTER V.

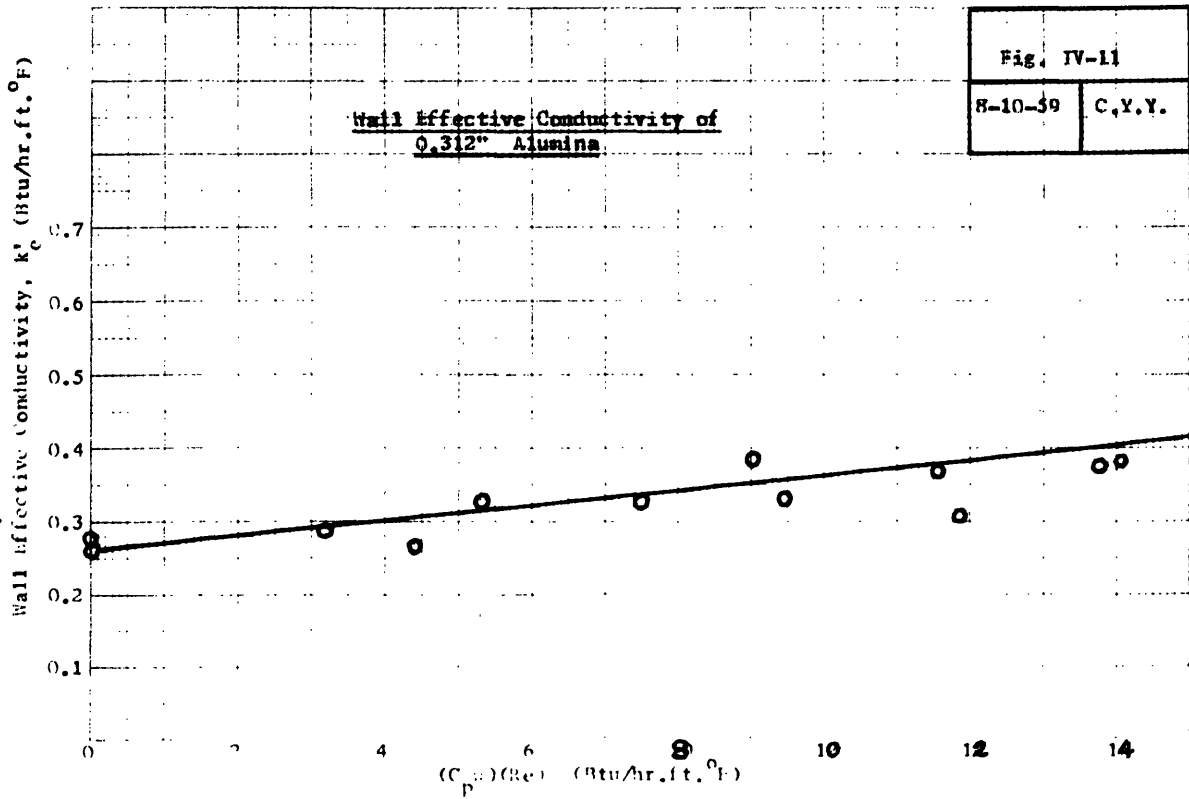
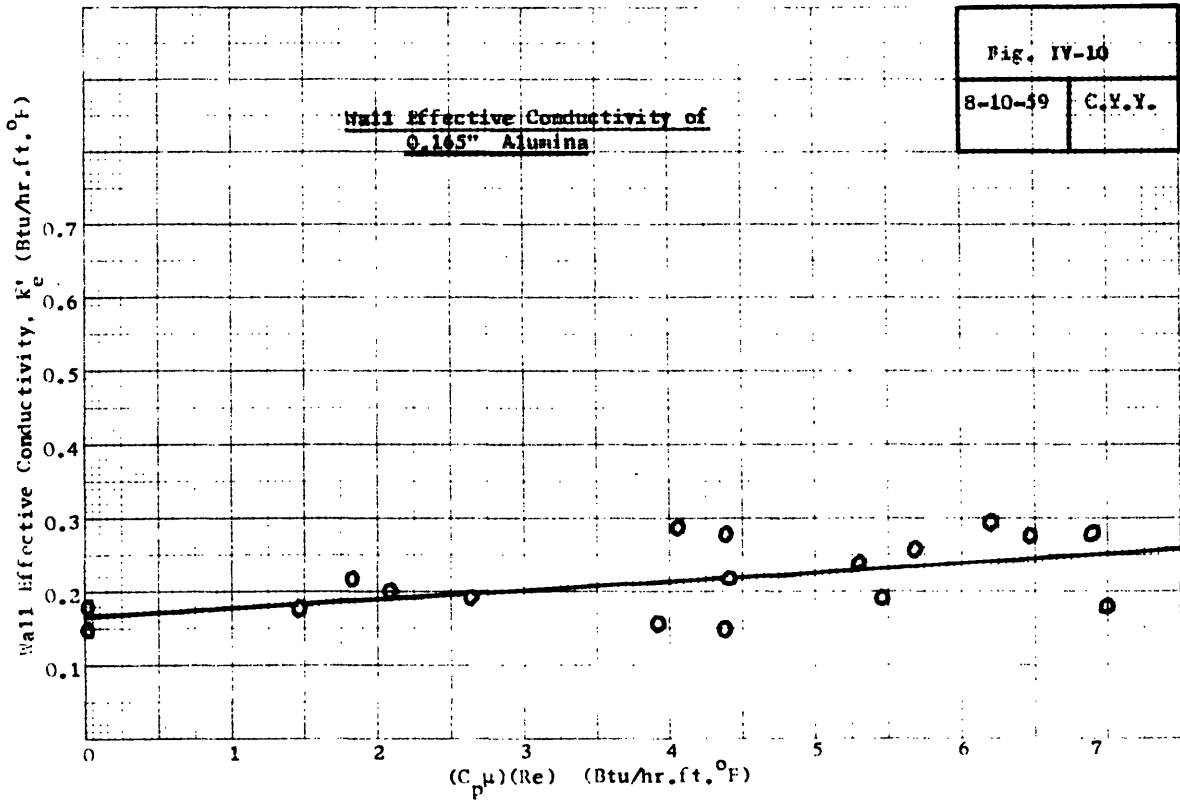


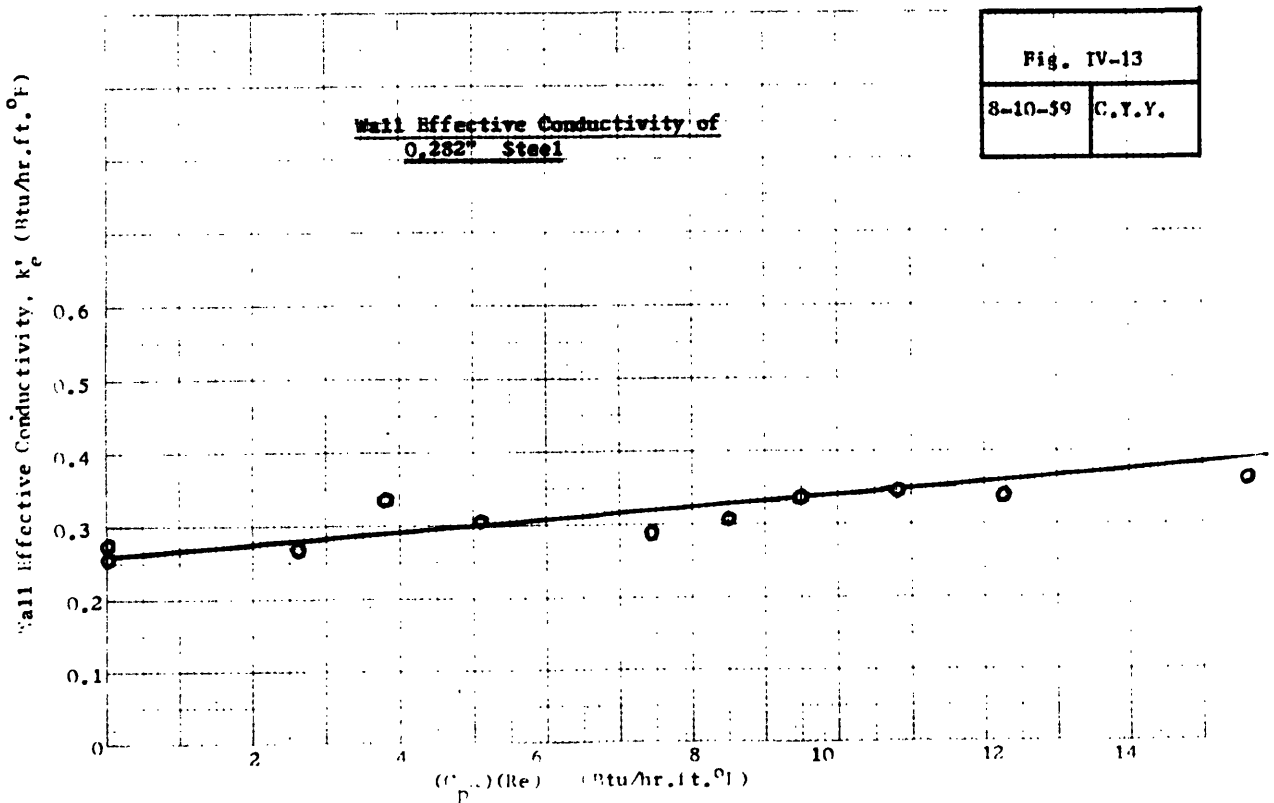
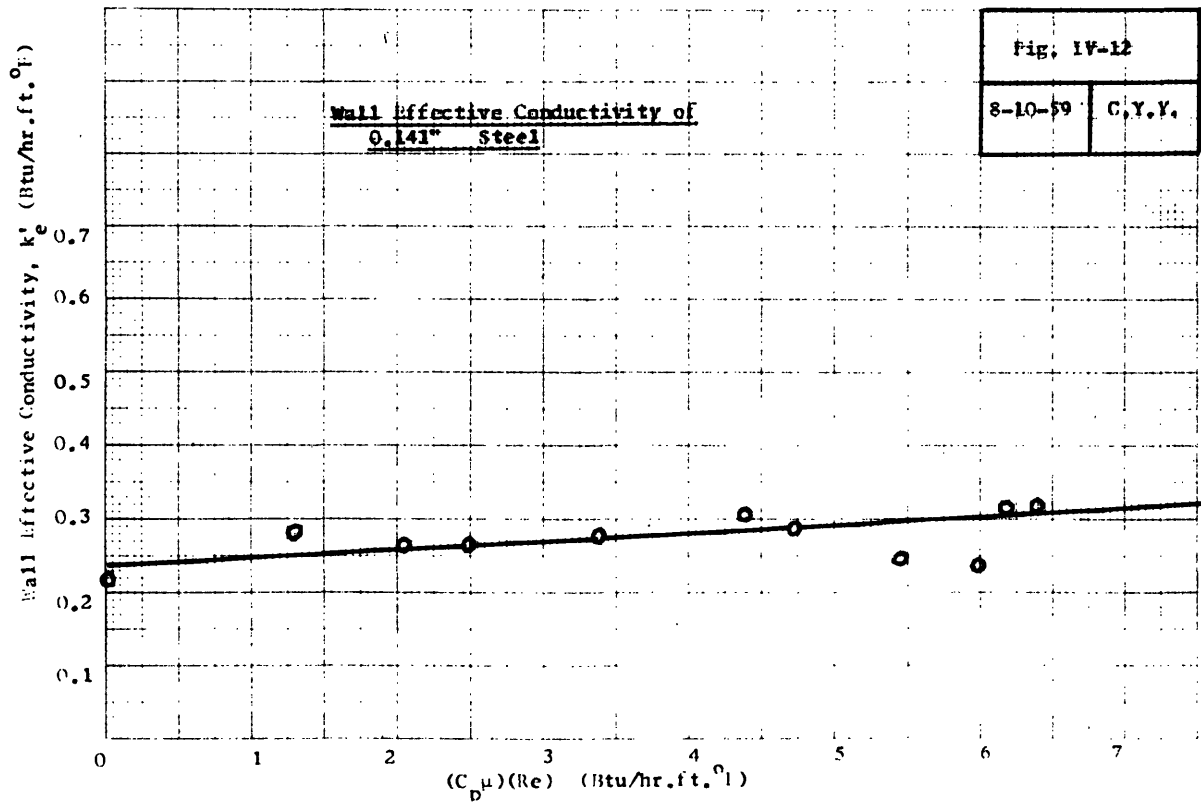


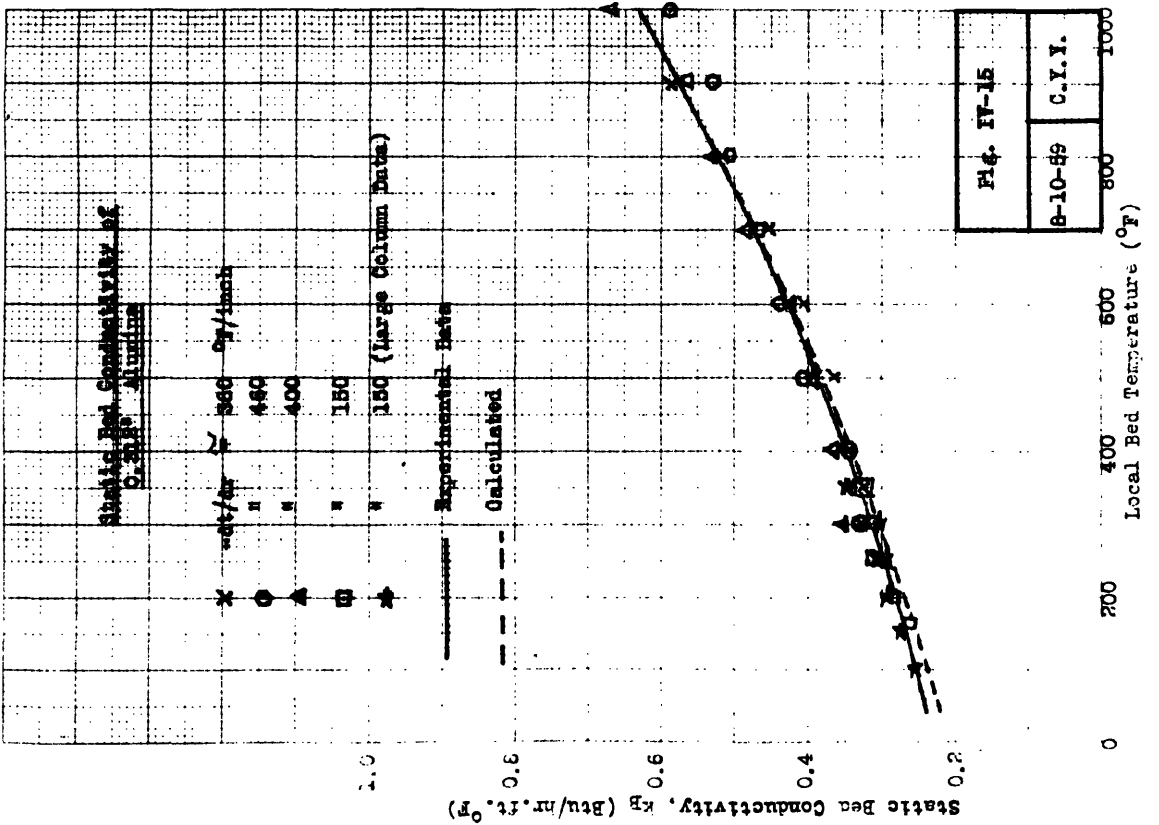
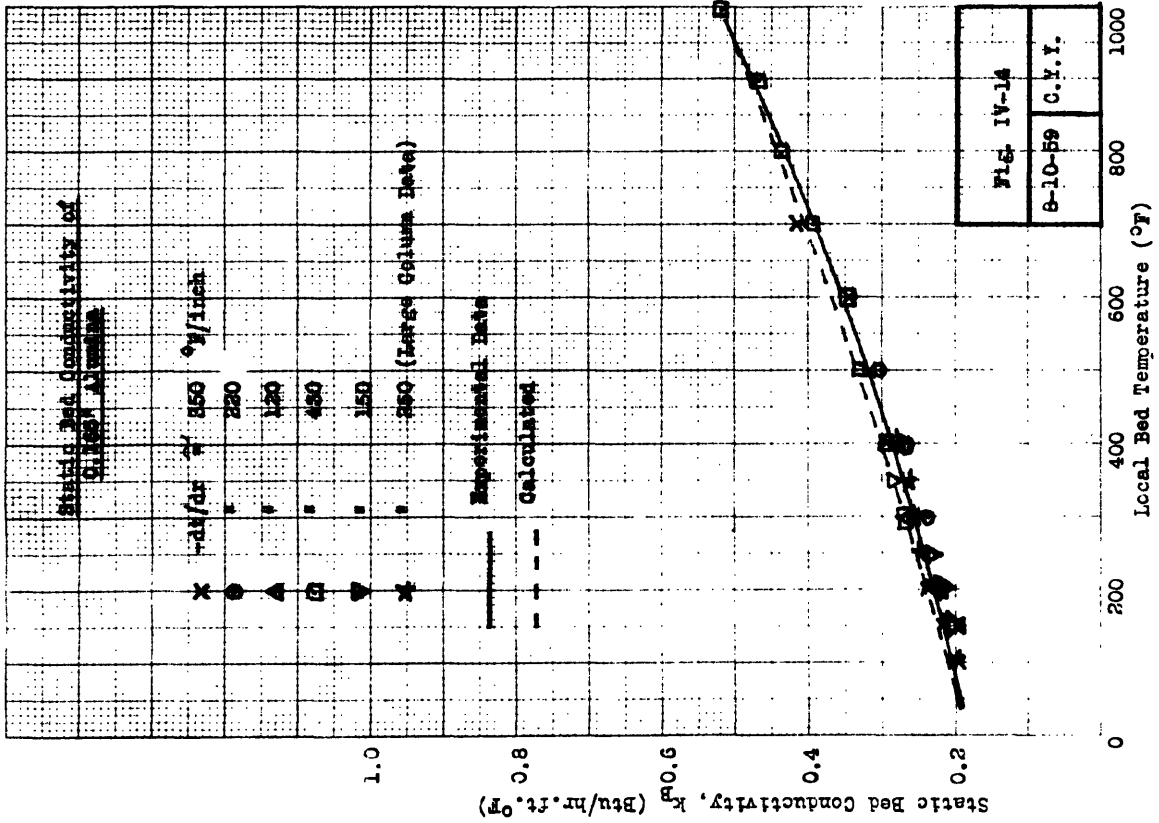












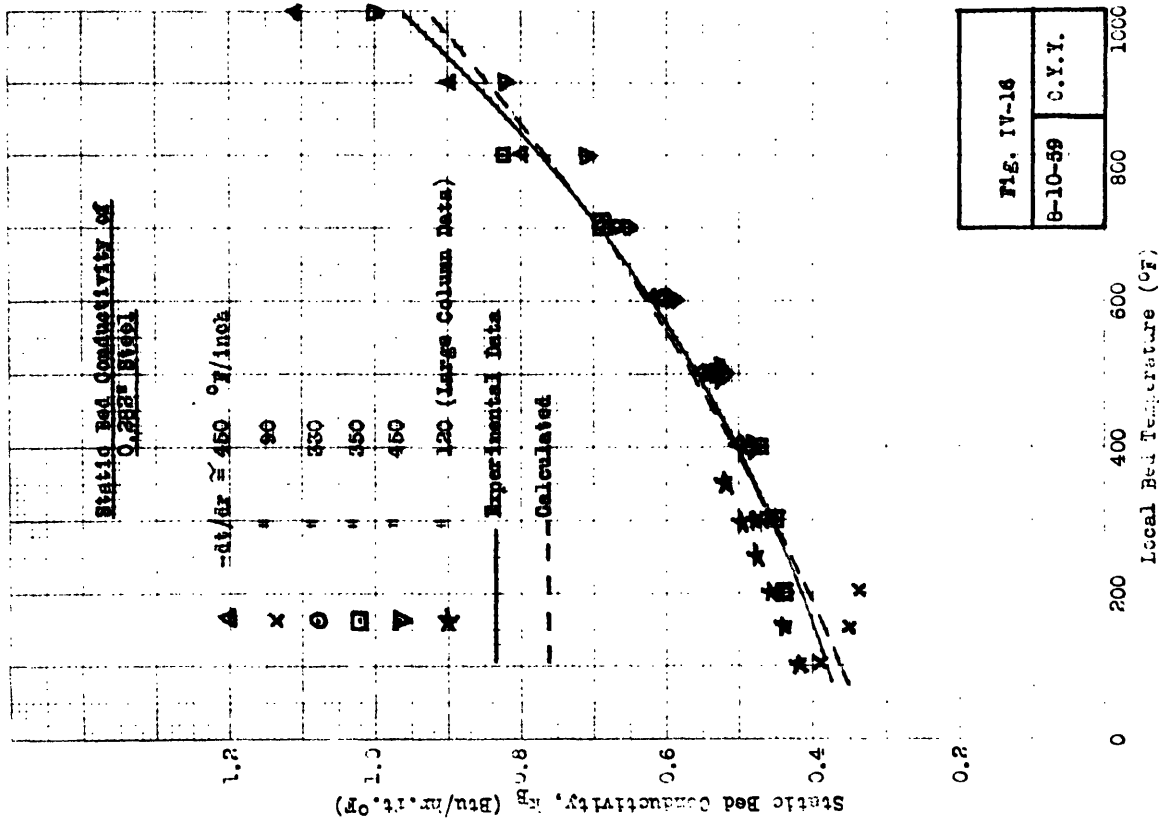


FIG. IV-16
B-10-59 C.Y.Y.

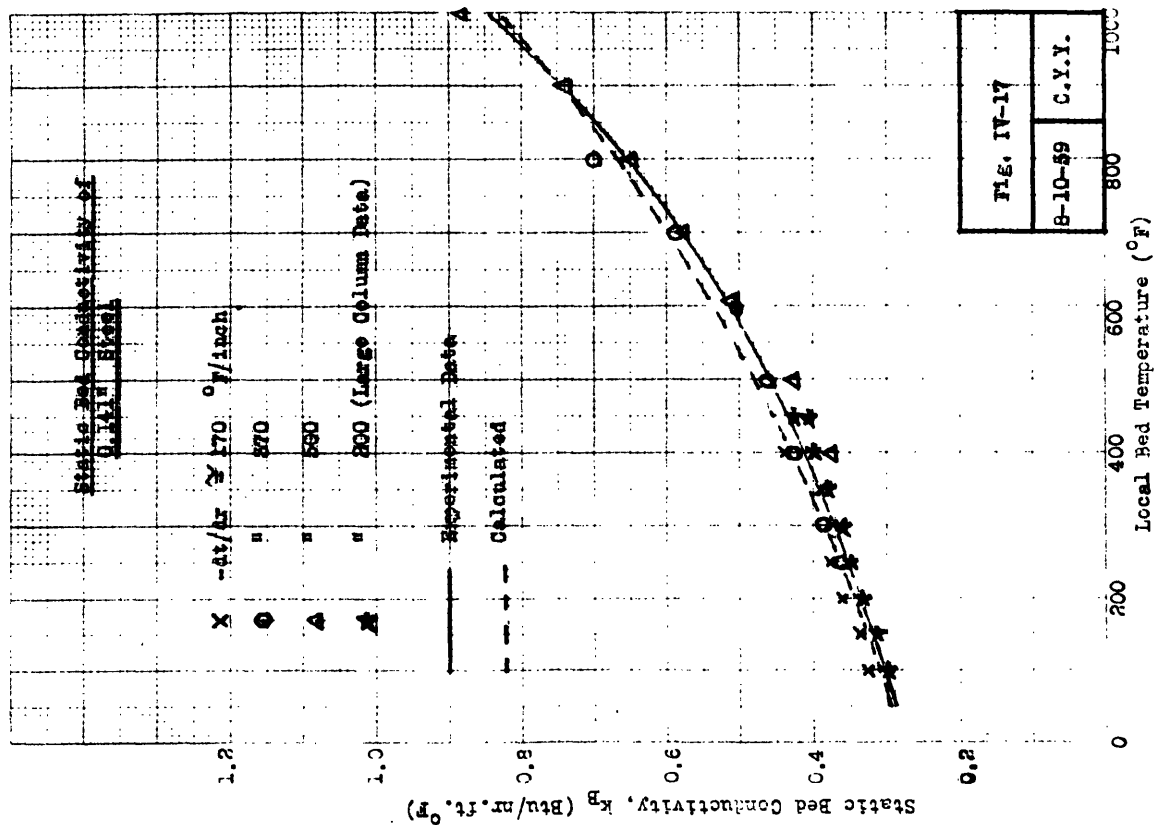
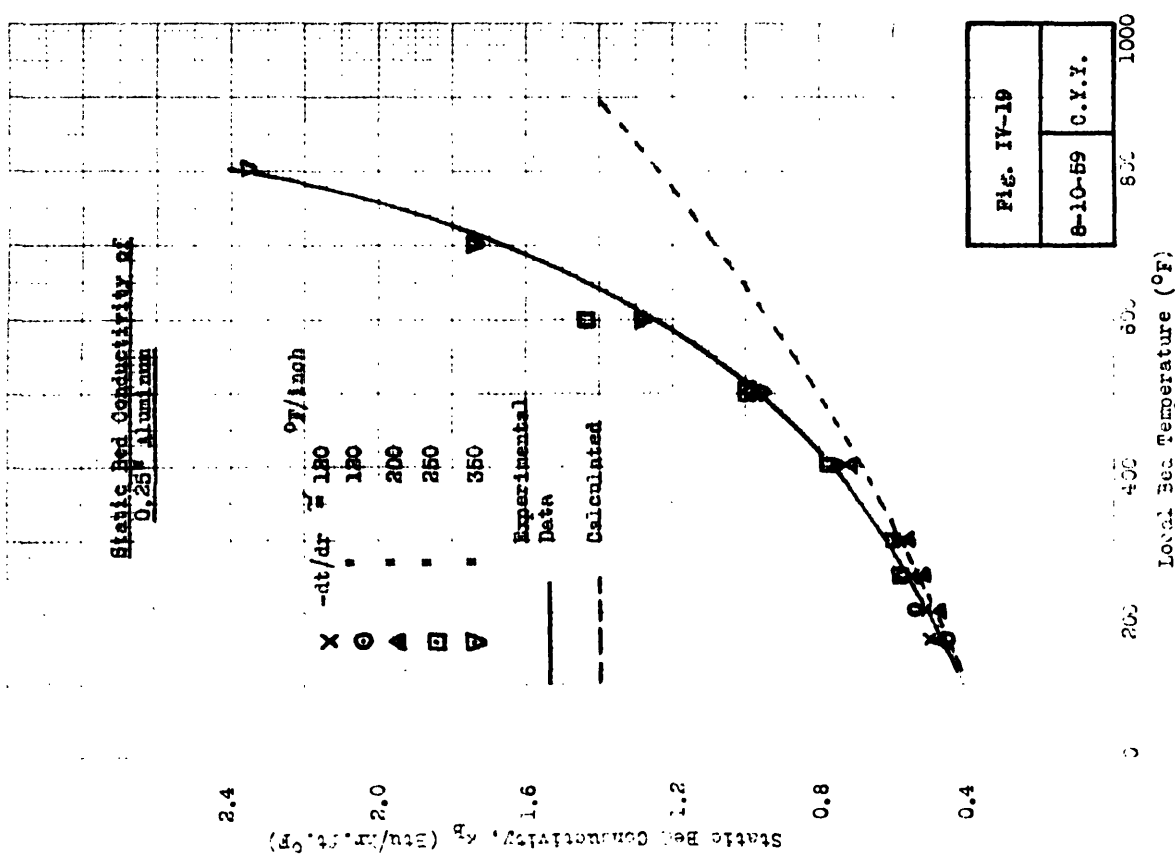
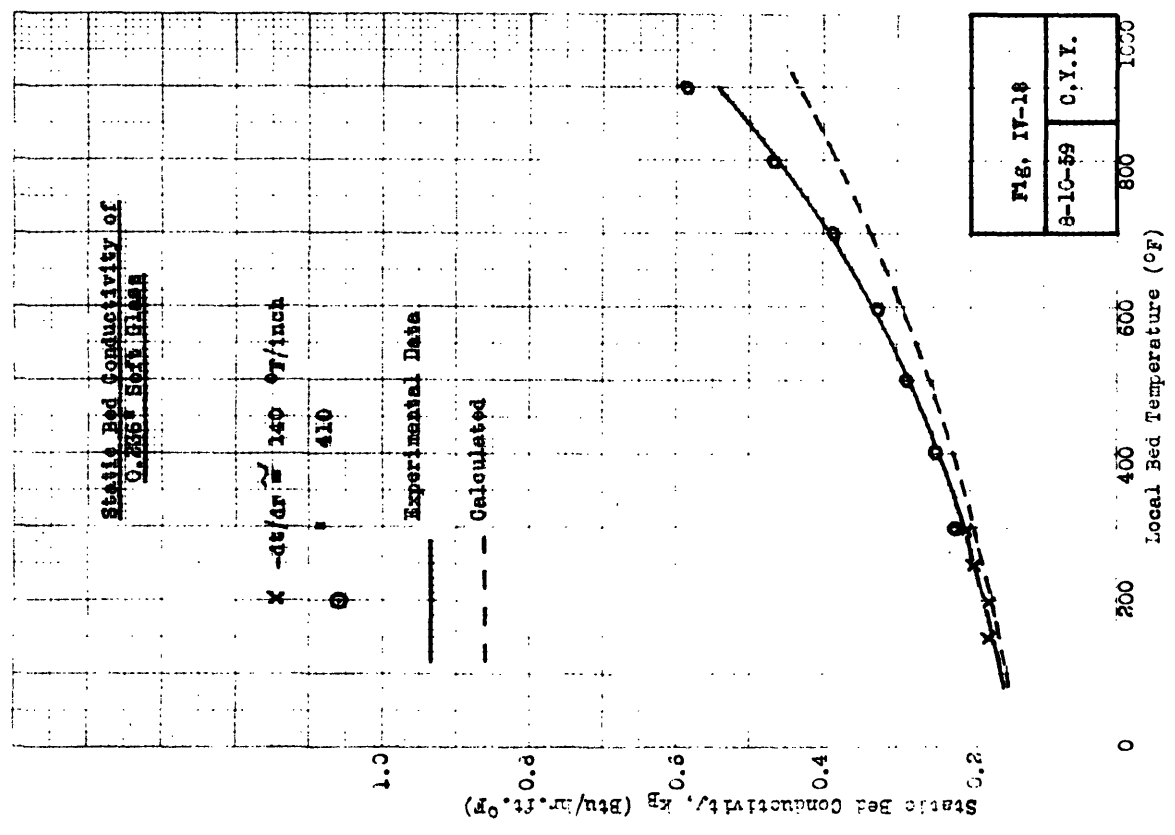


FIG. IV-17
B-10-59 C.Y.Y.



CHAPTER V. DISCUSSION OF RESULTS

(1) Radial Heat Transfer Peclet Number

The results presented in Figures (IV-1) through (IV-4) show that the local effective conductivity obtained in the interior of the bed outside a 1/2-particle-diameter distance from the confining walls is a linear function of the particle Reynolds number, and that the slope of the curve is not affected by the properties of the packing material. The slope, however, is a function of the local bed temperature at which the concerned values of k_e were observed. The manner in which the slope is related to the bed temperature is shown in Figures (IV-5) through (IV-9), where the modified Peclet number was plotted against the particle Reynolds number. The experimental points are somewhat scattered, but the tendency is evident that they are gathered around the Peclet number of 11. Furthermore, this tendency is common to all packing materials, regardless of the particle size, solid conductivity, or the bed temperature. Hence, the results in these figures may be generalized by the following equations:

$$Pe = \frac{d_p G C_p}{k_{td}} = 11 \quad \dots\dots\dots (V-1)$$

But $k_{td} = k_e - k_B$

Or $k_e = k_B + \frac{d_p G C_p}{11} \dots\dots\dots (V-2)$

Or $\frac{k_e}{k_g} = \frac{k_B}{k_g} + \left(\frac{1}{11}\right) \left(\frac{C_p \mu}{k_g}\right) \left(\frac{d_p G}{\mu}\right) \dots\dots (V-3)$

The significance of this result lies in its implications on the heat- and mass-transfer analogy. Equation (V-1) implies that the modified Peclet number calculated from the values of the local effective conductivity is essentially identical with the theoretical ^(4,46) or mass transfer Peclet number ⁽⁶⁾ of about 11. This fact is considered to indicate that the turbulent-diffusion contribution to heat transfer at any radial position of the bed outside a 1/2-particle-diameter distance from the confining walls is governed by the "random walk" analogy, in spite of the presence of widely varying temperature gradients.

In comparison with the above result, the discussions in CHAPTER I. on the previous work may be recalled. A number of authors who studied an average effective conductivity have recognized in the past that the heat transfer Peclet number approached the value of 11 at high Reynolds number and at low values of d_p/D_t . With the local effective conductivity, however, the results ^(31,48) have shown that the Peclet number

varied significantly across the radius of a bed, and the values were usually far below 11, ranging between approximately 0.9 and 5.0 at the center of the bed. These authors⁽³¹⁾ suspected that the uncertain assumptions on the flow profiles may have influenced their results.

In contrast to these previous data, the present results were obtained by a technique which permitted the calculations of local effective conductivity without involving the flow profile. The consequent higher reliability of the data, therefore, is believed to have contributed to the regularity of the present results. Further, the consistency with which the present results were correlated in agreement with the "random walk" analogy seems to indicate that the Reynolds number used in the correlations was an appropriate one.

(2) Solid-fluid-solid Series Conduction Mechanism

In CHAPTER I, it was pointed out that Mechanism No. 4, or the solid-fluid-solid series conduction mechanism was a controversial issue relative to its dependence on the Reynolds number. Singer and Wilhelm⁽⁵¹⁾ concluded that this mechanism was significantly affected by the Reynolds number especially for high-conductive packing materials. Plautz and Johnstone⁽⁴⁴⁾ suspected that this mechanism might be responsible for as much

as 25% of the total increase in k_e caused by an increase in the flow rate. On the other hand, the results of a number of other authors such as Polack⁽⁴⁵⁾ and Yagi et al.⁽⁶⁴⁾ indicated no such conclusions.

In the present analyses, the answer to this question was sought through the following considerations:

- a) If this mechanism is truly affected by the flow rate to such an extent, then, the difference between an observed value of k_e and the static bed conductivity, k_B should be appreciably larger than would be expected from the "random walk" analogy alone. Therefore, the heat transfer Peclet number calculated from the difference between k_e and k_B should be smaller than its mass transfer counterpart.
- b) Since the solid-fluid-solid series conduction mechanism involves the solid conductivity, the departure of the heat transfer Peclet number from its mass transfer counterpart should be larger for higher-conductive packing materials.

When the results presented in Fig. (IV-1) through (IV-9) are scrutinized in the light of these considerations, it is evident that the heat transfer Peclet number overall is no

smaller than the theoretical value of 11, and there is no significant difference between the values of different packing materials. For these reasons, it is believed that the solid-fluid-solid series conduction mechanism is not noticeably affected by the Reynolds number and is essentially the same as in a static bed.

The above conclusion implies that the fluid in the channel between pellets is essentially in a laminar state regardless of the superficial mass flow rate, at least within the range covered in this work. This is reasonable if the channel between pellets is pictured as a capillary tube, and the Reynolds number based on the diameter of the capillary is considered to determine the heat transfer rate within the capillary.

From a detailed geometrical analysis of a packed bed, Ranz⁽⁴⁶⁾ concluded that the true flow velocity within the channel was approximately 10.7 times as large as the superficial velocity based on the empty column diameter. Since the area available for flow would be proportionally smaller, the sum of the cross-sectional areas of all the capillaries in a cross-section of the column would be 1/10.7 of the cross-sectional area of the column. Assuming the tetrahedral close-packing model, there are 2 capillaries for each particle

on the average, and the capillary-to-particle diameter ratio is then equal to the square root of $1/(9.7)(2)$, or 0.227. This means that the Reynolds number based on the capillary diameter and the actual flow velocity is approximately 2.43 times the value of the particle Reynolds number. The present investigation covered up to the particle Reynolds number of about 1300, and this makes the maximum capillary Reynolds number about 3200 at most. This figure indicates that the fluid in the capillary was mostly within a laminar or transitional region in agreement with the experimental conclusions. It may be added that this conclusion does not contradict the results of pressure drop measurement,⁽⁵⁾ where the pressure drop was found to cease being linear with the particle Reynolds number at the value of the latter as low as 40. It is believed that the pressure drop in a packed bed occurs mostly due to the contraction and expansion of fluid, which take place before and after each capillary channel. If so, it is possible to observe the pressure drop phenomena characteristic of a turbulent flow, and yet the flow within the channel between pellets is still essentially laminar.

The above experimental result, that Mechanism No. 4 under flow conditions is essentially the same as in a static bed, indicates that Mechanism No. 4 is essentially additive to Mechanism No. 1 and they do not overlap with each other as

was said to be possible in the discussions in CHAPTER I.

As for the possible overlapping between Mechanisms No. 2 and No. 4, further discussion is given later in this chapter.

(3) The Wall Effect

In CHAPTER I, it was pointed out that the wall effect has been handled empirically either by including it into an average effective conductivity or by postulating a hypothetical resistance at zero distance from the column wall. It was further mentioned that the former technique necessitated a family of curves or group of equations to present the data over a reasonable range of variables, while the latter method often produced quite irregular results.

In the present investigation, the physical meaning of the wall effect and a general rule to express the wall effect over a wide range of variables were sought through the measurement of local effective conductivity near the column wall.

The results so far discussed in the preceding sections were concerned with the interior of the bed, that is, anywhere within the bed outside a 1/2-particle-diameter distance from the column wall. It has been shown that the results were correlated by Equation (V-3) without any particular bias on

account of the radial position. This was taken to mean that the same mechanisms govern the heat transfer process at everywhere in the bed within the interior region. As for the region within a 1/2-particle-diameter distance from the column wall, on the other hand, a different situation has been revealed.

Figures (IV-10) through (IV-13), where the wall effective conductivity was plotted against the product of $(C_p \mu)$ and the particle Reynolds number, clearly demonstrate the difference. Unlike in the interior of the bed, the wall effective conductivity hardly increases as the Reynolds number becomes larger, and its magnitude is comparable with the static-bed conductivity in the interior of the bed. If the slopes of these curves are compared with the equivalent quantities in the interior of the bed, the former are about 1/10 of the latter, and this ratio is essentially common to all 4 packing materials. Thus, the results in these figures are satisfactorily represented by the following equations:

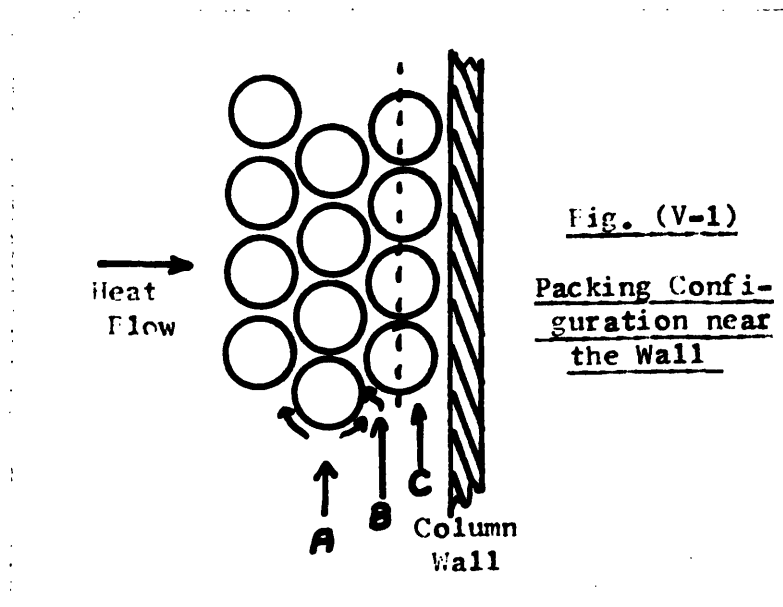
$$k'_e = k'_B + (0.01)(C_p \mu) \left(\frac{d_p G}{\mu} \right) \dots\dots\dots (V-4)$$

$$\frac{k'_e}{k_g} = \frac{k'_B}{k_g} + (0.01) \left(\frac{C_p \mu}{k_g} \right) \left(\frac{d_p G}{\mu} \right) \dots\dots\dots (V-5)$$

It is of interest to consider the physical significance of this result from the standpoint of the mechanics of the turbulent diffusion in packed beds. The so-called turbulent-diffusion in a packed bed is essentially the mechanical displacement of fluid parcels caused by the presence of discrete particles. When the passage of a fluid parcel is blocked by a particle, the fluid has no choice but to detour. In so doing, the fluid parcel would most likely split into smaller units and be displaced in all directions. Clearly, whichever offers the least resistance would be the most favored direction to move. When such a displacement happens to occur in parallel with the direction of heat transfer, a discrete unit of energy would be accordingly transported. If it is assumed that the displacement of fluid parcel is equally likely to occur in all directions, the probability of finding a particular fluid parcel at a particular radial position after a certain time lapse may be determined statistically. The results may then be converted into an equivalent diffusivity through Einstein's diffusion equation.^(4, 55) This type of mathematical treatment is what is known as the "random walk" analogy.

In spite of the presence of temperature and velocity gradients, the assumption of equal probability for all directions would be valid in the interior of the bed, because

the effect of small temperature and velocity differences across one particle would be insignificant in view of the ordinarily quite large momentum of fluid parcels. The result discussed earlier concerning the effective conductivity in the interior of the bed seems to support this point of view.



In the immediate vicinity of the column wall, however, the behavior of fluid parcels would not be the same as in the interior of the bed. Referring to Fig. (V-1), Fluid Parcel A would probably not feel the presence of the wall greatly and would split in all directions more or less with an equal probability. Fluid Parcel B, likewise, would not receive any direct influence of the wall and would be subject to practically the same torturous journey as Fluid Parcel A and

the intensity of the radial displacement would be about the same in both cases. As for Fluid Parcel C, clearly a different situation is expected. Firstly, as Roblee et al.⁽⁴⁷⁾ have found, the fraction void increases rapidly from a minimum value at 1/2-particle-diameter distance from the column wall to the value of unity at the surface of the wall. Therefore, Fluid Parcel C would find the journey much less torturous than either Fluid Parcel A or B, and the intensity of its radial displacement would be consequently much smaller. Secondly, the column wall poses as a permanent barrier to any fluid movement, and there is no traffic of fluid parcels across this barrier. Consequently, Fluid Parcel C would be more discouraged from moving toward the wall than if there were no wall. Thirdly, the large skin friction on the surface of the wall may develop a laminar boundary layer on the surface as was assumed by Yagi et al.⁽⁶⁴⁾ For these reasons, the turbulent-diffusion mechanism within a 1/2-particle-diameter distance from the wall would resemble more an ordinary tubular heat exchanger than the interior of a packed bed. Bernard and Wilhelm⁽⁶⁾ stated that the intensity of turbulence in a packed column is about 40%, whereas the same in an ordinary tube is only about 2.5--5.0%. Therefore, if the region within a 1/2-particle-diameter distance from the column wall is viewed as an ordinary tube, the transfer rate within this region should be only about 1/10 of that in the interior.

When the present experimental results are compared with the above physical picture, a close parallelism is evident. The experimental results showed a distinctive difference in the transfer rates between the two regions, within and without a $1/2$ -particle-diameter distance from the wall. Further, the experimental results indicated that the effective conductivity within a $1/2$ -particle-diameter distance was affected by the Reynolds number only about $1/10$ as much as in the interior of the bed, and this is in close agreement with the above physical picture. Therefore, it seems reasonable to consider that the so-called wall effect is satisfactorily explained by the above interpretations.

Equations (V-3) and (V-5) with the above physical interpretations can also satisfactorily explain the puzzling behavior of various previous data. The wall effect as observed by a group of authors such as Singer and Wilhelm⁽⁵¹⁾ was found more conspicuously at high Reynolds number and large d_p/D_t . It is clear from the above two equations that the effective conductivity in the interior of the bed is closer to the wall effective conductivity at low Reynolds number than at high values. As the Reynolds number is increased and the difference between the two regions is consequently increased, the wall effect should become more apparent, and this phenomenon would be further magnified with larger particles near the wall.

The reason why the experimental values of h_w were often found to be so irregular can be also explained. The two effective conductivities as expressed by Equations (V-3) and (V-5) are nearly equal at low Reynolds numbers, and therefore, a single value of average effective conductivity used for an entire bed would cause only an insignificant discrepancy. Therefore, h_w would be either infinite or very large at low Reynolds numbers. As the Reynolds number is increased, however, the difference in the effective conductivities would increase, and a single value of average effective conductivity would cause appreciable discrepancies when applied to an entire bed. Therefore, h_w would become smaller with increasing Reynolds number. As the Reynolds number is further increased, however, the effective conductivity in the interior of the bed would become so large, and the whole transfer process would be controlled by Equation (V-5). Then, the increase in the wall effective conductivity with increasing Reynolds number would be reflected on the magnitude of h_w , and it would become larger with increasing Reynolds number. Because of these ups and downs of h_w , the experimental data often appeared quite irregular to "straight-line-happy" chemical engineers.

(4) Comparison with Previous Expressions of Wall Effect

The overall results so far discussed in this chapter have been incorporated in two single equations, Equation (V-3) and Equation (V-5). The generality and versatility of these

equations can be best tested by demonstrating whether or not they are capable of reproducing a variety of previous data in which the wall effect was included in a number of different ways. The following comparisons were made for a cylindrical packed bed of 1/8-inch-diameter alumina balls flowed with air at an average bed temperature of 200 °F. These conditions were chosen because they were most frequently used in the previous investigations.

a) Singer and Wilhelm's Correlation

These authors⁽⁵¹⁾ studied an average effective conductivity and presented the results in terms of a modified Peclet number. The results showed that the Peclet number varied widely depending on the Reynolds number and d_p/D_t ratio. Equation (V-3) and Equation (V-5) were suitably transformed to calculate the same type of average effective conductivity as these authors obtained, and the results were compared in Fig. (V-2). (see APPENDIX VI for the derivation.)

The agreement is remarkable particularly at Reynolds number larger than 1000. At the Reynolds number of 500, however, some discrepancy exists. Recalling the discussions in CHAPTER I, Singer and Wilhelm correlated the data obtained from the experiments where air flowed downward while being heated. The possible presence of natural convection in the

opposite direction to the bulk flow may have influenced the data at low values of the Reynolds number and high values of d_p/D_t . The trend of discrepancy in Fig. (V-2) is in agreement with this explanation.

b) Vershoor and Schuit's Correlation

These authors⁽⁵⁴⁾ studied the same type of average effective conductivity as Singer and Wilhelm's, and correlated their data by Equation (I-10). The values obtained from their correlation are compared in Fig. (V-3) with the ones calculated through Equations (V-3) and (V-5). (see APPENDIX VI for the calculations.) The agreement is considered good.

c) Leva's Correlation

Leva and coworkers^(32,33,34) experimentally measured a mean heat transfer coefficient, h_o of packed tubes and correlated their data by a number of different equations depending on the experimental conditions and variable ranges used. In their experiment, air was invariably flowed downward either being heated or cooled. In order to avoid the possible influence of natural convection that might have affected their experiments of heating the air, the correlation for cooling the air was preferentially used for the present comparison. The values calculated from Equation (I-6) were compared in

Fig. (V-4) with the equivalent values calculated through Equations (V-3) and (V-5). (see APPENDIX VI for the details.)

Considering the large differences between the experimental methods, the agreement is considered good.

d) Yagi and Wakao's Correlation

As mentioned in CHAPTER I, a group of authors based their studies on the assumption that a finite resistance exists at zero distance from the column wall but otherwise a single effective conductivity is valid for the entire bed. Thus, these authors postulated a wall coefficient, h_w to account for the assumed resistance. Yagi and Wakao^(63,64) are of this type. These authors experimentally determined the values of h_w and correlated them by

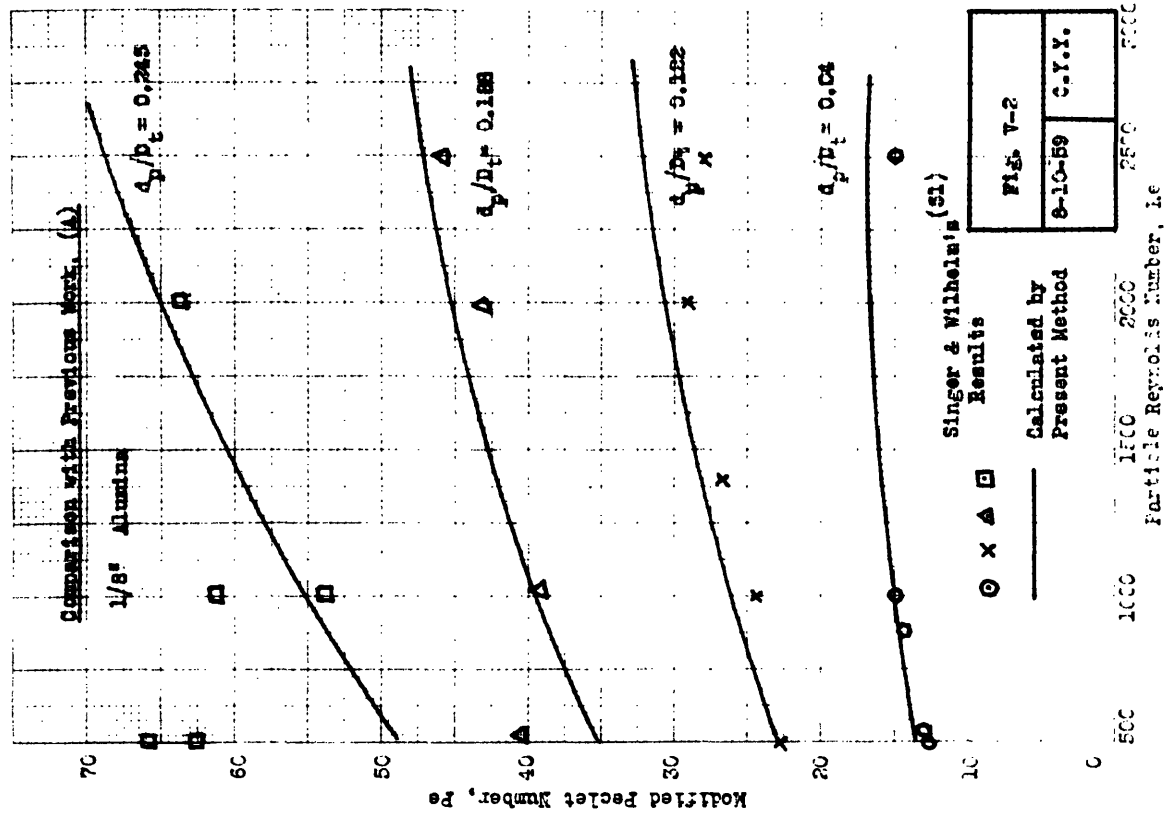
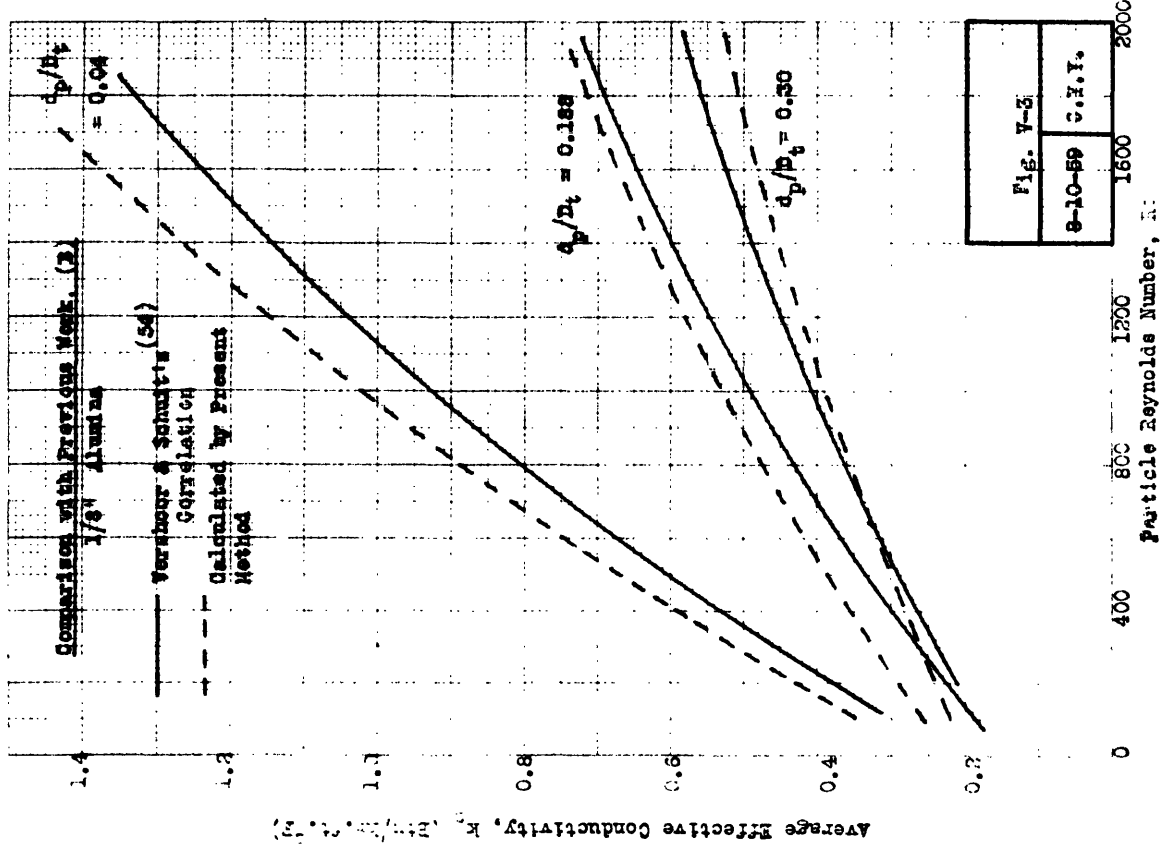
$$j = \left(\frac{h_w}{C_p G_o} \right) \left(\frac{C_p \mu}{k_g} \right)^{2/3} = 0.20 \left(\frac{d_p G_o}{\mu} \right)^{-0.20} \dots (I-17)$$

Under the physical picture of the wall effect as proposed in the present study, the wall coefficient, h_w is purely hypothetical. Nevertheless, it is possible to calculate the values which are equivalent to them through Equations (V-3) and (V-5). These were compared in Fig. (V-5) with the calculated values from Yagi's correlation.

Considering the extreme sensitivity of h_w to small errors, the agreement is good at high Reynolds number. As the Reynolds

approaches zero, however, the discrepancy becomes significant. Yagi's equation states that the wall coefficient should approach zero as the Reynolds number approaches zero. Considering the fact that a static bed does have a finite effective conductivity, and sometimes a quite significant one at that, it is difficult to see how h_w could possibly approach zero near a static condition. In a static bed, the conditions in the interior of the bed are believed to be more nearly like those in the vicinity of the wall than in a dynamic bed, and therefore, h_w could at times approach infinite if the bed conditions were ideally uniform. Recalling the discussion in CHAPTER I concerning Yagi's correlation, Equation (I-17) is suspected to reflect their concept of h_w , whereby it was treated as a film coefficient. As mentioned in the preceding section, a laminar boundary layer may develop on the column wall, but h_w would not be the measure of it. A film coefficient which represents the laminar boundary layer should indeed approach zero as the Reynolds number approaches zero. However, by definition, h_w is not a film coefficient, and its distinction becomes more striking as the Reynolds number decreases. This is considered to be an explanation for the discrepancy which exists in Fig. (V-5) at low Reynolds number.

The overall results of the comparisons with the above 4 different types of previous data are considered excellent.



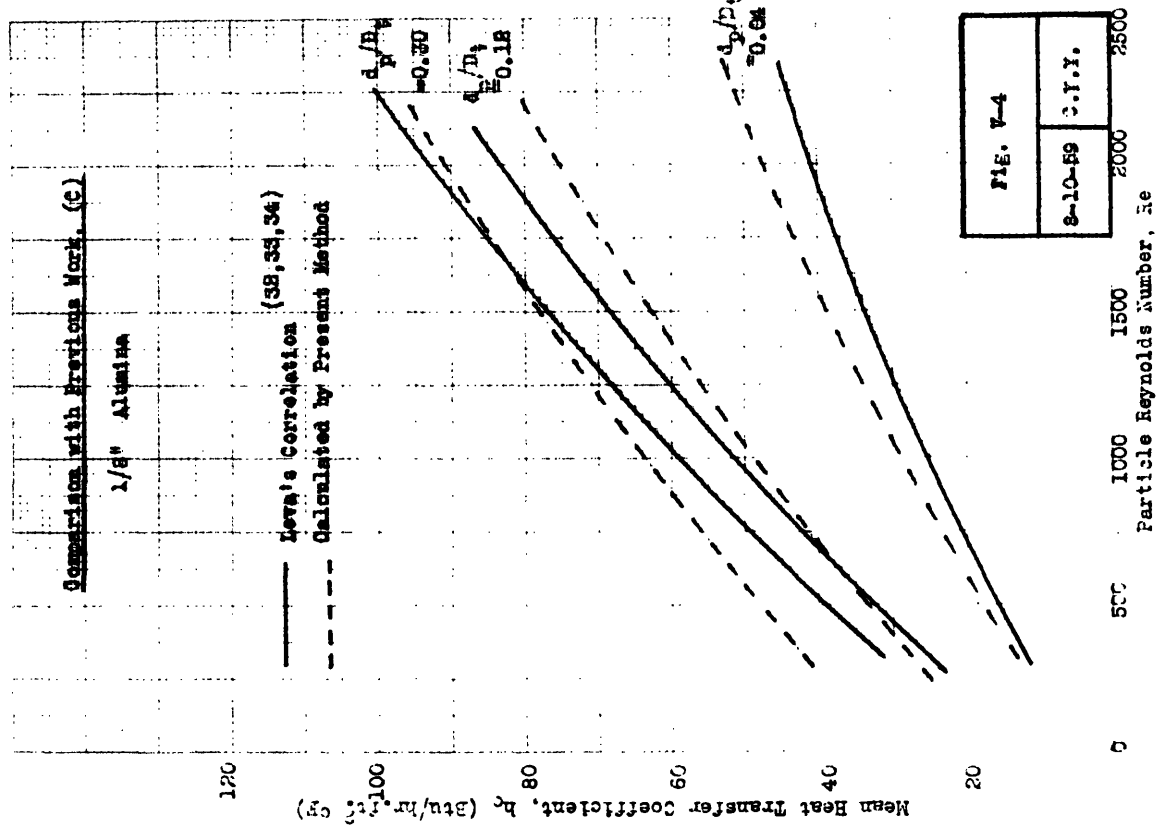


Fig. V-4
 8-10-59 C.Y.Y.

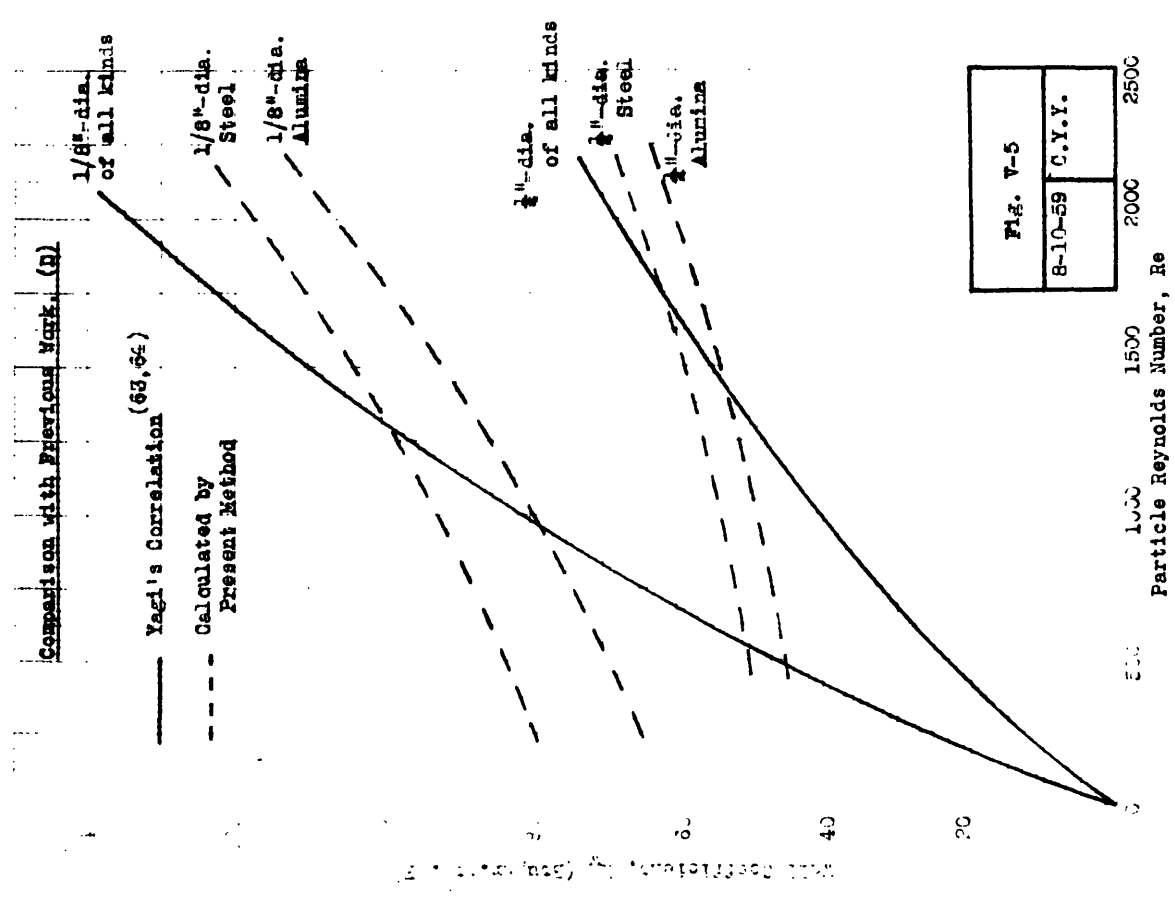


Fig. V-5
 8-10-59 C.Y.Y.

The fact that one single general rule expressed by Equation (V-5) can adequately replace the various types of previous correlations covering d_p/D_t ratio as large as 0.3 is believed to verify the correctness of its form as a general expression of the so-called wall effect.

(5) Static-bed Conductivity

Equations (V-3) and (V-5), which together generalize the heat transfer mechanisms in a packed bed, both involve a static-bed conductivity in their expressions. Therefore, a comparable significance must be attached to the heat transfer mechanisms which constitute the static-bed conductivity.

Recalling the discussions in CHAPTER I, the static-bed conductivity depends on 4 different mechanisms. These are Mechanism No. 2, or the molecular conduction in the fluid phase, Mechanism No. 3, the solid-solid conduction through the points of contact, Mechanism No. 4, or the solid-fluid-solid series conduction, and Mechanism No. 5, or thermal radiation. The experimental results on the static-bed conductivity presented in Fig. (IV-14) through (IV-19) all involve these 4 mechanisms.

As mentioned in CHAPTER I, a previous investigation has adequately demonstrated the insignificance of Mechanism No. 3. (30)

Referring to Figures (IV-14) through (IV-19), less than a 3-fold difference has been observed in the values of k_B at 100 °F between the materials covering as much as a 300-fold difference in the solid conductivities. Therefore, even if the total difference in k_B at 100 °F between the highest- and lowest-conductive materials were wholly attributed to the contact-point conduction mechanism, a simple calculation shows that less than a 2% error would be introduced in the value of k_B of alumina by neglecting this mechanism. Clearly, the contact-point conduction can not be wholly responsible for the differences in k_B between different materials, and the error which would arise from its neglect would be far smaller than the above value. Therefore, the present results are considered to be essentially in agreement with the conclusions of previous investigators. (29,30)

If Mechanism No. 3 is thus neglected and Mechanism No. 2 is disregarded for a moment, Mechanisms No. 4 and No. 5 are the remaining ones which are potentially non-additive to each other and to others. Beside being potentially non-additive, the radiation mechanism has a unique feature which could even more complicate the situation. Unlike other heat transfer mechanisms, the radiant heat transfer is expressed by

$$q = (C)(T_1^4 - T_2^4) \dots\dots\dots (V-6)$$

where C is a proportionality constant. To conform with the concept of effective conductivity, the above equation needs to be transformed into

$$q = (C)(T_1^3 + T_1^2 T_2 + T_1 T_2^2 + T_2^3)(\Delta x) \frac{\Delta T}{\Delta x} \dots\dots\dots (V-7)$$

where the quantity inside the large bracket is defined as a radiation conductivity, k_r . Or

$$k_r = (C)(T_1^3 + T_1^2 T_2 + T_1 T_2^2 + T_2^3)(\Delta x) \dots(V-8)$$

Clearly, this conductivity, k_r is a function of terminal temperatures as well as the local conditions, whereas other conductivities such as k_g or k_s are variables of local conditions only. If the dependence of k_r on terminal temperatures is an important one, Mechanism No. 5 would be not only non-additive but also a function of all the environment which participates in the determination of the terminal temperatures. If this is the case, it would be extremely difficult to handle the radiation contribution.

Whether k_r is significantly influenced by the terminal temperatures or not was examined in the present study by observing the static-bed conductivity at a fixed temperature level but at several different temperature gradients.

In Fig. (IV-14) through (IV-19), the observed values of k_B were plotted against the local temperature levels. The

observations were made at various temperature gradients differing up to 4 fold. The fact that the experimental points showed no biased deviations on account of the temperature gradient, plus the fact that several observations at the same temperature level but at different temperature gradients coincided in most cases, are considered to indicate the negligible influence of the terminal temperatures on the values of k_r . This experimental fact is not surprising, if it is remembered that the radiation path length between particles is a very small one and T_1 is usually close enough to T_2 in Equation (V-8). This would make k_r approximately equal to

$$k_r = (C)(4)(T^3)(\Delta x) \dots\dots\dots (V-9)$$

where T is a mean value of T_1 and T_2 . Therefore, it is considered reasonable to treat Mechanism No. 5 like the others as a function of the local conditions only, such as the local temperature level and other usual variables.

(6) General Correlations for Mechanisms No. 4 and No. 5

The experimental results on the static-bed conductivity have so far shown that Mechanism No. 3 is essentially negligible and Mechanism No. 5 is practically a function of the local conditions only. The remaining problems are now the question

of non-additivity between Mechanisms No. 4 and No. 5, and development of general correlations of these mechanisms.

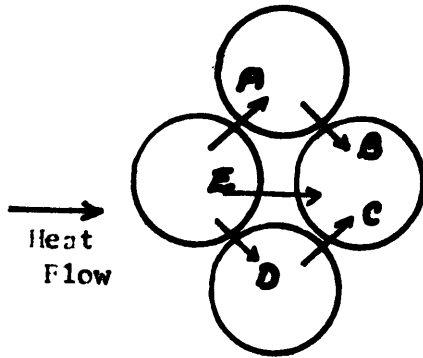


Fig. (V-6)
Magnified View of
Packed Bed

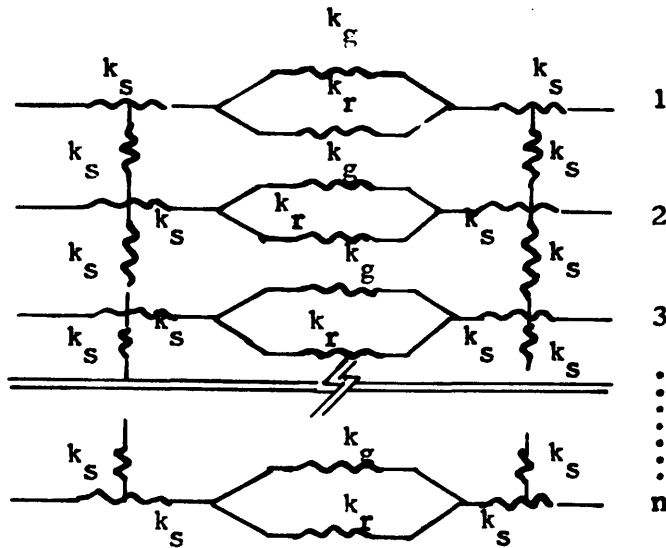
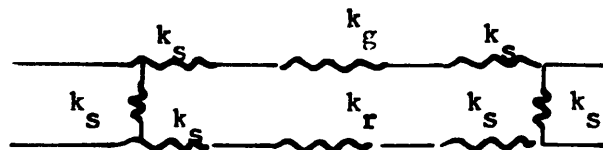
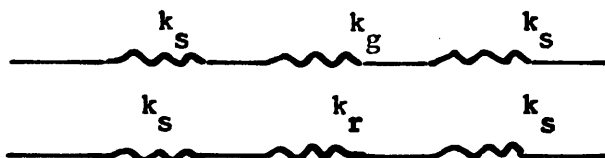


Fig. (V-7)
Electric Analog
of Static Bed
Conductivity

(Analog A)



(Analog B)



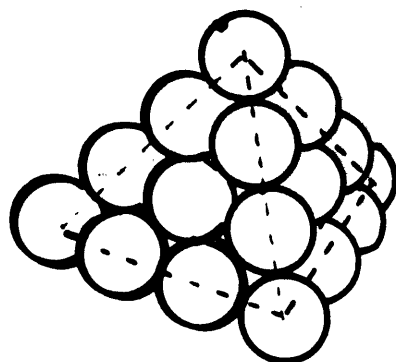
(Analog C)

The schematic diagram in Fig. (V-6) is a magnified view of a portion of a packed bed. In this figure, heat is shown to be transferred from one solid surface to another by the gas phase molecular conduction and radiation. The relative proportion of these two mechanisms, which are both in series with the solid conductivity, should vary from point to point throughout the surface of a pellet. This condition is expressed in terms of an electric analog by Analog A in Fig. (V-7). Now, confining attention to the solid-gas-solid paths, the conductivity of the gas generally controls this process, and therefore, the most favorable heat transfer paths would be where the void space is narrowest, such as Paths A, B, C, and D in Fig. (V-6). If the void distance is as large as in Path E, the amount of heat transferred by conduction would be relatively small. On the other hand, the radiation takes place approximately according to Equations (V-7) and (V-9). All other conditions remaining same, the amount of radiant energy transferred would be proportional to Δx or the distance between the terminals. Therefore, the radiant energy transfer would rapidly approach a negligible value where the solid surfaces are close together, such as in Paths A, B, C, and D in Fig. (V-6). Path E, on the other hand, would be the most favorable one. In other words, the void space may be quite approximately divided into

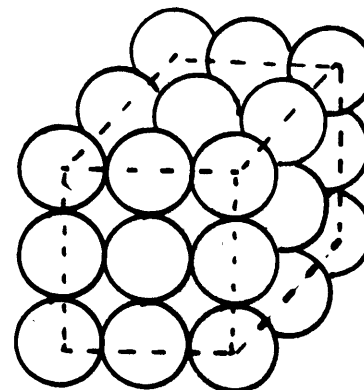
two regions, one where the gas molecular conduction is the principal mechanism and the other where radiation is the main mode of transfer. This condition is shown by Analog B in Fig. (V-7). Needless to say, the relative proportion of these two regions would be dependent on the temperature level, gas conductivity, emissivity, and so on. However, such a rigorous treatment would only make the problem unwieldy with relatively small benefit.

In Analog B in Fig. (V-7), the gas conductivity and radiation conductivity are in series with solid conductivity, and they are interlocked by the intra-particle conduction. Clearly, the difficulty involved in handling the intra-particle conduction is enormous, and it is desirable to neglect it. Where the solid conductivity, k_s is much larger than either k_g or k_r , this neglect would be quite reasonable. With this assumption, the electric analog in Fig. (V-7) is reduced from Analog B to Analog C. In other words, Mechanisms No. 4 and No. 5 are reduced to a pair of additive mechanisms. Further analyses in the present work were based on this assumption.

An aggregate of packed particles fused together from an accidental overheating was carefully observed of its geometric arrangement. As the result, the tetrahedral close-packing model was found to be the closest approximation to the true packing array, and subsequent theoretical analyses were based on this model. (see Fig. V-8).



Tetrahedral Model



Rectangular Model

Fig. (V-8)

Theoretical Model of Packing Arrangement

Heat was assumed to travel through the tetrahedral array in the radial direction only. In other words, this packing model was hypothetically divided into numerous parallel heat transfer paths, each having a differential quantity of heat transfer area and a series of solid and fluid segments occurring in a particular proportion. Through extensive numerical integrations, the amount of heat traveling through each of these paths was summed up over a unit area of the packed bed, and the result was expressed in terms of dimensionless groups, $(k_{B_c})/k_s$ vs. k_g/k_s , where (k_{B_c}) is the static-bed conductivity due to the conduction only. The integration was performed over the whole unit area of the packed bed, and it included also those paths where the solid phase was not involved and the molecular conduction in the fluid phase was the only transfer mechanism. This means that Mechanism No. 2, or the molecular conduction in the fluid phase was automatically incorporated in the obtained correlation. The details of the integrations are described in APPENDIX IV, and the obtained

correlation is represented in Fig. (V-9) by the top curve.

At this point, the relation between Mechanisms No. 2 and No. 4 needs to be clarified. Recalling the discussions in CHAPTER I, the "ferry-boat service" for Mechanism No. 4 was said to be provided by the transfer mechanisms in the fluid phase, namely, Mechanisms No. 1 and No. 2. Subsequent experimental results showed that Mechanism No. 4 was practically independent of the Reynolds number, meaning that Mechanism No. 1 did not participate in the "ferry-boat" function. Therefore, it was concluded that Mechanism No. 1 was additive to Mechanism No. 4 as well as to all other mechanisms. The above result indicates that the "ferry-boat service" is handled exclusively by Mechanism No. 2, or the molecular conduction in the fluid phase. Again recalling the discussion in CHAPTER I, Mechanism No. 2 has been found to be satisfactorily expressed by Equation (I-29), if it existed alone. When Mechanism No. 2 coexists in a system with Mechanism No. 4, these two mechanisms would overlap with each other, and Equation (I-29) would no longer be valid. Therefore, if a system involves both Mechanisms No. 2 and No. 4, it is best to incorporate them into a single correlation as was done in the above. If a system lacks Mechanism No. 4, as will be illustrated later, Mechanism No. 2 is believed to be represented by Equation (I-29), and is additive to all other mechanisms.

The top curve in Fig. (V-9) was found to coincide within about 15% with the empirical curve of Polack,⁽⁴⁵⁾ which was obtained through measurement of the static-bed conductivity at low temperature levels. Further, comparison with the present data (see Tables A1-17 through A1-22) shows that as the temperature level becomes lower, that is, as the radiation contribution becomes smaller, the experimental values of k_B approach closer to the theoretical values of $(k_B)_c$ predicted from Fig. (V-9), and their difference is reduced to an average 25% of the observed k_B at around 200 °F. This difference, of course, is mostly due to the radiation contribution and partially due to the ordinary experimental uncertainties. For the above reasons, the derived correlation is considered to be a satisfactory expression of Mechanisms No. 4 and No. 2 inclusive.

Assuming the additivity between Mechanisms No. 4 and No. 5, and using the above theoretical correlation for Mechanism No. 4 (plus No. 2), the static-bed conductivity due to the radiation contribution, $(k_B)_r$ was obtained by subtracting the value of $(k_B)_c$ from the observed value of k_B .

Recalling the discussions in CHAPTER I, Damköhler presented Equation (I-30) for an estimation of the radiation contribution.

He suggested that k_r calculated from Equation (I-30) was directly equivalent to the radiation contribution, or

$$(k_B)_r = k_r \dots\dots\dots(V-10)$$

where

$$k_r = (0.173)(\epsilon)(s)(\delta)(d_p)(4T^3/10^8)$$

s; proportionality constant, and was taken as 1 in this work

Damköhler's formular implies that the amount of radiation contribution is independent of the solid conductivity, and is equal for all materials of the same diameter and at the same average bed temperature. However, if the radiant energy is considered as something which links one solid to another, the solid conductivity should be involved as in Fig. (V-6) and (V-7). If so, the relation between $(k_B)_r$ and k_r would be approximately given by

$$(k_B)_r = \sum_{n=1}^n \left(\frac{C_n}{\frac{A_n}{k_s} + \frac{B_n}{k_r}} \right) \dots\dots(V-11)$$

A_n, B_n, C_n : constants

or,

$$\frac{(k_B)_r}{k_s} = \phi \left(\frac{k_r}{k_s} \right) \dots\dots\dots(V-12)$$

where ϕ is a functional form. A direct way of determining the true functional relationship is to plot $(k_B)_r/k_s$ against k_r/k_s on a log-log scale. If $(k_B)_r$ should indeed be directly equal or proportional to k_r as in Equation (V-10), a straight line with a slope of unity would be obtained. Otherwise, the slope would be different from unity.

Fig. (V-10) was prepared by the above technique from all the experimental values obtained in the present study. In spite of the scattering of points, the trend is clear that they are clustered around the indicated curve. This scattering might at first sight look appreciable, but if it is remembered that $(k_B)_r$ is a difference between a value and another value of comparable magnitude, its high sensitivity to small errors may be appreciated.

From Fig. (V-10), it is clear that the solid conductivity does indeed influence the radiation contribution as had been suspected, and the curve in the figure seems to be the general expression of the functional relationship. The generality of this empirical correlation can be best tested by demonstrating how closely the curves in Fig. (V-9) and (V-10) can reproduce experimental values of k_B . The calculated values obtained through these proposed correlations were indicated by the dashed lines in Fig. (IV-14) through (IV-19). It is seen that the agreement is reasonable for steel, alumina, and glass packing materials, but rather poor for aluminum balls. The precise cause for this deviation of aluminum balls is a matter of speculation, but the combination of the following reasons is considered mainly responsible: (1) Aluminum has a melting point of 1140 °F, and the material becomes considerably softer at relatively low temperature. Already around 700 to 800 °F,

the balls were often found fused together in the bed. When this occurs, the balls can no longer be considered as in a point contact, and the solid-solid conduction should increase rapidly on account of the extremely high solid conductivity of the material; (2) The aluminum balls used in the present study had much smoother surfaces than the other materials, and the reflection of radiant energy may have taken place specularly. This would have caused an effective increase in the view factor and consequently a larger amount of radiant heat transfer. The discrepancy between the experimental and calculated values were found in exactly the same manner as these explanations would have predicted.

Although the deviation is greater for the aluminum balls, relative to the other packing materials, the agreement is nevertheless reasonable especially up to 500 °F, with less than a 20% error. This is not particularly large, if all the various simplifying assumptions are taken into account.

As a further test of these correlations, some previous data involving such widely varying conditions as vacuum, helium-, and SO₂-atmosphere were compared with the values calculated through these correlations. They were also compared with the values calculated through Argo and Smith's theoretical correlation.⁽²⁾ The comparisons appear in Fig. (V-11) through (V-13). Considering the complexity of the problem and all the simplifying

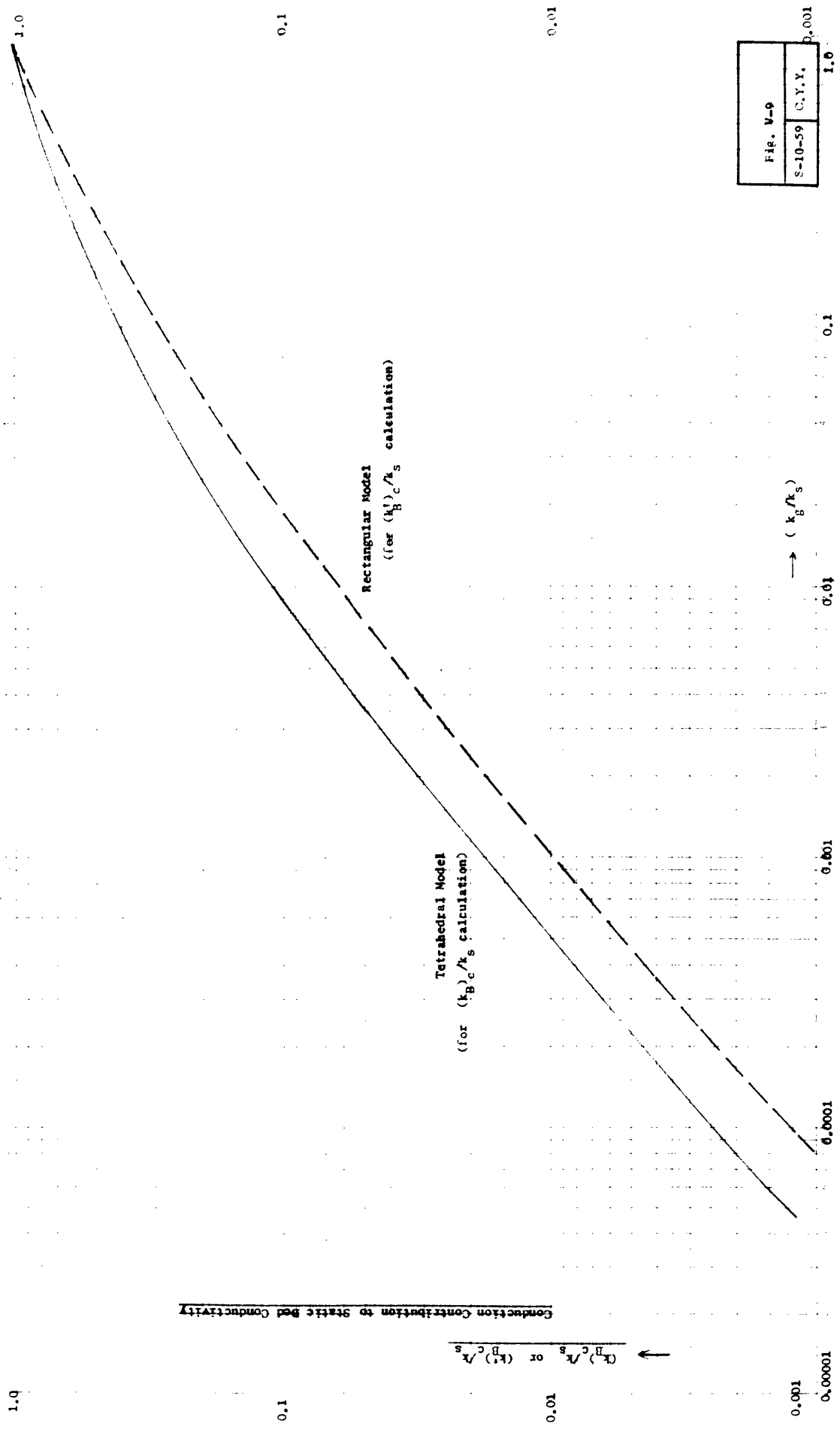
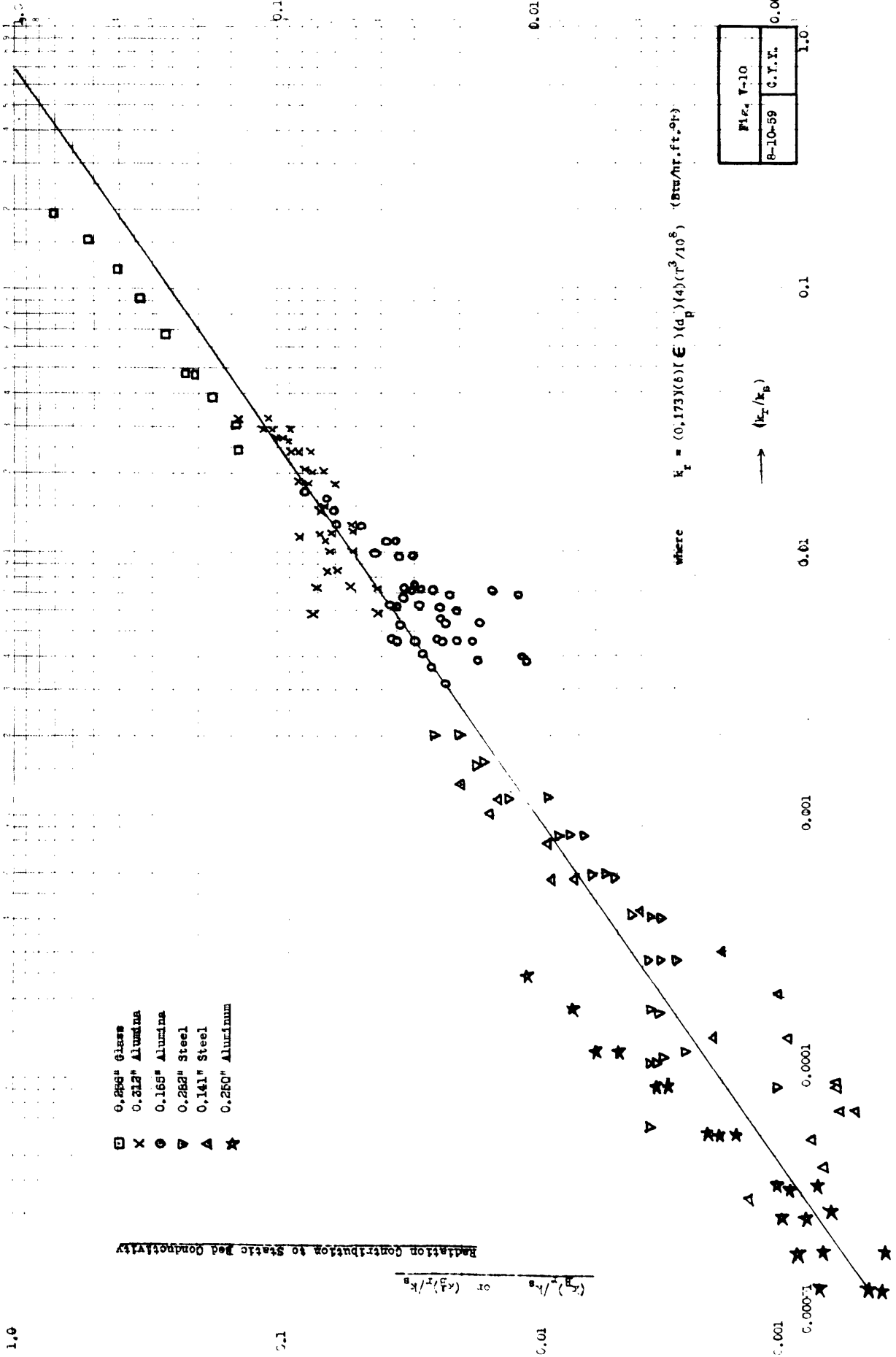


Fig. V-9	
S-10-59	C.Y.Y.



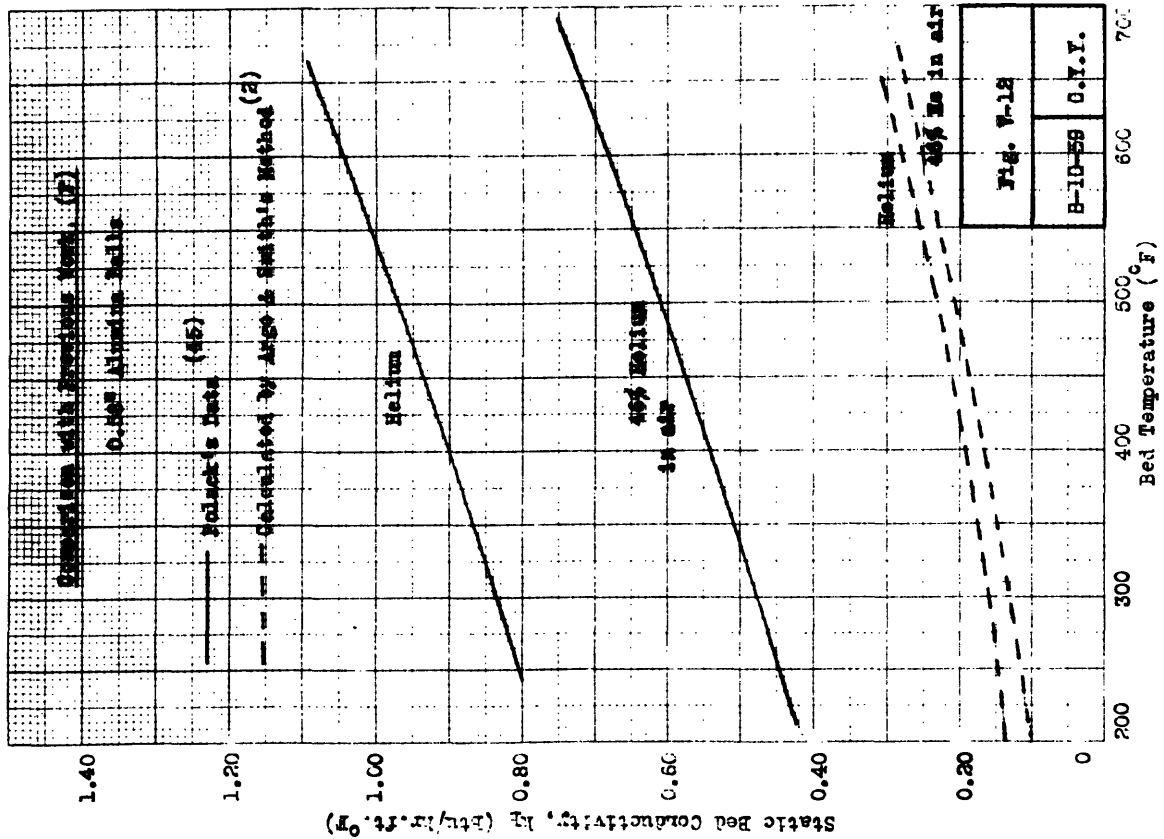
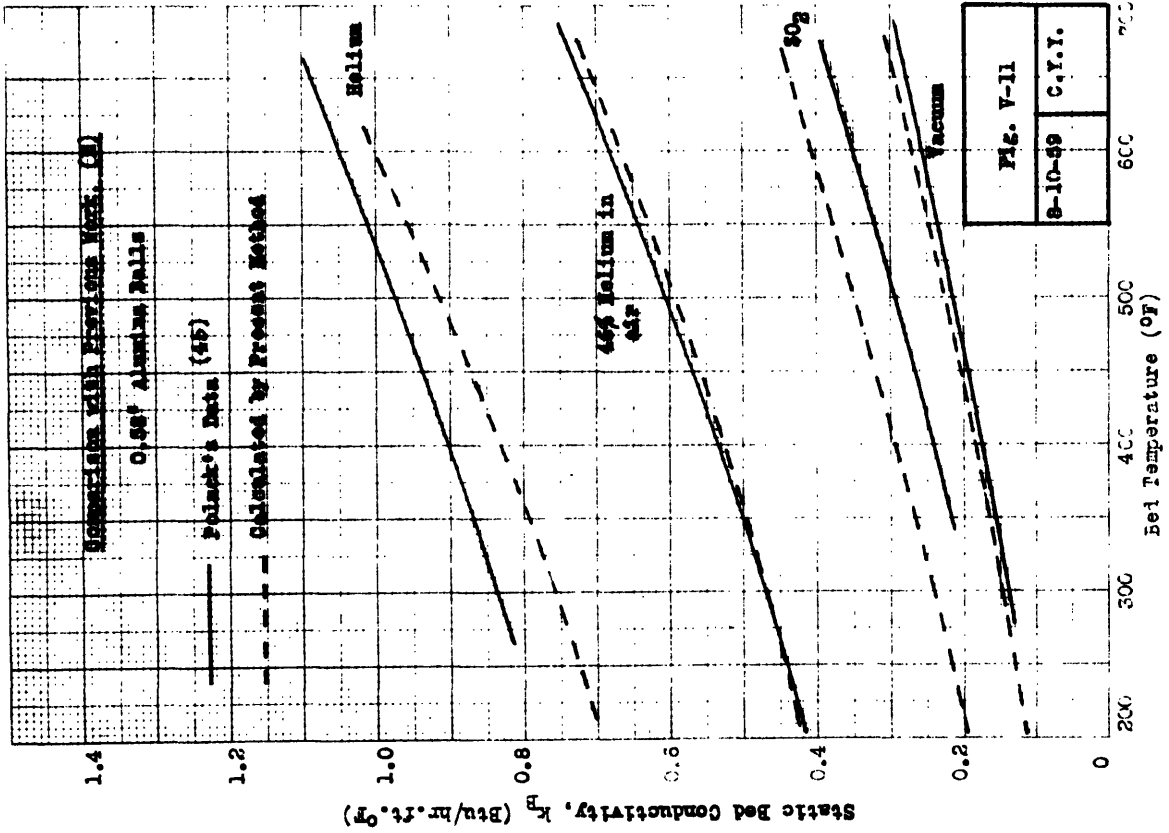
Radiation Contribution to Static Bed Conductivity

- 0.250" Glass
- X 0.312" Alumina
- 0.165" Alumina
- ▽ 0.283" Steel
- △ 0.141" Steel
- ★ 0.250" Aluminum

where $k_r = (0.173)(\delta T)(\epsilon)(d_p)^3(\rho_p)^3(r/10^6)^3(\delta T/10^3)^3$ (Btu/hr.ft.²)

Fig. 4, V-10	1.0
8-10-59	C.I.F.

→ (k_r/k_s)



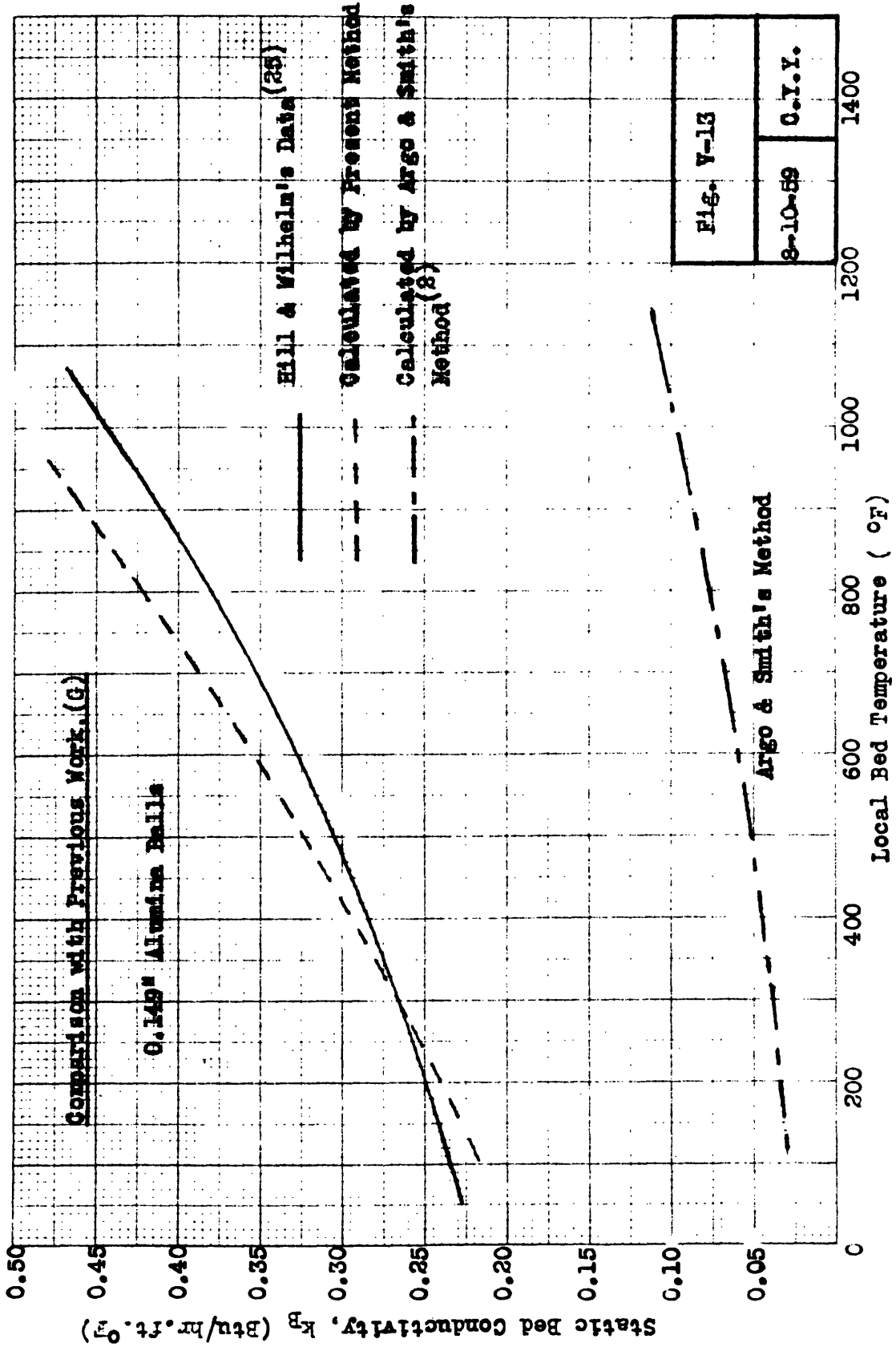


Fig. V-13
 8-10-59 O.Y.Y.

assumptions which were necessary to obtain these correlations, the agreement is believed rather remarkable.

The above results of various comparisons indicate that the proposed correlations which appear in Fig. (V-9) and (V-10) are satisfactory for their purpose.

(6) The Static-bed Conductivity near the Wall

The same basic principles, which were discussed relative to the static-bed conductivity in the interior of the bed, should also govern the static-bed conductivity within a 1/2-particle-diameter interval from the column wall. Thus, Mechanisms No. 2, No. 3, No. 4, and No. 5 are believed to constitute the static-bed conductivity near the wall.

However, because of a slight difference in the packing configurations between the interior of the bed and near the wall, a few modifications are in order. Referring to Fig. (V-1), the packing configuration right next to the wall is somewhat similar to a single layer of balls closely packed on a plane. In other words, the packing model closely resembles the rectangular close-packing array illustrated in Fig. (V-8). Based on this rectangular model, and by exactly the same technique as was used for the tetrahedral model, a theoretical correlation was obtained to express the magnitude of the conduction contribution to the wall static-bed conductivity.

As in the case of the tetrahedral model, this theoretical correlation based on the rectangular model includes both Mechanisms No. 2 and No. 4. The details of the derivations are included in APPENDIX IV, and the obtained correlation is presented in Fig. (V-9) by the bottom curve. So, the two curves in Fig. (V-9) are analogous in principles and purposes, but the top one is for the interior of the bed, whereas the bottom one is for the 1/2-particle-diameter interval from the wall.

As for the radiation contribution near the wall, no separate correlation was obtained, but instead, the same curve in Fig. (V-10) was found to be approximately applicable to this region, if the void fraction, δ is taken as one. This is reasonable because every point of the particle surface within this region can "see" the heat sink, or the column wall.

The values of k'_B calculated by the above technique are compared in the following table with the experimental values:

Table (V-1)

Experimental and Calculated Values of k'_B

<u>packing material</u>	<u>0.282-inch Steel</u>	<u>0.141-inch Steel</u>	<u>0.312-inch Alumina</u>	<u>0.165-inch Alumina</u>
$(k'_B)_{\text{exp.}}$	0.27	0.22	0.27	0.17
$(k'_B)_{\text{cal.}}$	0.23 (0.15)* (0.08)**	0.20 (0.16)* (0.04)**	0.22 (0.11)* (0.11)**	0.16 (0.10)* (0.06)**

where * (k'_{Bc}) and ** (k'_{Br})

The agreement is considered satisfactory for all the packing materials.

As mentioned previously, the wall effect is something which becomes conspicuous due to the difference in the conductivities between the interior of the bed and the near-wall region, and this relative magnitude is what determines its observable effect. For this reason, the wall effect has been found to be important only at large values of the Reynolds number. But at high Reynolds numbers, the effective conductivity in the interior of the bed is so much greater than the value of k'_B , that even a fairly significant percentage error in the latter would reflect but little on the actual observable effects. For this reason, the curve in Fig. (V-10) used with a proper δ should provide a satisfactory estimation of the static-bed conductivity near the wall. However, in the cases where either a high accuracy is demanded or the wall temperature level is considerably high, the estimation of k'_B should take into consideration the difference in the packing configurations between the interior of the bed and the near-wall region, and the difference in the total emissivities between the wall and the packed solids. In the present study, the wall temperature varied only within a limited range, and more rigorous analyses on the radiation contribution in the near-wall region were not carried out.

(8) Cases Where Solid and Fluid Temperatures Are Significantly Different from Each Other

All the materials so far presented have been discussed in terms of a packed bed where the temperatures of the solid and fluid phases are almost equal at every position in the bed. In practical applications of fixed beds, this ideal situation does not necessarily occur, and the temperatures of the two phases may significantly differ from each other. The question is then what type of effective conductivity may be used, and how the information so far obtained can be applied to such cases. It is precisely at this point that the full value of the "cookbook technique" mentioned in CHAPTER I is duly appreciated. The recipes are as follows:

If the temperature profiles of the two phases are significantly different from each other, a single energy balance is not sufficient to describe such a system completely, and two simultaneous equations such as Equations (I-2) and (I-3) are needed. These in turn require a separate postulation of the solid phase effective conductivity, K_s and the fluid phase effective conductivity, K_g . So, now the problem is how to calculate these two conductivities.

Mechanisms No. 1 and No. 2 are able to transfer heat due to the presence of a temperature gradient in the fluid phase. Once the temperature gradient is fixed, these mechanisms should

function in exactly the same manner, regardless of what is going on at the solid. Of course, the temperature gradient is dependent on what is going on at the solid, but this is accounted for by the energy balance equation and not by the effective conductivity. Therefore, K_g is simply the sum of the contributions of these two mechanisms, or

$$\frac{K_g}{k_g} = (1/11) \left(\frac{C_p \mu}{k_g} \right) \left(\frac{d_p G}{\mu} \right) + (\delta)^{1.3} \dots (V-13)$$

for the interior of the bed, and

$$\frac{K_g^*}{k_g} = (0.01) \left(\frac{C_p \mu}{k_g} \right) \left(\frac{d_p G}{\mu} \right) + (\delta)^{1.3} \dots (V-14)$$

for the 1/2-particle-diameter interval from the wall.

In these equations, $(k_g)(\delta)^{1.3}$ represents the contribution of Mechanism No. 2 (see Equation I-29), and it is additive in this case because, as will be shown later, Mechanism No. 4 does not coexist with Mechanism No. 2 in the system. Since Equation (I-29) was obtained from experiments which involved the whole bed, the result may not be rigorously correct if applied to a 1/2-particle-diameter interval from the column wall as was done in Equation (V-14). However, the magnitude of this contribution is ordinarily much smaller than the first term at reasonably high Reynolds numbers, and a slight error introduced from using Equation (I-29) for this region may be considered negligible.

As for the solid phase effective conductivity, both Mechanisms No. 3 and No. 5 should function independent of the fluid phase according to the inter-particle temperature gradient, which is, in this case, not identical with the fluid temperature profile. Rigorously speaking, however, these mechanisms should be a mild function of what is going on in the fluid phase, because, even with a given inter-particle temperature gradient, the intra-particle temperature gradient would be affected slightly by the overall transfer processes including those in the fluid phase. However, the neglect of such a complex factor is highly desirable, and it would probably make only a minor difference.

This leaves only Mechanism No. 4 to be considered. This mechanism represents the solid-fluid-solid series conduction and is able to function only with the aid of the fluid phase. If heat is to travel from Particle A to its neighboring Particle B through the fluid phase between them, the fluid temperature must be lower than that of Particle A but higher than that of B. This necessary condition is satisfied only if the inter-particle temperature profile at least nearly coincides with the overall fluid phase temperature profile, as shown in Fig. (V-14), where the heavy line represents the fluid phase temperature gradient, and the line-segments in the circles indicate the intra-particle temperature profiles.

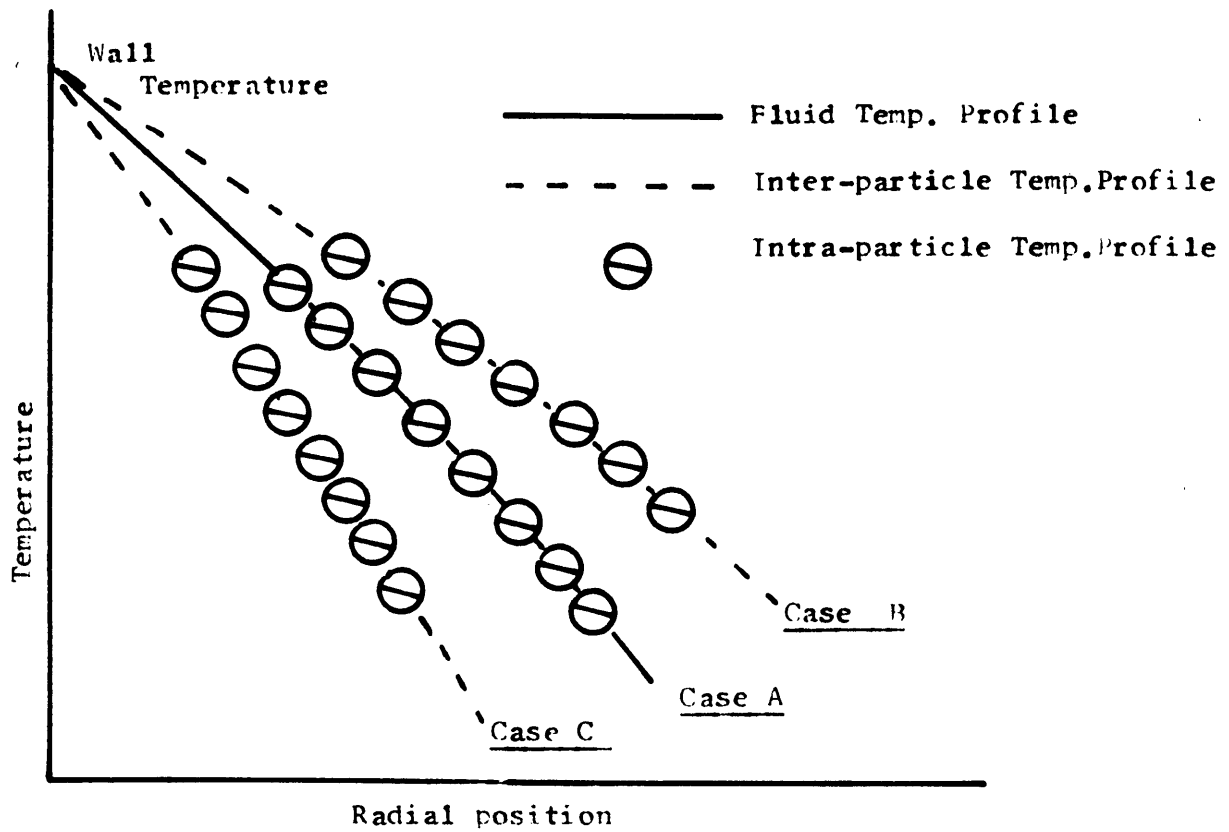


Fig. (V-14)

Solid-, and Fluid-temperature Profiles
under Various Circumstances

Owing to chemical reactions or otherwise, if the solid temperature is significantly higher than the fluid, the inter-particle temperature profile would be as in Case B, where the dashed line represents the inter-particle temperature profile. The fluid temperature profile, in this case, is still represented by the heavy line in Case A. If an endothermic chemical reaction causes the solid temperature to be much lower than the fluid, a situation as shown in Case C would arise.

In either of these two cases, the temperature of the fluid between two adjacent particles is either higher or lower than both of the particles, and consequently, the fluid phase can not transmit heat from one particle to next. Therefore, Mechanism No. 4 can not exist in these two cases. Instead, both of the neighboring particles would lose heat to (or gain from) the fluid. This net amount of heat loss from one phase to another is something that should be accounted for in the energy balance equation through a separate term, and is not anything an effective conductivity should be concerned with. This particular transfer mechanism, which represents the net heat loss from one phase to another, was in CHAPTER I classified under Mechanism No. 6, and the fluid-solid film coefficient (see APPENDIX VIII) was said to account for this mechanism. In Equation (I-3), the term involving the film coefficient, h is included to account for this inter-phase net heat transfer.

From the above discussion, it is clear that the solid phase effective conductivity, K_s depends on Mechanism No. 3 and Mechanism No. 5 only. Since Mechanism No. 3 is again considered negligible, K_s is essentially equal to the static bed conductivity due to the radiation, $(k_B)_r$, or

$$K_s = (k_B)_r \quad \dots\dots\dots (V-15)$$

where the values of $(k_B)_r$ may be obtained simply from the curve in Fig. (V-10). For an approximate estimation of K_s for the region within a 1/2-particle-diameter distance from the wall, the same curve in Fig. (V-10) may be used with δ of 1.

In conclusion, a packed column, where the solid and fluid temperatures are significantly different from each other, can be handled through two simultaneous energy balance equations with the solid and fluid-phase effective conductivities given by Equations (V-13) through (V-15).

CHAPTER VI. CONCLUSIONS

Local values of the "combined" radial effective conductivity, k_e were measured experimentally at various radial positions of the bed both with and without a flow of air. As the result, the following conclusions were obtained:

- (1) The local effective conductivity at any radial position outside a 1/2-particle-diameter distance from the wall is given by

$$k_e/k_g = k_B/k_g + (1/11) \left(\frac{C_p \mu}{k_g} \right) \left(\frac{d_p G}{\mu} \right) \dots (V-3)$$

On the other hand, for the region within a 1/2-particle-diameter distance from the wall, the same is given by

$$k'_e/k_g = k'_B/k_g + (0.01) \left(\frac{C_p \mu}{k_g} \right) \left(\frac{d_p G}{\mu} \right) \dots (V-5)$$

- (2) The occurrence of unequal effective conductivities in these two regions as indicated by the above two equations is believed to be what constitutes the phenomenon generally known as the "wall effect."

Implied in the above 2 equations are the following conclusions concerning the various individual mechanisms:

- (3) Mechanism No. 1, or the turbulent-diffusion in the fluid phase, is characterized by the modified Peclet number of .11,

in the region outside a 1/2-particle-diameter distance from the column wall, regardless of the radial position, the Reynolds number, particle diameter, solid conductivity, or the temperature level. Or

$$k_{td} = (1/11)(C_p \mu)(Re).$$

This is believed to indicate that the random displacement of fluid parcels is the principal mode of heat transfer in the fluid phase at everywhere in the bed outside a 1/2-particle-diameter distance from the wall. The same mechanism, however, is expressed by

$$k'_{td} = (0.01)(C_p \mu)(Re)$$

for the region inside a 1/2-particle-diameter distance from the wall. The heat transfer process within this region is believed to resemble more an ordinary tubular heat exchanger than the interior of a packed bed.

- (4) Mechanism No. 3, or the solid-solid conduction through the points of contact is believed to be negligible in comparison with other mechanisms.
- (5) Mechanism No. 4, or the solid-fluid-solid series conduction is essentially independent of the Reynolds number, indicating that the fluid in the channel between pellets is essentially in a laminar state, regardless of the

superficial mass flow rate, at least within the range covered in this work. This result also indicates that Mechanism No. 1 is additive to Mechanism No. 4 as well as to the others.

- (6) The tetrahedral, and rectangular close-packing models satisfactorily represent the packing configurations in the interior of the bed and in the immediate vicinity of the wall, respectively. The theoretical correlations based on these models are believed to be adequate for an estimation of Mechanisms No. 2 and No. 4 inclusive.
- (7) Mechanism No. 5, or the radiation mechanism is essentially independent of the temperature gradient of the bed and is a function of the local conditions only.
- (8) Mechanism No. 5 is not independent of the solid conductivity. The empirical correlation obtained in the present work, Fig. (V-10), is believed to express the functional relationship between them with reasonable accuracy.
- (9) Judging from the results of comparisons with various types of previous data, Equations (V-3) and (V-5) and the proposed correlations in Fig. (V-9) and (V-10) are believed to be sufficiently general over most of the practical variable ranges.

- (10) As the result of a theoretical consideration, the correlations obtained in the present work are believed to be applicable, with proper combinations, to the cases where the solid and fluid temperatures are significantly different from each other.

CHAPTER VII. RECOMMENDATIONS

Concerning the methods of applications of the present results, the following procedures are recommended:

(1) Cases Where Fluid and Solid Temperatures Are Nearly Equal at Every Position in the Bed

- a) The local effective conductivity of the interior of the bed and the near-wall region (1/2-particle-diameter distance from the wall) may be calculated through Equations (V-3) and (V-5), respectively. The calculations should be based on the local physical properties of the bed, and the Reynolds number should be determined as described in CHAPTER III.

The static-bed conductivity, k_B may be obtained by summing the conduction contribution, $(k_B)_c$ and the radiation contribution, $(k_B)_r$, which are obtainable from the top curve of Fig. (V-9) and Fig. (V-10), respectively. The wall static-bed conductivity, k_B^* should be obtained by the similar procedure from the bottom curve of Fig. (V-9) and Fig. (V-10).

- b) For a less accurate estimation, if an average effective conductivity is preferred to the more accurate local effective conductivity, such is obtainable through the same equations by simply replacing the local

physical properties by the corresponding mean values for the entire bed.

- c) If an average effective conductivity of the Singer and Wilhelm type is desired (i.e. incorporating the wall effect into the average effective conductivity), the same two equations can be used according to the procedures described in APPENDIX VI.
- d) If a mean heat transfer coefficient of the Leva type is needed, again the same equations may be used as described in APPENDIX VI.
- e) If an average effective conductivity plus the wall coefficient of the Yagi type are required, the procedures described in APPENDIX VI should be followed to convert the same two equations into the required forms.

(2) Cases Where the Fluid and Solid Temperatures Are Significantly Different from Each Other

- a) In such cases, 2 simultaneous energy balance equations must be used, and a separate postulation of the solid phase effective conductivity, K_s and the fluid phase effective conductivity, K_g is necessary. (see Equations I-2 and I-3.)
- b) The fluid phase effective conductivity, K_g is obtainable by merely adding the contributions of Mechanisms No. 1

and No. 2, as in Equations (V-13) and (V-14).

The calculations should be based on the fluid phase physical properties.

- c) For the solid phase effective conductivity, K_s , simply the value obtained from Fig. (V-10) may be used. The curve should be used with the solid phase temperature.
- d) The energy balance equation should include a term to account for the inter-phase net heat transfer. The pertinent fluid-solid film coefficient, h may be estimated from the equations in APPENDIX VIII.

APPEND IX

APPENDIX I

SUMMARY OF DATA AND CALCULATED VALUES

The summary of data and calculated values are presented in the following tables. The original data and calculation sheets are in the custody of Prof. R. F. Baddour.

(1) Tables (A1-1) through (A1-12)

The values of k_e , k_{td} , and P_e are tabulated in these tables as a function of the local bed temperature and Reynolds number. The values of k_B obtained with the large experimental column are included.

(2) Tables (A1-13) through (A1-16)

The values of k_e' , the effective conductivity within a 1/2-particle-diameter interval from the column wall, are tabulated against the local bed temperature and $(C_p \mu)(Re)$. The values of k_B' , the static bed conductivity within the same interval, are also shown.

(3) Tables (A1-17) through (A1-22)

The values of k_B , the static bed conductivity, are shown as a function of the local bed temperature. The values of $(k_B)_c/k_s$, the conduction contribution to k_B , as calculated from Fig. (V-9) were subtracted from the experimental values of $(k_B/k_s)_{exp}$ to obtain $(k_B)_r/k_s$, the radiation contribution to k_B . The data shown in these tables are primarily those obtained with the small experimental column.

Table (A1-1)

k_e of 0.165-inch alumina

<u>Run No.</u>	<u>Local Bed Temperature ($^{\circ}$F)</u>					<u>350</u>	<u>400</u>
	<u>100</u>	<u>150</u>	<u>200</u>	<u>250</u>	<u>300</u>		
60	0.41 (194)	0.44 (173)	0.44 (156)	0.43 (143)	0.43 (140)		
61	0.68 (400)	0.635 (360)	0.65 (328)	0.66 (300)			
62	0.585 (397)	0.595 (357)	0.605 (322)	0.65 (293)			
63	0.74 (475)	0.73 (425)	0.755 (383)				
64	0.90 (620)	0.83 (552)					
65	1.05 (710)	0.93 (635)	0.92 (577)				
69	0.60 (361)	0.57 (325)	0.59 (295)				
70	0.35 (135)	0.34 (124)	0.35 (112)	0.35 (103)	0.36 (94)		
72	0.41 (167)	0.39 (150)	0.39 (136)	0.41 (129)			
73	0.49 (250)	0.45 (222)	0.41 (204)	0.43 (189)	0.435 (169)		
75	0.89 (570)	0.85 (510)	0.82 (465)	0.825 (423)			
76	0.71 (400)	0.62 (366)	0.59 (332)	0.61 (303)	0.62 (278)		
77	0.655 (373)	0.63 (337)	0.63 (303)	0.635 (281)	0.635 (256)		
78	0.81 (635)	0.785 (575)	0.90 (520)				

The numbers inside the parentheses are the corresponding values of the Reynolds number.

Table (A1-1) (Cont'd)

<u>Run No.</u>	<u>100</u>	<u>150</u>	<u>200</u>	<u>250</u>	<u>300</u>	<u>350</u>	<u>400</u>
79	0.61 (500)	0.60 (450)	0.635 (415)				
80	0.775 (596)	0.795 (525)	0.795 (492)				
81	0.69 (525)	0.69 (477)	0.75 (445)	0.76 (390)			

Static Bed Conductivity, k_B

59	0.20	0.20	0.22	0.23	0.25	0.25	0.26
68	- - -	0.25	0.25	0.26	0.26	0.27	0.29
74	- -	- -	0.25	0.26	0.26	0.29	0.29
$(k_B)_{ave}$	0.20	0.22	0.24	0.25	0.26	0.27	0.28

The numbers inside the parentheses are the corresponding values of the Reynolds number.

Table (A1-2)

k_{td} of 0.165-inch alumina

<u>Run No.</u>	<u>Local Bed Temperatures (^oF)</u>						<u>400</u>
	<u>100</u>	<u>150</u>	<u>200</u>	<u>250</u>	<u>300</u>	<u>350</u>	
60	0.21 (194)	0.22 (173)	0.20 (156)	0.18 (143)	0.17 (140)		
61	0.48 (400)	0.415 (360)	0.41 (328)	0.41 (300)			
62	0.385 (397)	0.375 (357)	0.365 (322)	0.40 (293)			
63	0.54 (475)	0.51 (425)	0.515 (383)				
64	0.70 (620)	0.61 (552)					
65	0.85 (710)	0.71 (635)	0.68 (577)				
69	0.40 (361)	0.35 (325)	0.35 (295)				
70	0.13 (135)	0.12 (124)	0.11 (112)	0.10 (103)	0.10 (94)		
72	0.21 (167)	0.17 (150)	0.15 (136)	0.16 (129)			
73	0.29 (250)	0.23 (222)	0.17 (204)	0.18 (189)	0.175 (169)		
75	0.69 (570)	0.63 (510)	0.58 (465)	0.575 (423)			
76	0.51 (400)	0.40 (366)	0.35 (332)	0.36 (303)	0.36 (278)		
77	0.355 (373)	0.41 (337)	0.39 (303)	0.385 (281)	0.375 (256)		
78	0.61 (635)	0.565 (575)	0.66 (520)				

Table (A1-2) (Cont'd)

<u>Run No.</u>	<u>100</u>	<u>150</u>	<u>Local Bed Temperature (°F)</u>				<u>400</u>
			<u>200</u>	<u>250</u>	<u>300</u>	<u>350</u>	
79	0.41 (500)	0.38 (450)	0.395 (415)				
80	0.575 (596)	0.575 (525)	0.555 (492)				
81	0.49 (525)	0.47 (477)	0.51 (445)	0.51 (390)			

$$k_{td} = k_e - (k_B)_{ave}$$

The numbers inside the parentheses are the corresponding values of the Reynolds number.

Table (A1-3)

Pe of 0.165-inch alumina

<u>Run No.</u>	<u>Local Bed Temperature (°F)</u>						
	<u>100</u>	<u>150</u>	<u>200</u>	<u>250</u>	<u>300</u>	<u>350</u>	<u>400</u>
60	10.5 (194)	9.4 (173)	9.9 (156)	10.7 (143)	11.6 (140)		
61	9.4 (400)	10.4 (360)	10.2 (328)	9.9 (300)			
62	11.6 (397)	11.4 (357)	11.2 (322)	9.9 (293)			
63	9.9 (475)	10.0 (425)	9.5 (383)				
64	10.0 (620)	10.9 (552)					
65	9.4 (710)	10.7 (635)	10.8 (577)				
69	10.2 (361)	10.5 (325)	10.7 (295)				
70	11.7 (135)	12.4 (124)	12.9 (112)	13.8 (103)	13.3 (94)		
72	9.0 (167)	10.6 (150)	11.5 (136)	10.8 (129)			
73	9.7 (250)	11.6 (222)	15.3 (204)	14.1 (189)	13.6 (169)		
75	9.3 (570)	9.7 (510)	10.2 (465)	9.9 (423)			
76	8.8 (400)	11.0 (366)	12.1 (332)	11.3 (303)	10.9 (278)		
77	11.8 (373)	9.9 (337)	9.9 (303)	9.8 (281)	9.7 (256)		
78	11.7 (635)	12.2 (575)	10.0 (520)				

Table (A1-3) (Cont'd)

<u>Run No.</u>	<u>100</u>	<u>150</u>	<u>Local Bed Temperature (°F)</u>			<u>350</u>	<u>400</u>
			<u>200</u>	<u>250</u>	<u>300</u>		
79	13.7 (500)	14.2 (450)	13.3 (415)				
80	11.7 (596)	10.9 (525)	11.2 (492)				
81	12.0 (525)	12.2 (477)	11.1 (445)	10.3 (390)			

$$Pe = C_p \cdot G \cdot d_p / k_{td}$$

The numbers inside the parentheses are the corresponding values of the Reynolds number.

Table (A1-4)

k_e of 0.312-inch Alumina

<u>Run No.</u>	<u>Local Bed Temperature ($^{\circ}$F)</u>						
	<u>100</u>	<u>150</u>	<u>200</u>	<u>250</u>	<u>300</u>	<u>350</u>	<u>400</u>
101	1.41 (1295)	1.42 (1160)	1.66 (1050)				
102	1.312 (1070)	1.24 (965)	1.36 (880)				
103	1.05 (870)	1.10 (785)	1.14 (712)				
104	0.89 (712)	0.94 (642)	1.02 (581)	1.05 (527)	1.00 (478)		
105	0.65 (422)	0.69 (380)	0.72 (345)	0.69 (314)	0.74 (289)	0.81 (267)	
107	1.48 (1260)	1.41 (1130)	1.55 (1020)				
108	1.25 (1055)	1.26 (955)	1.31 (862)				
109	1.12 (840)	1.10 (760)	1.12 (692)	1.15 (628)	1.13 (576)		
110	0.82 (504)	0.79 (450)	0.78 (408)	0.78 (372)	0.79 (342)	0.81 (314)	
111	0.62 (306)	0.61 (274)	0.58 (248)	0.56 (227)	0.57 (208)	0.56 (192)	
<hr/> <u>Static Bed Conductivity, k_B</u> <hr/>							
100	0.23	0.25	0.28	0.29	0.32		
106	0.30	0.30	0.30	0.31	0.32	0.33	
<hr/>							
$(k_B)_{ave}$	0.26	0.28	0.29	0.30	0.32	0.33	

The numbers inside the parentheses are the corresponding values of the Reynolds number.

Table (A1-5)

k_{td} of 0.312-inch Alumina

<u>Run No.</u>	<u>Local Bed Temperature (^oF)</u>						
	<u>100</u>	<u>150</u>	<u>200</u>	<u>250</u>	<u>300</u>	<u>350</u>	<u>400</u>
101	1.15 (1295)	1.14 (1160)	1.37 (1050)				
102	1.06 (1070)	0.96 (965)	1.07 (880)				
103	0.79 (870)	0.82 (785)	0.85 (712)				
104	0.63 (712)	0.66 (642)	0.73 (581)	0.75 (527)	0.68 (478)		
105	0.39 (422)	0.41 (380)	0.43 (345)	0.39 (314)	0.42 (289)	0.48 (267)	
107	1.22 (1260)	1.13 (1130)	1.26 (1020)				
108	0.99 (1055)	0.98 (955)	1.02 (862)				
109	0.86 (840)	0.82 (760)	0.83 (692)	0.85 (628)	0.81 (576)		
110	0.56 (504)	0.51 (450)	0.49 (408)	0.48 (374)	0.47 (342)	0.48 (312)	
111	0.36 (306)	0.33 (274)	0.29 (248)	0.26 (227)	0.25 (208)	0.23 (192)	

The numbers inside the parentheses are the corresponding values of the Reynolds number.

Table (A1-6)

Pe of 0.312-inch Alumina

<u>Run No.</u>	<u>Local Bed Temperature (°F)</u>						
	<u>100</u>	<u>150</u>	<u>200</u>	<u>250</u>	<u>300</u>	<u>350</u>	<u>400</u>
101	12.8 (1295)	12.2 (1160)	9.7 (1050)				
102	11.3 (1070)	12.1 (965)	10.5 (880)				
103	12.4 (870)	11.5 (785)	11.7 (712)				
104	12.7 (712)	11.6 (642)	10.2 (581)	9.5 (527)	9.9 (478)		
105	12.2 (422)	11.1 (380)	9.9 (345)	10.8 (314)	9.8 (289)	8.3 (267)	
107	11.6 (1260)	12.0 (1130)	10.1 (1020)				
108	12.0 (1055)	11.7 (955)	10.7 (862)				
109	11.0 (840)	11.3 (760)	10.6 (692)	9.9 (628)	10.1 (576)		
110	10.1 (504)	10.6 (450)	10.6 (408)	10.4 (374)	10.3 (342)	9.6 (314)	
111	9.6 (306)	10.0 (274)	10.9 (248)	11.7 (227)	11.8 (208)	12.4 (192)	

The numbers inside the parentheses are the corresponding values of the Reynolds number.

Table (A1-7)

k_e of 0.141-inch Steel

<u>Run No.</u>	<u>Local Bed Temperature ($^{\circ}$F)</u>						<u>400</u>
	<u>100</u>	<u>150</u>	<u>200</u>	<u>250</u>	<u>300</u>	<u>350</u>	
200	0.99 (581)	0.92 (524)	0.91 (475)	0.97 (434)			
201	0.99 (562)	0.95 (507)	0.90 (461)	0.90 (425)			
202	1.06 (718)	1.05 (645)	1.05 (588)				
203	0.89 (545)	0.845 (490)	0.825 (441)	0.825 (405)			
204	0.87 (495)	0.78 (445)	0.75 (403)	0.79 (369)			
205	0.76 (398)	0.74 (356)	0.735 (324)	0.70 (294)	0.70 (270)		
206	0.605 (306)	0.625 (278)	0.63 (250)	0.63 (228)	0.64 (208)	0.63 (191)	
207	0.525 (187)	0.54 (168)	0.535 (153)	0.54 (140)	0.56 (128)	0.57 (118)	0.60 (109)
208	0.79 (430)	0.715 (384)	0.755 (348)	0.775 (318)	0.805 (292)		
209	0.55 (227)	0.555 (204)	0.59 (184)	0.57 (167)	0.575 (153)	0.575 (141)	0.585 (132)
210	0.445 (116)	0.47 (105)	0.47 (95)	0.48 (86)	0.48 (79)	0.48 (73)	0.49 (68)
Static Bed Conductivity, k_B							
211	0.30	0.32	0.34	0.35	0.37	0.39	0.40

The numbers inside the parentheses are the corresponding values of the Reynolds number.

Table (A1-8)

k_{td} of 0.141-inch Steel

<u>Run No.</u>	<u>Local Bed Temperature ($^{\circ}$F)</u>						
	<u>100</u>	<u>150</u>	<u>200</u>	<u>250</u>	<u>300</u>	<u>350</u>	<u>400</u>
200	0.69 (581)	0.60 (524)	0.57 (475)	0.62 (434)			
201	0.69 (562)	0.63 (507)	0.56 (461)	0.55 (425)			
202	0.76 (718)	0.73 (645)	0.71 (588)				
203	0.59 (545)	0.525 (490)	0.485 (441)	0.47 (405)			
204	0.57 (495)	0.46 (445)	0.41 (403)	0.44 (369)			
205	0.46 (398)	0.42 (356)	0.395 (324)	0.35 (294)	0.33 (270)		
206	0.305 (306)	0.305 (278)	0.290 (250)	0.28 (228)	0.27 (208)	0.24 (191)	
207	0.225 (187)	0.21 (168)	0.195 (153)	0.19 (140)	0.19 (128)	0.18 (118)	0.20 (109)
208	0.49 (430)	0.40 (384)	0.415 (348)	0.425 (318)	0.435 (292)		
209	0.25 (227)	0.235 (204)	0.25 (184)	0.22 (167)	0.205 (153)	0.185 (141)	0.185 (132)
210	0.145 (116)	0.15 (105)	0.13 (95)	0.13 (86)	0.11 (79)	0.09 (73)	0.09 (68)

The numbers inside the parentheses are the corresponding values of the Reynolds number.

Table (A1-9)
Pe of 0.141-inch Steel

<u>Run No.</u>	<u>Local Bed Temperature (°F)</u>						<u>400</u>
	<u>100</u>	<u>150</u>	<u>200</u>	<u>250</u>	<u>300</u>	<u>350</u>	
200	9.5 (581)	10.5 (524)	10.6 (475)	9.5 (434)			
201	9.2 (562)	9.7 (507)	10.5 (461)	10.4 (425)			
202	10.6 (718)	10.6 (645)	10.5 (588)				
203	10.4 (545)	11.2 (490)	11.6 (441)	11.6 (405)			
204	9.8 (495)	11.6 (445)	12.5 (403)	11.3 (369)			
205	9.7 (398)	10.2 (356)	10.4 (324)	11.3 (294)	11.5 (270)		
206	11.3 (306)	10.9 (278)	11.0 (250)	10.9 (228)	10.9 (208)	11.9 (191)	
207	9.3 (187)	9.6 (168)	10.0 (153)	9.9 (140)	9.5 (128)	9.8 (118)	8.5 (109)
208	9.8 (430)	11.5 (384)	10.7 (348)	10.1 (318)	9.5 (292)		
209	10.2 (227)	10.4 (204)	9.4 (184)	10.2 (167)	10.6 (153)	11.3 (141)	11.1 (132)
210	8.9 (116)	8.4 (105)	9.3 (95)	8.9 (86)	10.2 (79)	12.1 (73)	11.7 (68)

The numbers inside the parentheses are the corresponding values of the Reynolds number.

Table (A1-10)

k_e of 0.282-inch Steel

<u>Run No.</u>	<u>Local Bed Temperature ($^{\circ}$F)</u>						<u>400</u>
	<u>100</u>	<u>150</u>	<u>200</u>	<u>250</u>	<u>300</u>	<u>350</u>	
300	1.77 (1422)	1.75 (1280)					
301	1.40 (1100)	1.44 (990)	1.55 (895)				
302	1.35 (977)	1.33 (885)	1.40 (800)				
303	1.23 (768)	1.21 (692)	1.28 (624)				
304	1.30 (855)	1.22 (770)	1.28 (697)				
305	1.08 (667)	1.08 (605)	1.12 (547)	1.15 (495)			
306	0.945 (458)	0.95 (420)	0.95 (382)	0.97 (345)	0.98 (312)		
308	0.81 (348)	0.82 (320)	0.83 (289)	0.86 (261)	0.90 (240)	0.91 (218)	
309	0.78 (240)	0.73 (218)	0.76 (198)	0.75 (180)	0.765 (165)	0.80 (151)	
Static Bed Conductivity, k_B							
310	0.42	0.44	0.465	0.48	0.515	0.55	
311	0.42	0.435	0.46	0.48	0.49	- - -	
$(k_B)_{ave}$	0.42	0.44	0.46	0.48	0.50	0.55	

The numbers inside the parentheses are the corresponding values of the Reynolds number.

Table (A1-11)

k_{td} of 0.282-inch Steel

<u>Run No.</u>	<u>Local Bed Temperature (°F)</u>						<u>400</u>
	<u>100</u>	<u>150</u>	<u>200</u>	<u>250</u>	<u>300</u>	<u>350</u>	
300	1.35 (1422)	1.31 (1280)					
301	0.98 (1100)	1.00 (990)	1.09 (895)				
302	0.93 (977)	0.89 (885)	0.94 (800)				
303	0.81 (768)	0.77 (692)	0.82 (624)				
304	0.88 (855)	0.78 (770)	0.82 (697)				
305	0.66 (667)	0.64 (605)	0.66 (547)	0.67 (495)			
306	0.525 (458)	0.51 (420)	0.49 (382)	0.49 (345)	0.48 (312)		
308	0.39 (348)	0.38 (320)	0.37 (289)	0.38 (261)	0.40 (240)	0.36 (218)	
309	0.36 (240)	0.29 (218)	0.30 (198)	0.27 (180)	0.265 (165)	0.25 (151)	

The numbers inside the parentheses are the corresponding values of the Reynolds number.

Table (A1-12)

Pe of 0.282-inch Steel

<u>Run No.</u>	<u>Local Bed Temperature (°F)</u>						
	<u>100</u>	<u>150</u>	<u>200</u>	<u>250</u>	<u>300</u>	<u>350</u>	<u>400</u>
300	11.9 (1422)	11.7 (1280)					
301	12.6 (1100)	11.9 (990)	10.5 (895)				
302	11.8 (977)	11.9 (885)	10.8 (800)				
303	10.7 (768)	10.8 (692)	9.7 (624)				
304	10.9 (855)	11.8 (770)	10.8 (697)				
305	11.4 (667)	11.3 (605)	10.5 (547)	10.0 (495)			
306	9.8 (458)	9.9 (420)	9.9 (382)	9.5 (345)	9.2 (312)		
308	10.1 (348)	10.1 (320)	10.0 (289)	9.3 (261)	8.5 (240)	9.0 (218)	
309	7.5 (240)	9.0 (218)	8.4 (198)	9.0 (180)	8.8 (165)	9.0 (151)	

The numbers inside the parentheses are the corresponding values of the Reynolds number.

Table (A1-13)

k'_e of 0.165-inch Alumina

<u>Run No.</u>	<u>k'_e</u>	<u>Re</u>	<u>$t(^{\circ}F)$</u>	<u>$(C_p \mu)$</u>	<u>$(C_p \mu)(Re)$</u>
59	0.15	0	50	0.0106	0
60	0.20	198	50	0.0106	2.10
61	0.21	415	55	0.01066	4.40
62	0.15	411	50	0.01060	4.36
63	0.22	500	50	0.01060	5.30
64	0.18	660	50	0.01060	7.00
65	0.18	745	55	0.01066	7.95
68	0.18	0	50	0.01060	0
69	0.16	365	60	0.01072	3.92
70	0.18	139	60	0.01072	1.49
72	0.21	170	60	0.01072	1.83
73	0.19	248	60	0.01072	2.66
74	0.18	0	60	0.01072	0
75	0.30	575	65	0.01080	6.21
76	0.28	405	65	0.01080	4.37
77	0.29	375	65	0.01080	4.05
78	0.28	640	65	0.01080	6.91
79	0.19	505	65	0.01080	5.45
80	0.28	598	65	0.01080	6.47
81	0.26	522	70	0.01088	5.67

See Table of Nomenclature for the units.

Table (A1-14)

 k'_e of 0.312-inch Alumina

<u>Run No.</u>	<u>k'_e</u>	<u>Re</u>	<u>$t(^{\circ}\text{F})$</u>	<u>$(C_p \mu)$</u>	<u>$(C_p \mu)(\text{Re})$</u>
100	0.28	0	65	0.01080	0
101	0.38	1290	75	0.01093	14.10
102	0.31	1090	75	0.01093	11.90
103	0.33	870	75	0.01093	9.50
104	0.33	692	75	0.01093	7.56
105	0.27	405	75	0.01093	4.43
106	0.27	0	75	0.01093	0
107	0.38	1265	75	0.01093	13.85
108	0.37	1060	75	0.01093	11.60
109	0.39	825	79	0.01098	9.05
110	0.33	482	85	0.01105	5.33
111	0.29	293	80	0.01098	3.22

Table (A1-15)

 k'_e of 0.141-inch Steel

<u>Run No.</u>	<u>k'_e</u>	<u>Re</u>	<u>$t(^{\circ}\text{F})$</u>	<u>$(C_p \mu)$</u>	<u>$(C_p \mu)(\text{Re})$</u>
200	0.32	590	70	0.01088	6.40
201	0.32	568	70	0.01088	6.18
202	0.33	720	70	0.01088	7.82
203	0.24	550	75	0.01093	6.01
204	0.25	500	75	0.01093	5.46
205	0.31	402	75	0.01093	4.40
206	0.28	310	75	0.01093	3.39

See Table of Nomenclature for the units.

Table (A1-15) (Cont'd)

<u>Run No.</u>	<u>k'_e</u>	<u>Re</u>	<u>$t(^{\circ}F)$</u>	<u>$(C_p \mu)$</u>	<u>$(C_p \mu)(Re)$</u>
207	0.27	190	70	0.01088	2.06
208	0.29	435	70	0.01088	4.73
209	0.27	230	70	0.01088	2.50
210	0.29	120	70	0.01088	1.31
211	0.22	0	70	0.01088	0

Table (A1-16)

k'_e of 0.282-inch Steel

<u>Run No.</u>	<u>k'_e</u>	<u>Re</u>	<u>$t(^{\circ}F)$</u>	<u>$(C_p \mu)$</u>	<u>$(C_p \mu)(Re)$</u>
300	0.36	1429	80	0.01098	15.70
301	0.34	1110	85	0.01105	12.30
302	0.35	980	85	0.01105	10.81
303	0.31	770	85	0.01105	8.51
304	0.34	860	85	0.01105	9.50
305	0.29	670	90	0.01110	7.45
306	0.31	460	90	0.01110	5.11
308	0.34	350	85	0.01105	3.87
309	0.27	242	90	0.01110	2.68
310	0.26	0	80	0.01098	0
311	0.28	0	75	0.01093	0

See Table of Nomenclature for the units.

Table (A1-17)

- 176 -

 k_B of 0.165-inch Alumina

Run No.	t(°F)	$(k_B)_{exp}$	$(k_B/k_s)_{exp}$	k_g/k_s	* $(k_B)_c/k_s$	** $(k_B)_r/k_s$	*** k_r/k_s
2014	200	0.24	0.141	0.0106	0.111	0.030	0.0045
	300	0.27	0.150	0.0111	0.115	0.035	0.0061
	400	0.285	0.148	0.0117	0.120	0.028	0.0071
	500	0.32	0.160	0.0125	0.125	0.035	0.0096
	600	0.345	0.163	0.0127	0.127	0.036	0.0110
	700	0.42	0.191	0.0132	0.131	0.060	0.0127
2015	150	0.21	0.127	0.0103	0.110	0.017	0.0038
	200	0.23	0.135	0.0106	0.111	0.024	0.0045
	300	0.245	0.136	0.0111	0.115	0.021	0.0061
	400	0.28	0.146	0.0117	0.120	0.026	0.0071
	500	0.31	0.155	0.0125	0.125	0.030	0.0096
2016	150	0.20	0.121	0.0103	0.110	0.011	0.0038
	200	0.225	0.132	0.0106	0.111	0.021	0.0045
	250	0.24	0.137	0.0109	0.114	0.023	0.0053
	300	0.27	0.150	0.0111	0.115	0.035	0.0061
2027	300	0.274	0.152	0.0111	0.115	0.037	0.0061
	400	0.294	0.153	0.0117	0.120	0.033	0.0071
	500	0.334	0.167	0.0125	0.125	0.042	0.0096
	600	0.35	0.165	0.0127	0.127	0.038	0.0110
	700	0.394	0.179	0.0132	0.131	0.048	0.0127
	800	0.44	0.195	0.0137	0.133	0.062	0.0143
	900	0.47	0.200	0.0141	0.135	0.065	0.0156
	1000	0.52	0.220	0.0148	0.140	0.080	0.0170

* Calculated from Fig. (V-9); ** These are plotted in Fig. (V-10).

*** where $k_r = (0.173)(\delta)(\epsilon)(d_p)(4T^3/10^8)$

Table (A1-17) (Cont'd)

k_B of 0.165-inch Alumina

Run No.	t(°F)	k_B of 0.165-inch Alumina					
		$(k_B)_{exp}$	$(k_B/k_s)_{exp}$	k_g/k_s	* $(k_B)_c/k_s$	** $(k_B)_r/k_s$	*** k_r/k_s
2028	150	0.21	0.127	0.0103	0.110	0.017	0.0038
	200	0.23	0.135	0.0106	0.111	0.024	0.0045
	250	0.24	0.137	0.0109	0.114	0.023	0.0053
	300	0.26	0.144	0.0111	0.115	0.029	0.0061
	350	0.29	0.153	0.0116	0.120	0.033	0.0068
59	100	0.20	0.125	0.0094	0.102	0.023	0.0031
	150	0.20	0.121	0.0103	0.110	0.011	0.0038
	200	0.22	0.129	0.0106	0.111	0.018	0.0045
	250	0.23	0.131	0.0109	0.114	0.017	0.0053
	300	0.25	0.139	0.0111	0.115	0.024	0.0061
	350	0.25	0.132	0.0116	0.120	0.012	0.0068
	400	0.26	0.135	0.0117	0.120	0.015	0.0071
68	200	0.25	0.147	0.0106	0.111	0.036	0.0045
	250	0.26	0.149	0.0109	0.114	0.035	0.0053
	300	0.26	0.144	0.0111	0.115	0.029	0.0061
	350	0.27	0.142	0.0116	0.120	0.022	0.0068
	400	0.29	0.151	0.0117	0.120	0.031	0.0071
69	200	0.25	0.147	0.0106	0.111	0.036	0.0045
	250	0.26	0.149	0.0109	0.114	0.035	0.0053
	300	0.26	0.144	0.0111	0.115	0.029	0.0061
	350	0.29	0.153	0.0116	0.120	0.033	0.0068
	400	0.29	0.151	0.0117	0.120	0.031	0.0071

* Calculated from Fig.(V-9); ** These are plotted in Fig.(V-10).

*** where $k_r = (0.173)(\delta)(\epsilon)(d_p)^3(4T^3/10^8)$

Table (A1-18)

Run No.	t(°F)	k_B of 0.312-inch Alumina					
		$(k_B)_{exp}$	$(k_B/k_s)_{exp}$	k_g/k_s	* $(k_B)_c/k_s$	** $(k_B)_r/k_s$	*** k_r/k_s
2005	250	0.31	0.178	0.0109	0.114	0.064	0.0100
	300	0.33	0.183	0.0111	0.115	0.068	0.0116
	400	0.35	0.182	0.0117	0.120	0.062	0.0146
	500	0.37	0.185	0.0125	0.125	0.060	0.0181
	600	0.41	0.193	0.0127	0.127	0.066	0.0209
	700	0.455	0.207	0.0132	0.131	0.076	0.0241
	800	0.52	0.230	0.0137	0.133	0.097	0.0271
	900	0.59	0.251	0.0141	0.135	0.116	0.0295
	2006	300	0.33	0.183	0.0111	0.115	0.068
400		0.36	0.188	0.0117	0.120	0.068	0.0146
500		0.405	0.203	0.0125	0.125	0.078	0.0181
600		0.435	0.205	0.0127	0.127	0.078	0.0209
700		0.475	0.216	0.0132	0.131	0.085	0.0241
800		0.51	0.226	0.0137	0.133	0.093	0.0271
900		0.53	0.225	0.0141	0.135	0.090	0.0295
1000		0.59	0.250	0.0148	0.140	0.110	0.0321
2029	300	0.36	0.200	0.0111	0.115	0.085	0.0116
	400	0.365	0.190	0.0117	0.120	0.070	0.0146
	500	0.40	0.200	0.0125	0.125	0.085	0.0181
	600	0.43	0.202	0.0127	0.127	0.075	0.0209
	700	0.485	0.220	0.0132	0.131	0.089	0.0241
	800	0.53	0.234	0.0137	0.133	0.101	0.0271
	900	0.57	0.242	0.0141	0.135	0.107	0.0295
	1000	0.675	0.286	0.0148	0.140	0.146	0.0321

Table (A1-18) (Cont'd)

k_B of 0.312-inch Alumina

Run No.	t(°F)	$(k_B)_{exp}$	$(k_B/k_s)_{exp}$	k_g/k_s	* $(k_B)_c/k_s$	** $(k_B)_r/k_s$	*** k_r/k_s
2030	150	0.27	0.164	0.0103	0.110	0.054	0.0073
	200	0.29	0.171	0.0106	0.111	0.060	0.0085
	250	0.31	0.177	0.0109	0.114	0.063	0.0100
	300	0.32	0.178	0.0111	0.115	0.063	0.0116
	350	0.33	0.173	0.0116	0.120	0.053	0.0128
100	100	0.23	0.144	0.0094	0.102	0.042	0.0059
	150	0.25	0.152	0.0103	0.110	0.042	0.0073
	200	0.28	0.165	0.0106	0.111	0.054	0.0085
	250	0.29	0.166	0.0109	0.114	0.052	0.0100
	300	0.32	0.178	0.0111	0.115	0.063	0.0116
106	100	0.30	0.188	0.0094	0.102	0.086	0.0059
	150	0.30	0.182	0.0103	0.110	0.072	0.0073
	200	0.30	0.176	0.0106	0.111	0.065	0.0085
	250	0.31	0.177	0.0109	0.114	0.063	0.0100
	300	0.32	0.178	0.0111	0.115	0.063	0.0116
	350	0.33	0.174	0.0116	0.120	0.054	0.0128

* Calculated from Fig.(V-9); ** These are plotted in Fig. (V-10).

*** where $k_r = (0.173)(\delta)(\epsilon)(d_p)(4T^3/10^8)$

Table (A1-19)

k_B of 0.141-inch Steel

Run No.	$t(^{\circ}F)$	$(k_B)_{exp}$	$(k_B/k_s)_{exp}$	k_g/k_s	* $(k_B)_c/k_s$	** $(k_B)_r/k_s$	*** k_r/k_s
2020	100	0.33	0.0126	0.00057	0.0110	0.0016	0.000033
	150	0.34	0.0130	0.00065	0.0122	0.0008	0.000044
	200	0.365	0.0139	0.00069	0.0130	0.0009	0.000057
	250	0.37	0.0142	0.00073	0.0135	0.0007	0.000073
	300	0.38	0.0146	0.00077	0.0139	0.0007	0.000091
	400	0.44	0.0177	0.00087	0.0155	0.0022	0.000140
2021	250	0.365	0.0139	0.00073	0.0133	0.0006	0.000073
	300	0.385	0.0148	0.00077	0.0141	0.0007	0.000091
	400	0.43	0.0166	0.00087	0.0155	0.0011	0.000140
	500	0.465	0.0183	0.00098	0.0171	0.0012	0.000204
	600	0.51	0.0206	0.00109	0.0186	0.0020	0.000300
	700	0.585	0.0247	0.00122	0.0205	0.0042	0.000420
	800	0.71	0.0313	0.00137	0.0221	0.0092	0.000570
2022	400	0.38	0.0147	0.00087	0.0155	- - -	0.000140
	500	0.43	0.0169	0.00098	0.0171	- - -	0.000204
	600	0.51	0.0206	0.00109	0.0186	0.0020	0.000300
	700	0.585	0.0247	0.00122	0.0205	0.0042	0.000420
	800	0.65	0.0286	0.00137	0.0221	0.0065	0.000570
	900	0.74	0.0336	0.00150	0.0242	0.0094	0.000770
	1000	0.89	0.0412	0.00162	0.0255	0.0157	0.001000
	1100	1.02	0.0476	0.00175	0.0274	0.0202	0.001300

* Calculated from Fig.(V-9); ** These are plotted in Fig. (V-10).

*** where $k_r = (0.173)(\delta)(\epsilon)(d_p)(4T^3/10^8)$

Table (A1-20)

k_B of 0.282-inch Steel

<u>Run No.</u>	<u>t(°F)</u>	<u>(k_B)_{exp}</u>	<u>(k_B/k_s)_{exp}</u>	<u>k_g/k_s</u>	<u>* (k_B)_c/k_s</u>	<u>** (k_B)_r/k_s</u>	<u>*** k_r/k_s</u>
2017	100	0.39	0.0149	0.00057	0.0110	0.0039	0.000065
	150	0.35	0.0134	0.00065	0.0122	0.0012	0.000090
	200	0.34	0.0130	0.00069	0.0130	0.0000	0.000115
2018	200	0.435	0.0166	0.00069	0.0130	0.0036	0.000115
	300	0.46	0.0177	0.00077	0.0141	0.0036	0.000180
	400	0.49	0.0189	0.00087	0.0155	0.0034	0.000280
	500	0.53	0.0208	0.00098	0.0171	0.0037	0.000410
	600	0.61	0.0246	0.00109	0.0186	0.0060	0.000590
	700	0.665	0.0280	0.00122	0.0205	0.0075	0.000840
2019	300	0.465	0.0179	0.00077	0.0141	0.0038	0.000180
	400	0.50	0.0193	0.00087	0.0155	0.0038	0.000280
	500	0.55	0.0216	0.00098	0.0171	0.0045	0.000410
	600	0.615	0.0248	0.00109	0.0186	0.0062	0.000590
	700	0.69	0.0291	0.00122	0.0205	0.0086	0.000840
	800	0.80	0.0352	0.00137	0.0221	0.0131	0.001150
	900	0.90	0.0410	0.00150	0.0242	0.0168	0.001550
	1000	1.11	0.0512	0.00162	0.0255	0.0257	0.002005

Table (A1-20) (Cont'd)

k_B of 0.282-inch Steel

<u>Run No.</u>	<u>t(°F)</u>	<u>(k_B)_{exp}</u>	<u>(k_B/k_s)_{exp}</u>	<u>k_g/k_s</u>	<u>* (k_B)_c/k_s</u>	<u>** (k_B)_r/k_s</u>	<u>*** k_r/k_s</u>
2040	200	0.44	0.0168	0.00069	0.0130	0.0038	0.000115
	300	0.455	0.0175	0.00079	0.0141	0.0034	0.00018
	400	0.475	0.0183	0.00087	0.0155	0.0028	0.00028
	500	0.53	0.0208	0.00098	0.0171	0.0037	0.00041
	600	0.60	0.0242	0.00109	0.0186	0.0056	0.00059
	700	0.69	0.0291	0.00122	0.0205	0.0086	0.00084
	800	0.83	0.0365	0.00137	0.0221	0.0144	0.00115
	2041	300	0.465	0.0179	0.00077	0.0141	0.0038
400		0.48	0.0185	0.00087	0.0155	0.0030	0.00028
500		0.525	0.0206	0.00098	0.0171	0.0035	0.00041
600		0.595	0.0240	0.00109	0.0186	0.0054	0.00059
700		0.65	0.0274	0.00122	0.0205	0.0069	0.00084
800		0.71	0.0312	0.00137	0.0221	0.0091	0.00115
900		0.92	0.0418	0.00150	0.0242	0.0176	0.00155
1000		1.00	0.0462	0.00162	0.0255	0.0207	0.0020

* Calculated from Fig. (V-9); ** These are plotted in Fig. (V-10).

*** where $k_r = (0.173)(\delta)(E)(d_p)(4T^3/10^8)$

Table (A1-21)

k_B of 0.236-inch Glass

<u>Run No.</u>	<u>t(°F)</u>	<u>(k_B)_{exp}</u>	<u>(k_B/k_s)_{exp}</u>	<u>k_g/k_s</u>	<u>* (k_B)_c/k_s</u>	<u>** (k_B)_r/k_s</u>	<u>*** k_r/k_s</u>
2031	150	0.175	0.398	0.0387	0.257	0.141	0.0245
	200	0.182	0.413	0.0409	0.270	0.143	0.0307
	250	0.200	0.455	0.0432	0.275	0.180	0.0382
	300	0.215	0.489	0.0455	0.282	0.207	0.0465
2032	300	0.224	0.510	0.0455	0.282	0.228	0.0465
	400	0.254	0.578	0.0512	0.303	0.275	0.0670
	500	0.290	0.660	0.0570	0.321	0.339	0.0910
	600	0.330	0.750	0.0614	0.340	0.410	0.1200
	700	0.390	0.886	0.0660	0.346	0.540	0.1530
	800	0.470	1.070	0.0705	0.360	0.710	0.1930
	900	0.590	1.340	0.0750	0.370	0.970	0.2390

* Calculated from Fig. (V-9); ** These are plotted in Fig. (V-10).

*** where $k_r = (0.173)(\delta)(\epsilon)(d_p)(4T^3/10^8)$

Table (A1-22)

- 184 -

Run No.	t(°F)	k_B of 0.250-inch Aluminum					
		$(k_B)_{exp}$	$(k_B/k_s)_{exp}$	k_g/k_s	* $(k_B)_c/k_s$	** $(k_B)_r/k_s$	*** k_r/k_s
2008	150	0.475	0.00402	0.000144	0.00344	0.00058	0.000015
	200	0.48	0.00402	0.000151	0.00355	0.00047	0.000021
	250	0.535	0.00446	0.000158	0.00370	0.00076	0.000028
	300	0.57	0.00471	0.000165	0.00383	0.00088	0.000037
	400	0.73	0.00590	0.000181	0.00408	0.00182	0.000060
	500	1.005	0.00785	0.000195	0.00422	0.00363	0.000091
2009	250	0.59	0.00491	0.000158	0.00370	0.00121	0.000028
	300	0.615	0.00509	0.000165	0.00383	0.00126	0.000037
	400	0.79	0.00638	0.000181	0.00408	0.00230	0.000060
	500	1.03	0.00791	0.000195	0.00422	0.00369	0.000091
	600	1.45	0.01090	0.000203	0.00465	0.00625	0.000125
2010	300	0.605	0.00500	0.000165	0.00383	0.00117	0.000037
	400	0.77	0.00620	0.000181	0.00408	0.00212	0.000060
	500	0.98	0.00765	0.000195	0.00422	0.00343	0.000091
	600	1.29	0.00970	0.000203	0.00465	0.00505	0.000125
	700	1.75	0.01250	0.000208	0.00475	0.00775	0.000180
	800	2.37	0.01630	0.000214	0.00490	0.01140	0.000240
2023	150	0.465	0.00394	0.000144	0.00344	0.00050	0.000015
	200	0.55	0.00461	0.000151	0.00355	0.00106	0.000021
	250	0.59	0.00491	0.000158	0.00370	0.00121	0.000028
2035	150	0.51	0.00432	0.000144	0.00344	0.00088	0.000015
	200	0.52	0.00437	0.000151	0.00355	0.00082	0.000021
	250	0.56	0.00467	0.000158	0.00370	0.00097	0.000028

* Calculated from Fig.(V-9); **These are plotted in Fig. (V-10).

*** where $k_r = (0.173)(\delta)(\epsilon)(d_p)(4T^3/10^8)$

SAMPLE CALCULATIONS

(1) Calculation of the Effective Conductivity in the Interior of the Bed

At any radial position r , the basic Fourier equation gives

$$q = - (k_e)(A)(dt/dr) \dots\dots\dots (I-1)$$

or

$$\begin{aligned} k_e &= \frac{q}{(A)(-dt/dr)} \quad \frac{\text{Btu}}{(\text{hr})(\text{ft})(\text{oF})} \\ &= \frac{(3413)(\text{KW})}{(2\pi r)(L)(-dt/dr)} \\ &= \frac{(3413)(\text{KW})}{(2\pi)(65/12)(r)(-dt/dr)} \\ &= (100.1) \left(\frac{\text{KW}}{(r)(-dt/dr)} \right) \end{aligned}$$

where KW: Amount of energy-input measured in Kilowatts.

For an illustration, the value of k_e at the bed temperature of 150 oF observed in Run 109 is calculated as follows: (c.f. Fig.III-1) The bed temperature of 150 oF was observed in this run at $r=2.1$ inches. The temperature profile in Fig. (III-1) was graphically differentiated at that particular location to obtain $(-dt/dr) = 86$ oF/inch. The total power input in this run was 1.99 KW. Substituting these values into Equation (I-1),

$$k_e = (100.1) \frac{(1.99)}{(2.10)(86)} = 1.103 \frac{\text{Btu}}{(\text{hr})(\text{ft})(\text{oF})}$$

This value was attributed to the bed temperature of 150 °F and the Reynolds number of 760.

The calculations of k_p for both the large and small experimental columns were carried out by exactly the same method as above.

(2) Calculation of the Effective Conductivity within 1/2-particle-diameter Distance from the Wall

Again Run 109 (see Fig. III-1) is used here for an illustration. The inside diameter of the large heat transfer column is 6.065 inches, or the radius, R is 3.033 inches. The packing material used in this run was 0.312-inch alumina, and 1/2 of the diameter is 0.156 inch. At 1/2-particle-diameter distance from the column wall ($r = 3.033 - 0.156 = 2.877$ inches), the temperature profile in Fig. (III-1) gives the local bed temperature of 93 °F.

The average outer wall temperature was 65 °F during this run. Assuming 26.2 Btu/hr.ft.°F for the solid conductivity of the column wall, the inner wall temperature is given by

$$\begin{aligned} t_{\text{inner wall}} &= 65 + \frac{(q)(\text{thickness of the wall})}{(2\pi r)(L)(k_s \text{ of the wall})} \\ &= 65 + \frac{(3413)(1.99)(0.28/12)}{(2\pi)(3.173/12)(65/12)(26.2)} \\ &= 65.7 \text{ } ^\circ\text{F.} \end{aligned}$$

Therefore, the temperature drop within the 1/2-particle-diameter interval was $93 - 65.7 = 27.3$ °F, or the average temperature

gradient within this interval was $(-dt/dr) = (27.3/0.156)$
 $= 175 \text{ } ^\circ\text{F/inch}$. The arithmetic mean value of r within this
interval was

$$r_{\text{mean}} = \frac{2.87 + 3.033}{2} = 2.95 \text{ inches.}$$

Substituting these values into Equation (I-1),

$$k'_e = (100.1) \frac{(1.99)}{(2.95)(175)}$$

$$= 0.386 \text{ Btu/hr.ft.}^\circ\text{F.}$$

This value was attributed to the local bed temperature of
 $(93 + 65.7)/2 = 79.3 \text{ } ^\circ\text{F}$. The Reynolds number at that location
was calculated to be 825.

(3) Calculation of Flow Profile and the Reynolds Number

The values of the local mass flow rate, G at $r=0.75$,
1.25,1.75,2.25, and 2.75 inches are approximately related to
the overall mass flow rate, G_o by Equation (III-6) and Equation
(III-7) as follows:

$$G_1 = \frac{(G_o)(35.8)}{3 + (5)\left(\frac{T_1}{T_2}\right)^{1/1.8} + (7)\left(\frac{T_1}{T_3}\right)^{1/1.8} + (9)\left(\frac{T_1}{T_4}\right)^{1/1.8} + (11.8)\left(\frac{T_1}{T_5}\right)^{1/1.8}}$$

.....(III-6)

$$G_2 = (G_1)\left(\frac{T_1}{T_2}\right)^{1/1.8}, \quad G_3 = (G_1)\left(\frac{T_1}{T_3}\right)^{1/1.8}, \quad \text{etc.(III-7)}$$

where G_1, G_2, \dots, G_5 and T_1, T_2, \dots, T_5 are the approximate local mass flow rates and local bed temperatures at $r = 0.75, 1.25, 1.75, 2.25, 2.75$ inches, respectively. (see Chapter III)

In Run 109, The overall mass flow rate, G_o was $1380 \frac{\text{lbs.}}{(\text{hr})(\text{ft}^2)}$, and the values of T_1, T_2, \dots, T_5 were 790, 700, 642, 597, and 561 $^{\circ}\text{R}$, respectively. (see Fig. III-1)

Substituting these values into Equation (III-6),

$$G_1 = \frac{(1380)(35.8)}{3 + (5)\left(\frac{790}{700}\right)^{1/1.8} + (7)\left(\frac{790}{642}\right)^{1/1.8} + (9)\left(\frac{790}{597}\right)^{1/1.8} + (11.8)\left(\frac{790}{561}\right)^{1/1.8}}$$

$$= \frac{(1380)(35.8)}{(41.02)} = 1203 \text{ lbs.}/(\text{hr})(\text{ft}^2)$$

$$G_2 = (1203)\left(\frac{790}{700}\right)^{1/1.8} = 1290 \text{ lbs.}/(\text{hr})(\text{ft}^2)$$

$$G_3 = (1203)\left(\frac{790}{642}\right)^{1/1.8} = 1350 \text{ "}$$

$$G_4 = (1203)\left(\frac{790}{597}\right)^{1/1.8} = 1408 \text{ "}$$

$$G_5 = (1203)\left(\frac{790}{561}\right)^{1/1.8} = 1460 \text{ "}$$

The flow profile in Fig. (III-2) was constructed using the above values of G . The Reynolds number profile was then obtained by calculating $d_p G / \mu$, from the above G and the air viscosity at the local bed temperature. Thus, in Run 109, the bed temperature at $r = 2.10$ inches was 150°F , and the value of G was $1395 \text{ lbs.}/(\text{hr})(\text{ft}^2)$. But μ at 150°F is $0.0477 \text{ lbs}/(\text{hr})(\text{ft})$. This gives the Reynolds number at $r = 2.10$ inches the value of

$$\text{Re} = (0.312)(1395)/(12)(0.0477) = 760.$$

(3) Examples of Estimating the Values of k_e and k'_e

For an illustration of how to use the obtained correlations, the value of k_e is estimated in the following under these conditions:

- packing material: 0.312-inch-diameter alumina balls
- local bed temperature: 200 oF
- fluid: air
- mass flow rate: 2000 lbs/(hr)(ft)²
- volume fraction void: 0.35
- emissivity of packing material: 0.80

The effective conductivity, k_e is given by Equation (V-3),

$$k_e = k_B + (1/11)(C_p \mu)(Re) \dots\dots\dots(V-3)$$

First, the value of k_B is estimated from Figures (V-9) and (V-10).

At 200 oF,

- the solid conductivity, $k_s = 1.7$ Btu/(hr)(ft)(oF)
- the air conductivity, $k_g = 0.018$ "
- or $k_g/k_s = 0.0106$

From the top curve of Fig. (V-9), $(k_B)_c/k_s = 0.113$.

The conduction contribution to the static bed conductivity is then,

$$(k_B)_c = (0.113)(1.7) = 0.192 \text{ Btu}/(\text{hr})(\text{ft})(\text{oF}).$$

The radiation conductivity, k_r is given by Damköler's equation,

or

$$k_r = (0.173)(\epsilon_s)(\delta)(d_p)(4T^3/10^8) \dots\dots\dots(I-30)$$

Figure (V-10) was established assuming that the proportionality constant, s in the above equation was equal to 1. Therefore, $s = 1$ should be used consistently. Also, the volume fraction void was used to approximate the area fraction void originally used in Damköler's equation.

$$k_r = (0.173)(0.80)(0.35)(0.312/12)(4)(660)^3/10^8$$

$$= 0.0145$$

$$k_r/k_s = 0.00852$$

From Figure (V-10), $(k_B)_r/k_s = 0.046$

Or, the radiation contribution to the static bed conductivity is,

$$(k_B)_r = (0.046)(1.7) = 0.078 \text{ Btu/(hr)(ft)(}^\circ\text{F)}.$$

Thus, the static bed conductivity is given by

$$k_B = (k_B)_c + (k_B)_r = 0.192 + 0.078 = 0.270 \text{ Btu/(hr)(ft)(}^\circ\text{F)}.$$

At 200 $^\circ\text{F}$, C_p for air = 0.253 Btu/(lb)($^\circ\text{F}$)

and μ for air = 0.0503 lb/(hr)(ft)

Substituting these values into Equation (V-3), the effective conductivity is obtained as

$$k_e = (0.270) + (1/11)(0.253)(0.0503) \frac{(0.312)(2000)}{(12)(0.0503)}$$

$$= 0.27 + 1.20 = 1.47 \text{ Btu/(hr)(ft)(}^\circ\text{F)}.$$

The wall effective conductivity, k'_e is estimated under the following conditions:

- packing material: 0.282-inch-diameter steel
- local bed temperature: 90 $^\circ\text{F}$
- fluid: air
- mass flow rate: 2000 lb/(hr)(ft)²
- emissivity of packing material: 0.18

The wall effective conductivity is given by Equation (V-5),

$$k'_e = k'_B + (0.01)(C_p \mu)(\text{Re}) \dots\dots\dots(\text{V-5})$$

First, the wall static bed conductivity, k'_B is estimated from Figures (V-9) and (V-10). At 90°F ,

$$\begin{aligned} \text{the solid conductivity, } k_s &= 26.2 \text{ Btu/(hr)(ft)}(^{\circ}\text{F}) \\ \text{the air conductivity, } k_g &= 0.0153 \text{ " " } \\ k_g/k_s &= 0.000585 \end{aligned}$$

From the bottom curve in Figure (V-9), $(k'_{Bc})/k_s = 0.0060$, or the conduction contribution to k'_B is

$$(k'_{Bc}) = (0.0060)(26.2) = 0.157 \text{ Btu/(hr)(ft)}(^{\circ}\text{F}).$$

At the column wall, the area fraction void is nearly 1, and this gives

$$\begin{aligned} k_r &= (0.173)(0.18)(1.0)(0.282/12)(4)(550)^3/10^8 \\ &= 0.00487 \text{ Btu/(hr)(ft)}(^{\circ}\text{F}) \end{aligned}$$

$$k_r/k_s = 0.000186$$

From Fig. (V-10), $(k'_{Br})/k_s = 0.00305$, or the radiation contribution to k'_B is

$$(k'_{Br}) = (0.00305)(26.2) = 0.081 \text{ Btu/(hr)(ft)}(^{\circ}\text{F}).$$

Thus, the wall static bed conductivity, k'_B is given by

$$k'_B = (k'_{Bc}) + (k'_{Br}) = 0.157 + 0.081 = 0.238 \text{ Btu/(hr)(ft)}(^{\circ}\text{F}).$$

At 90°F ,

$$\begin{aligned} C_p \text{ for air} &= 0.25 \text{ Btu/(lb)}(^{\circ}\text{F}) \\ \mu \text{ for air} &= 0.0445 \text{ lb/(hr)(ft)} \end{aligned}$$

Substituting these values into Equation (V-5), the wall effective conductivity, k'_e is given by

$$\begin{aligned} k'_e &= 0.238 + (0.01)(0.25)(0.0445) \frac{(0.282)(2000)}{(12)(0.0445)} \\ &= 0.238 + 0.117 = 0.355 \text{ Btu/(hr)(ft)}(^{\circ}\text{F}). \end{aligned}$$

APPENDIX III

ERROR ANALYSES

The accuracies of various measurements taken in this study are estimated, and their effects on the obtained correlations are discussed in the following:

(1) Effective Conductivity

The calculations of the effective conductivity were carried out through Equation (I-1), or

$$\begin{aligned} k_e &= \frac{q}{(A) (-dt/dr)} \\ &= \frac{q}{(2\pi r)(L) (-dt/dr)} \end{aligned}$$

where the amount of heat input, q was measured with a watt-meter, and both the radial position, r and the temperature gradient, $(-dt/dr)$ were obtained graphically. The length of the calorimeter heater, L was determined by an actual measurement. The watt-meter employed in this study was reportedly calibrated at the Instrument Shop, Electrical Engineering Department, M.I.T., and the accuracy was said to be good to $\pm 0.1\%$. The calorimeter heater was specially tailor-made to assure an even heat flux throughout its heated length of 61 inches, but the 2-inch cold-ends on its top and bottom were expected to draw some heat away from the heated section and cause a small non-uniformity near the both ends. In the calculation of k_e , the total amount of heat input, q was

assumed to be uniformly distributed throughout the total length of the calrod, 65 inches. Since the thermal conductivity of the stainless-steel sheath of the calrod is much larger than the effective conductivity of the bed, this assumption of uniform heat liberation throughout the entire 65 inches, including the total 4-inch non-heated section, is considered reasonable, and the error introduced in the value of q/L by this assumption is estimated to be no larger than 2%. The temperature measurement was carried out with iron-constantan thermocouples, and the EMF registered on a potentiometer was converted to temperature through a standard conversion table. Several trial measurements of the boiling-water temperature by the above procedure checked with an accuracy of $\pm 0.5\%$. Therefore, the total error in the temperature measurement is conservatively estimated at $\pm 1.0\%$. The most error in the values of k_e is believed to come from the graphically obtained r and $(-dt/dr)$. Since the temperature measurement is believed to be accurate to $\pm 1.0\%$, the error in the values of r and $(-dt/dr)$ would largely depend on the accuracies of thermocouple placement in the bed and the graphical differentiation. The position of a thermocouple was determined from the distance between a reference point on the wire outside the column and the outer wall of the column. The distance was measured accurately to $1/32$ -inch, but the wire inside the column may have been slightly disturbed by the packing material and have caused uncertainty of another $1/32$ inch. Therefore, total

1/16-inch uncertainty was believed to exist with the values of the thermocouple locations. The temperature traverses measured with total 30 thermocouples involving 7 different radial positions were plotted on a graph to obtain the radial temperature profile. During this process, the uncertainties associated with the thermocouple locations were partially smoothed out by drawing the best line through the multitude of experimental points. Therefore, the inaccuracy in placing any one particular thermocouple would have affected the final temperature profile only slightly. For this reason, the error in the values of $(r)(-dt/dr)$ is believed to depend mostly on the accuracy of graphical differentiation. Since the error associated with the graphical differentiation under the above circumstances would be essentially a "random error," it is considered reasonable to estimate the accuracy of graphical differentiation through the reproducibility. The results of many repeated measurements of the same temperature gradient were found to agree within $\pm 10\%$. If it is assumed that the error in the values of $(r)(-dt/dr)$ is of the same magnitude as the above reproducibility, the maximum error in the value of k_e is considered to be no larger than $\pm 15\%$. It is seen, therefore, that about 2/3 of the total error in the values of k_e is attributed to the graphical differentiation, where the error is equally likely to occur with either plus or minus sign. Therefore, the accuracy of the final correlation, which was obtained by drawing the best line through a large number of experimental values of k_e as in Figures (IV-1) through (IV-9), is believed to be better than $\pm 15\%$.

(2) Measurement of Air Flow Rate

The flow rates of air were measured with commercial high-precision sharp-edge orifice meters, and the calculations were carried out by the procedures described in an ASTM manual.⁽³⁾ The manometer and pressure gauge readings were believed to be accurate to + 2%. The 3 orifice meters used in this study were checked against one another, and the maximum discrepancy between them was found to be less than +3%. Since the values of the orifice coefficient recommended in the ASTM manual are believed to be accurate to +0.5%, the maximum error in the measured values of air flow rate is conservatively estimated to be less than +5%.

From the measured overall flow rate, the radial flow profile was calculated by the procedures described in Chapter III. The question of whether the calculated profile truly represented the local flow rates or not is beyond the scope of this error analysis, because the true flow profile in a non-isothermal packed bed has never been adequately established. Furthermore, the above question is immaterial from the standpoint of this thesis, because the calculated flow profile was used only for the purpose of correlating the data. As long as the obtained correlation is used consistently according to the original definitions of variables, its accuracy should not be affected by the way the variables were defined originally.

(3) Physical Properties of Materials Used

Various physical properties, such as k_s , k_g , C_p , μ , ϵ , ρ were estimated through the data published in the literature. In all cases, efforts were made to use the best data available, and when necessary, interpolations and extrapolations were carried out as carefully as possible.

The values of the physical properties of various materials used in this study are tabulated in APPENDIX VII, and the sources of the data are therein indicated.

APPENDIX IV

CONDUCTION CONTRIBUTION TO THE STATIC
BED CONDUCTIVITY (Fig. V-9)

(1) Rectangular Close-packing Model

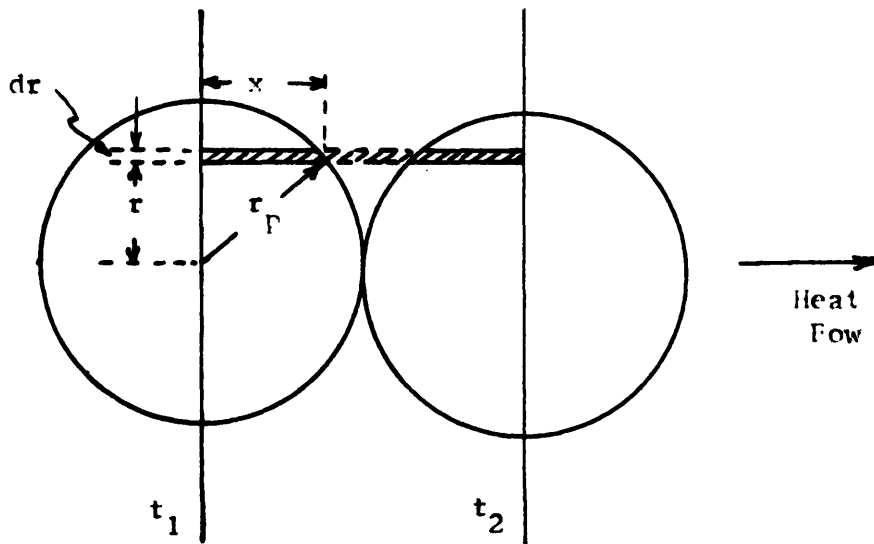


Fig. (A4-1)

Unit Structure of Rectangular
Model (Side View)

A side view of the unit structure of the rectangular close-packing model (Fig. V-8) is shown in Fig. (A4-1). The center-plane temperatures of the two adjacent spheres are assumed to be t_1 , and t_2 , respectively, and uniform throughout on each plane. The heat is assumed to travel in the horizontal direction only through a series of solid- and fluid-phase resistances. Only the molecular conduction is assumed to exist in the fluid phase.

Under the above assumptions, the amount of heat which travels through a differential area dA_s is given by

$$dq = k (dA_s) \frac{t_1 - t_2}{d_p} \dots\dots\dots (A4-1)$$

where

$$\begin{aligned} 1/k &= (1/k_s)(x/r_p) + (1/k_g)(r_p - x)/r_p \\ &= \frac{1}{k_s} \frac{\sqrt{r_p^2 - r^2}}{r_p} + \frac{1}{k_g} \frac{r_p - \sqrt{(r_p^2 - r^2)}}{r_p} \end{aligned} \dots\dots\dots (A4-2)$$

and $dA_s = r d\theta dr$

where θ is the angle in the polar coordinate system.

Substituting Equation (A4-2) into Equation (A4-1), and integrating over the entire major cross-sectional area of a particle, the total amount of heat which travels through a particle is given by

$$q_s = \int_{\theta=0}^{2\pi} \int_{r=0}^{r_p} \frac{-r d\theta dr}{\frac{1}{k_s} \frac{\sqrt{r_p^2 - r^2}}{r_p} + \frac{1}{k_g} \frac{r_p - \sqrt{(r_p^2 - r^2)}}{r_p}} \left(\frac{t_2 - t_1}{d_p} \right) \dots\dots\dots (A4-3)$$

where q_s represents only that portion of heat which travels through the solid-fluid-solid series paths. In addition to this, there is q_v which travels through the fluid path only without involving any solid paths. The ratio of the heat transfer areas available for q_s and q_v is, in the case of a rectangular close-packing model, equal to $(\pi/4)/(1 - \pi/4)$. In other words, approximately 78.6% of the total heat transfer area is available for q_s and the rest for q_v . If the total amount of heat which travels by both

means is denoted by q,

$$q = q_s + q_v = (k'_{Bc})(A) \frac{t_1 - t_2}{d_p} \dots\dots\dots(A4-4)$$

but

$$q_v = (k_g)(A)(0.214) \frac{t_1 - t_2}{d_p} \dots\dots\dots(A4-5)$$

Therefore,

$$q_s = \left[(k'_{Bc}) - (k_g)(0.214) \right] \frac{t_1 - t_2}{d_p} (A) \dots\dots(A4-6)$$

If the total heat-transfer area, A is taken as $(d_p)^2$, Equation (A4-6) is equivalent to Equation (A4-3).

Or,

$$(k'_{Bc}) - (k_g)(0.214) = \frac{1}{(d_p)^2} \int_0^{2\pi} \int_0^{r_p} \frac{r \, d\theta \, dr}{\frac{1}{k_s} \frac{r_p}{\sqrt{r_p^2 - r^2}} + \frac{1}{k_g} \frac{r_p}{\sqrt{r_p^2 - r^2}}}$$

The above integration can be facilitated by substituting

$$\sqrt{r_p^2 - r^2} = x$$

whence $r \, dr = -x \, dx$, and hence

$$(k'_{Bc}) - (k_g)(0.214) = \frac{k_s k_g}{2 d_p} \int_0^{2\pi} \int_{r_p}^0 \frac{-x \, d\theta \, dx}{(k_g - k_s) x + k_s r_p}$$

$$= \frac{k_s k_g (\pi)}{2(k_g - k_s)} \left[1 + \frac{k_s}{k_g - k_s} \ln(k_s/k_g) \right]$$

or

$$(k'_{Bc}) = \frac{k_s k_g (\pi)}{2(k_g - k_s)} \left[1 + \frac{k_s}{k_g - k_s} \ln(k_s/k_g) \right] + (0.214)k_g$$

\dots\dots\dots(A4-7)

Equation (A4-7) may be rearranged to obtain a dimensionless equation as follows:

$$\begin{aligned} \frac{(k'_B)_c}{k_s} &= \frac{(\pi)}{4} \frac{2 k_g}{(k_g - k_s)} \left[1 + \frac{k_s}{k_g - k_s} \ln \left(\frac{k_s}{k_g} \right) \right] + (0.214) \frac{k_g}{k_s} \\ &= \frac{\pi}{4} \frac{2 \left(\frac{k_g}{k_s} \right)}{(1 - k_g/k_s)^2} \left[\frac{k_g}{k_s} - 1 - \ln \left(\frac{k_g}{k_s} \right) \right] + (0.214) \frac{k_g}{k_s} \\ &\dots\dots\dots (A4-8) \end{aligned}$$

Equation (A4-8) is represented by the bottom curve in Figure (V-9), where $(k'_B)_c/k_s$ is plotted against k_g/k_s .

It should be noted that Equation (A4-8) represents both Mechanisms No. 2 and No.4, because the total amount of heat which travels through the solid-fluid-solid series paths as well as the fluid path alone was accounted for in the derivation. However, the term which represents the conduction through the fluid path alone is given by $(0.214)(k_g)$ in Equation (A4-8), and this is not equal to Equation (I-29), where Mechanism No.2 is represented by $(k_g)(\delta)^{1.3}$. This difference is believed to arise from the fact that Equation (I-29) was obtained from an experiment where Mechanism No. 2 was the only transfer mechanism present in the system, i.e. Mechanism No. 4 was not present. Under such conditions, the molecular conduction which takes place in the entire void space is observed as a whole, and consequently

Equation (I-29) represents the second term of Equation (A4-8) plus some extra contribution. This extra contribution is none other than what serves in Mechanism No. 4 as the bridge between two solid particles. Therefore, if Mechanism No. 4 is absent as in the cases of significantly different solid and fluid temperatures, then, Mechanism No. 2 may be expressed by Equation (I-29), but when Mechanism No. 4 is also present as in the cases of nearly equal fluid and solid temperatures, Mechanisms No. 2 and No. 4 are not completely separable, and it is advantageous to express them together as in Equation (A4-8). The same idea is also true with the tetrahedral close-packing model, which is derived in the following section.

(2) Tetrahedral Close-packing Model

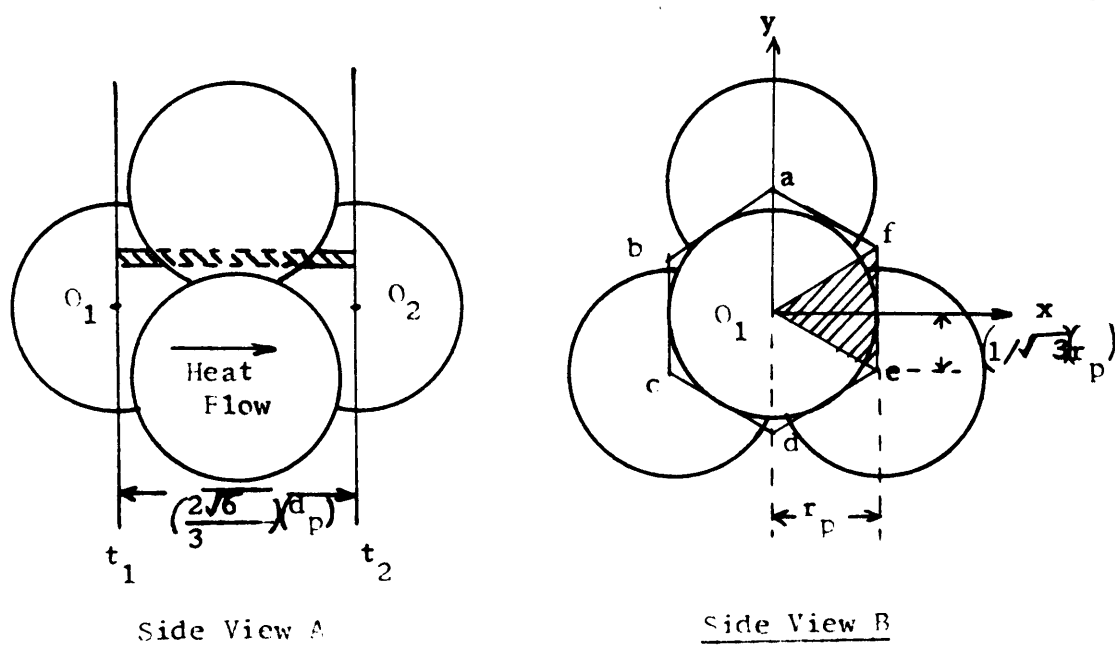


Fig. (A4-2)

Unit Structure of Tetrahedral Model

2 different side views of the unit structure of the tetrahedral close-packing model is shown in Fig. (A4-2). In Side View A, the heat transfer path is in parallel with the paper, but in Side View B the same is perpendicular to the paper. As before, the heat is assumed to travel in one direction only, horizontally in Side View A and perpendicularly in Side View B, through either a solid-fluid-solid series path or a fluid path alone. The center-plane temperatures of the two symmetric neighboring particles, O_1 and O_2 are assumed to be t_1 and t_2 , respectively, and uniform throughout on each plane.

Under the above assumptions, the amount of heat which travels through a differential heat transfer area, dA is given by

$$dq = \frac{dA}{\frac{1}{k_s} \left(\frac{\Delta x_s}{\Delta x} \right) + \frac{1}{k_g} \left(\frac{\Delta x_g}{\Delta x} \right)} \left(\frac{t_1 - t_2}{\Delta x} \right) \dots\dots(A4-9)$$

where Δx is the distance between O_1 and O_2 , or $(2/3)\sqrt{6} d_p$, and Δx_s and Δx_g are the lengths of solid and fluid paths, respectively, which occur in series on a particular heat transfer path between O_1 and O_2 . Integrating Equation (A4-9) over the area abcdef shown in Side View B, the total amount of heat which travels through this area is given by

$$q = \int_A \frac{dA}{(1/k_s)(\Delta x_s/\Delta x) + (1/k_g)(\Delta x_g/\Delta x)} \left(\frac{t_1 - t_2}{\Delta x} \right)$$

$$= (k_B)_c (A) \left(\frac{t_1 - t_2}{\Delta x} \right) \dots\dots\dots(A4-10)$$

Or, $(k_B)_c = (1/A) \int_A \frac{dA}{(1/k_s)(\Delta x_s/\Delta x) + (1/k_g)(\Delta x_g/\Delta x)}$

$$\frac{(k_B)_c}{k_s} = \frac{1}{A} \int_A \frac{dA}{\frac{\Delta x_s}{\Delta x} + \frac{k_s}{k_g} \left(\frac{\Delta x_g}{\Delta x} \right)} \dots\dots(A4-11)$$

It should be noted that the area \overline{abcdef} is a basic unit, and the repetition of the area constitutes the entire heat-transfer area in the bed. This basic unit includes the solid-fluid-solid series paths as well as the fluid path alone, and therefore, Mechanisms No. 2 and No. 4 are already included in Equation (A4-11).

For the tetrahedral close-packing model, Equation (A4-11) can not be integrated by any simple analytical method, and therefore, numerical integration must be used in this case. The base unit \overline{abcdef} may be further divided into 6 identical sub-base areas, one of which is indicated by the shaded area in Side View B, Fig. (A4-2).

Referring to the shaded area $\overline{O_1 ef}$ in Side View B, the values of $\Delta x_s/\Delta x$ and $\Delta x_g/\Delta x$ at any point within this area may be expressed in terms of its x, y coordinates as follows:

$$\frac{\Delta x_s}{\Delta x} = \frac{\sqrt{r_p^2 - y^2 - x^2} + \sqrt{r_p^2 - (r_p/\sqrt{3} + y)^2 - (r_p - x)^2}}{\frac{2\sqrt{6}}{3} (r_p)}$$

$$= \frac{\sqrt{r_p^2 - y^2 - x^2} \sqrt{-r_p^2/3 - y^2 - 2r_p y/\sqrt{3} + 2r_p x - x^2}}{\frac{2\sqrt{6}}{3} (r_p)} \dots\dots\dots (A4-12)$$

and $\Delta x_g / \Delta x = 1 - \Delta x_s / \Delta x \dots\dots\dots (A4-13)$

where $\Delta x_s / \Delta x$ is given by Equation (A4-12).

Equations (A4-11) and (A4-12) may be numerically integrated over the area $\overline{O_1ef}$ to obtain the relation between $(k_B)_c/k_s$ and k_g/k_s .

In the present work, the area $\overline{O_1ef}$ was divided into numerous small incremental square areas of $r_p/30 \times r_p/30$ size. These incremental squares were numbered 1.....n along the x-axis, and 1.....m along the y-axis.

$$0 \leq n \leq 30$$

$$-17.3 \leq m \leq 17.3$$

$$\begin{aligned} x &= (r_p/30) n \\ y &= (r_p/30) m \\ dx &= (r_p/30)(\Delta n) \dots\dots\dots(A4-14) \\ dy &= (r_p/30)(\Delta m) \end{aligned}$$

Substituting Equation (A4-14) into Equations (A4-11) through (A4-13), we obtain

$$\frac{(k_B)_c}{k_s} = 0.00314 \int_1^m \int_1^n \frac{\Delta n \Delta m}{\sqrt{1 - \frac{n^2}{900} - \frac{m^2}{900} + \frac{n}{15} - \frac{m^2}{3} - \frac{m}{900} - \frac{m}{26} + \left(\frac{r_p}{k_g}\right) \left[1.632 - \sqrt{1 - \frac{m^2}{900} - \frac{n}{15} - \frac{m^2}{3} - \frac{m}{900} - \frac{m}{26} \right]}} \dots\dots\dots(A4-15)$$

At a fixed value of (k_s/k_g) and "n", Equation (A4-14) was evaluated at various values of "m", and these were summed between $m = -n/\sqrt{3}$ and $m = n/\sqrt{3}$. The similar summation was carried out at the same fixed value of k_s/k_g for each value of "n" between $n=0$ and $n=30$, and the sums were added together. The grand total represented $(k_{Bc})/k_s$ for that particular value of k_g/k_s . Next, another value of k_g/k_s was picked, and the above procedures were repeated to obtain the corresponding value of $(k_{Bc})/k_s$. When a sufficient number of different values of k_g/k_s are thus covered, the results may be plotted in a smooth curve. The top curve in Fig. (V-9) represents the results of the above numerical integration. The computation sheets which contain all the numbers obtained during the numerical integration process are in the custody of Prof. R. F. Baddour.

APPENDIX V

MATHEMATICAL DERIVATIONS

(1) Separate Postulation of K_s and K_g

Equations (I-2) and (I-3) may be integrated analytically under the following assumptions: ⁽⁵¹⁾ The system is a symmetric cylinder and is in a steady-state without any chemical reactions. The fluid flow is unidirectional with negligible net radial components. The axial conduction both in the solid and fluid phases are negligible and all the physical parameters are constant, including the values of K_s and K_g . Under these conditions, Equations (I-2) and (I-3) are reduced to

$$G_o C_p \int_0^r r \frac{\partial t_g}{\partial x} dr - K_g r \frac{\partial t_g}{\partial r} - K_s r \frac{\partial t_s}{\partial r} = 0 \quad \dots(A5-1)$$

$$K_s r \frac{\partial t_s}{\partial r} - h \int_0^r r (t_s - t_g) dr = 0 \quad \dots\dots\dots(A5-2)$$

where the boundary conditions are

$$t_g = t_o, \quad x = 0 \quad (0 < r < R)$$

$$t_s = t_w, \quad r = R \quad (0 < x < L)$$

Let

$$t_s = U_o(x) + \sum_{n=1}^{\infty} U_n(x) J_o(a_n r) \quad \dots\dots\dots(A5-3)$$

$$t_g = V_o(x) + \sum_{n=1}^{\infty} V_n(x) J_o(a_n r)$$

where U_n, V_n are functions of x to be determined.

From the boundary conditions,

$$(t_s)_{r=R} = U_0(x) + \sum_{n=1}^{\infty} U_n(x) J_0(a_n R) = t_w \dots\dots\dots (A5-4)$$

set

$$U_0(x) = t_w, \text{ and } J_0(a_n R) = 0$$

whence

$$a_n = \alpha_n / R \quad \text{where } \alpha_n: \text{nth root of } J_0(\alpha_n) = 0$$

Also

$$(t_g)_{x=0} = t_0 = V_0(0) + \sum V_n(0) J_0(a_n r) \dots\dots\dots (A5-5)$$

$t_0 - V_0(0)$ is a constant and may be expanded in a

Bessel series:

$$t_0 - V_0(0) = \sum A_r J_0(\alpha_r r) \dots\dots\dots (A5-6)$$

$$\alpha_r: \text{ rth root of } J_0(\alpha_r) = 0$$

Comparing (A5-5) and (A5-6), (see Reference No. 52)

$$A_r = V_n(0) = \frac{2 \int_0^r y [t_0 - V_0(0)] J_0(\alpha_n y) dy}{[J_1(a_n R)]^2} \dots\dots\dots (A5-7)$$

where $y = r/R$

$$\text{Or, } V_n(0) = A_r = \frac{2[t_0 - V_0(0)]}{\alpha_n J_1(\alpha_n)} \dots\dots\dots (A5-8)$$

Substituting (A5-3) into (A5-2),

$$\begin{aligned} -K_s r \sum U_n a_n J_1(a_n r) - h \int_0^r [(U_0 - V_0) + \sum (U_n - V_n) J_0(a_n r)] r dr = 0 \\ -K_s r \sum U_n a_n J_1(a_n r) - \frac{hr^2}{2} (U_0 - V_0) + h \sum (U_n - V_n) \frac{r}{a_n} J_1(a_n r) = 0 \end{aligned} \dots\dots\dots (A5-9)$$

Equating the coefficients of like terms in J_1 , the following relationships can be arrived at for U_n and V_n :

$$U_o = V_o = t_w \quad (\text{Recalling Eq. A5-4}) \quad \dots\dots(A5-10)$$

$$U_n = \frac{h}{h + K_s a_n^2} (V_n) \quad \dots\dots\dots(A5-11)$$

Substituting (A5-3) into (A5-1),

$$\frac{G C_p V_n' r}{a_n} J_1(a_n r) + K_s r \sum U_n a_n J_1(a_n r) + K_g r \sum V_n a_n J_1(a_n r) = 0 \dots(A5-12)$$

Equating the coefficients of like terms in J_1 , further relationships for U_n and V_n can be found:

$$K_s U_n a_n + K_g V_n a_n = \frac{-G C_p V_n'}{a_n} \quad \dots\dots\dots(A5-13)$$

Combining (A5-11) and (A5-13),

$$\frac{V_n'}{V_n} = \frac{-a_n^2 (h K_s + h K_g + K_g K_s a_n^2)}{G C_p (h + K_s a_n^2)} \quad \dots\dots\dots (A5-14)$$

Integrating:

$$V_n(x) = V_n(0) \exp \left[\frac{-a_n^2 x (h K_s + h K_g + K_g K_s a_n^2)}{G C_p (h + K_s a_n^2)} \right] \quad \dots\dots\dots (A5-15)$$

The values of V_n from (A5-8), (A5-10), and (A5-15) are substituted in the expressions for the fluid temperature at any position in the bed, t_g to obtain

$$t_g = t_w + \sum_{n=1}^{\infty} \frac{2(t_o - t_w)}{d_n J_1(d_n)} J_0(a_n r) \exp \left[\frac{-a_n^2 x (hK_s + hK_g + K_g K_s a_n^2)}{G_o C_p (h + K_s a_n^2)} \right]$$

.....(A5-16)

The values of t_s may be obtained from Equations (A5-10), (A5-11), and (A5-16).

(2) "Combined" Effective Conductivity, k_e

Neglecting axial conduction, and assuming a unidirectional fluid flow and constant k_e , C_p , and G_o , Equation (I-4) may be reduced to the following equation for a steady-state operation in a cylindrical bed with no chemical reactions: (k_a : constant k_e)

$$\frac{\partial t}{\partial x} = \frac{k_a}{G_o C_p} \left(\frac{1}{r} \frac{\partial t}{\partial r} + \frac{\partial^2 t}{\partial x^2} \right) \dots\dots\dots(A5-17)$$

The boundary conditions are

- (1) t is finite at $r = 0$ ($0 \leq x \leq L$)
- (2) $t = t_o$ at $x = 0$ ($0 \leq r < R$)
- (3) $k \left(\frac{\partial t}{\partial r} \right)_{r=R} = h_w (t_w - t_{r=R})$ (A5-18)

Or alternately (4) $t = t_w$ at $r = R$ ($0 \leq x \leq L$)

Equation (A5-17) may be solved by separation of variables to obtain the general solution as follows:

$$\frac{t_w - t}{t_w - t_o} = e^{\frac{-\alpha^2 k_a x}{C_p G_o R^2}} \left[C_1 J_0(\alpha \xi) + C_2 Y_0(\alpha \xi) \right] \dots\dots\dots (A5-19)$$

where $\xi = r/R$

From the boundary condition (1), $C_2 = 0$ in order to make t finite at $\xi = 0$ between $x = 0$ and L .

From the boundary condition (3),

$$k_a \left(\frac{\partial t}{\partial r} \right)_{r=R} = h_w (t_w - t_{r=R})$$

Differentiating Equation (A5-19),

$$\begin{aligned} \left(\frac{\partial t}{\partial r} \right)_{r=R} &= \frac{(t_w - t_o)}{R} e^{\frac{-\alpha^2 k_a x}{C_p G_o R^2}} C_1 \alpha J_1(\alpha) \\ &= \frac{h_w}{k_a} (t_w - t_o) e^{\frac{-\alpha^2 k_a x}{C_p G_o R^2}} C_1 J_1(\alpha) \end{aligned}$$

Or
$$\frac{J_0(\alpha)}{\alpha J_1(\alpha)} = \frac{k_a}{h_w R} = m \dots\dots\dots (A5-20)$$

There are an infinite number of α 's which satisfy Equation (A5-20), and therefore, Equation (A5-19) is given by

$$\frac{t_w - t}{t_w - t_o} = \sum_{n=1}^{\infty} e^{\frac{-\alpha_n^2 k_a x}{C_p G_o R^2}} C_n J_0(\alpha_n \xi) \dots\dots\dots (A5-21)$$

Now, from the boundary condition (2),

$$1 = \sum_{n=1}^{\infty} C_n J_0(\alpha_n \xi)$$

Or,

$$C_n = \frac{2}{\alpha_n J_1(\alpha_n) \left[\left(\frac{J_0(\alpha_n)}{J_1(\alpha_n)} \right)^2 + 1 \right]} \dots\dots (A5-22)$$

(see Reference No. 24)

Substituting Equation (A5-22) into (A5-21), the final solution is given by

$$\frac{t_w - t}{t_w - t_o} = \sum_{n=1}^{\infty} \frac{2 J_0(\alpha_n \xi)}{\alpha_n J_1(\alpha_n) \left[\left(\frac{J_0(\alpha_n)}{J_1(\alpha_n)} \right)^2 + 1 \right]} e^{\frac{-k_a \alpha_n^2 x}{C_p G_o R^2}} \dots\dots (A5-23)$$

where

α_n is the nth root of

$$\frac{J_0(\alpha_n)}{\alpha_n J_1(\alpha_n)} = \frac{k_a}{h_w R} = m \dots\dots (A5-20)$$

and $\xi = r/R$

If boundary condition (4) is used instead of (3), the eigenvalue, α_n is defined by $J_0(\alpha_n) = 0$, and the solution of Equation (A5-17) is given by

$$\frac{t_w - t}{t_w - t_o} = \sum_{n=1}^{\infty} \frac{2 J_0(\alpha_n \xi)}{\alpha_n J_1(\alpha_n)} e^{\frac{-k_a \alpha_n^2 x}{C_p G_o R^2}} \dots\dots (A5-24)$$

and $J_0(\alpha_n) = 0 \dots\dots (A5-25)$

and $\xi = r/R$

APPENDIX VI

CALCULATIONS OF EQUIVALENT WALL COEFFICIENT,
AVERAGE EFFECTIVE CONDUCTIVITY, & MEAN HEAT TRANSFER
COEFFICIENT

(1) Calculation of Wall Coefficient, h_w

The results of the present investigation show that the local effective conductivity is given by

$$k_e = k_B + (1/11)(C_p \mu)(Re) \dots\dots\dots(V-3)$$

for anywhere outside a 1/2-particle-diameter distance from the column wall, whereas the same is given by

$$k'_e = k'_B + (0.01)(C_p \mu)(Re) \dots\dots\dots(V-5)$$

for the region within a 1/2-particle-diameter interval from the column wall.

These equations were originally designed to be used for the local effective conductivity, but they may be used for an approximate estimation of an average effective conductivity, by substituting the mean physical properties into the equations.

A group of authors, such as Yagi and Wakao,^(63,64) assume that a single value of an average effective conductivity applies to the entire bed, but there is a finite resistance at zero distance from the column wall, which is expressed by wall coefficient, h_w .

Illustrated in the following is an approximate method of calculating the Yagi-type wall coefficient, h_w through Equations (V-3) and (V-5).

Equation (V-5) states that the resistance to heat flow is greater within the near-wall region (i.e. 1/2-particle-diameter interval from the column wall) than in the interior of the bed. On the other hand, the assumption of Yagi and others is that the resistance is uniform throughout the bed, but there is an additional resistance at zero distance from the wall. For the purpose of an approximation, if the amount of heat gain by the fluid which flows within a 1/2-particle-diameter interval from the column wall is neglected in comparison with the total heat input, and if the heat transfer area within the annular space (1/2-particle-diameter distance from the wall) is assumed to be equal to the column-wall area, the relation between h_w and (k'_e) is given by

$$\frac{r_p}{k'_e} \approx \frac{r_p}{k_e} + \frac{1}{h_w}$$

Or,

$$h_w \approx \frac{1}{(r_p) \left[\frac{1}{k'_e} - \frac{1}{k_e} \right]} \dots\dots (A6-1)$$

The above approximation is considered reasonable, because the fluid which flows in the immediate vicinity of the column wall rapidly reaches the wall temperature after a short distance

from the inlet end, and the amount of heat gain by it is insignificant thereafter in comparison with the heat gain by the fluid in the interior of the bed. Since h_w reported in the literature was obtained in general from an overall heat balance of a considerably tall column, the above approximation should be particularly suited for an estimation of h_w to be compared with the literature values.

(2) Calculation of Average Effective Conductivity

A group of authors, such as Singer and Wilhelm,⁽⁵¹⁾ experimentally obtained an average effective conductivity assuming that a single value of k_a applied to the entire column. Under such an assumption, the temperature within a cylindrical bed is given by

$$\frac{t_w - t}{t_w - t_o} = \sum_{n=1}^{\infty} \frac{2 J_0(\alpha_n \xi)}{\alpha_n J_1(\alpha_n)} e^{\frac{-k_a \alpha_n^2 x}{C_p G_o R^2}} \dots\dots(A5-24)$$

$$J_0(\alpha_n) = 0 \dots\dots(A5-25)$$

$$\xi = r/R$$

Then, the average exit temperature of the bulk fluid is given

by

$$(t_{\text{exit}})_{\text{ave}} = \frac{\int_0^R C_p G_o t 2 \pi r dr}{\pi R^2 G_o C_p} = \int_0^1 2 t \xi d \xi \dots\dots(A6-2)$$

But from Equation (A5-24),

$$t_{\text{exit}} = t_w - (t_w - t_o) \sum_{n=1}^{\infty} \frac{2 J_0(\alpha_n)}{\alpha_n J_1(\alpha_n)} e^{\frac{-k_a \alpha_n^2 L}{C_p G_o R^2}} \dots (A6-3)$$

Substituting (A6-3) into (A6-2), and integrating, we obtain

$$(t_{\text{exit}})_{\text{ave}} = t_w - (t_w - t_o) \sum_{n=1}^{\infty} \left[\frac{4 e^{\frac{-k_a \alpha_n^2 L}{C_p G_o R^2}}}{\alpha_n^2} \right] \dots (A6-4)$$

and $J_0(\alpha_n) = 0$

In order to obtain a similar expression from Equations (V-3) and (V-5), it is best to convert k'_e into an equivalent h_w by the method described in the preceding section. The wall coefficient, h_w so obtained is used together with k_e calculated from Equation (V-3) to express the average bulk temperature of the exiting fluid. By the same procedures as were used to derive Equation (A6-4), the exiting fluid temperature expressed by Equations (A5-23) and (A5-20) is averaged by integrating over the entire cross-sectional area of the bed. As the result, we obtain

$$(t_{\text{exit}})_{\text{ave}} = t_w - (t_w - t_o) \sum_{n=1}^{\infty} \frac{4}{a_n^2 (m^2 a_n^2 + 1)} e^{\frac{-k_e a_n^2 L}{C_p G_o R^2}} \dots (A6-5)$$

$$m = \frac{J_0(a_n)}{a_n J_1(a_n)} = \frac{k_e}{h_w R}$$

Note that k_e is originally a local effective conductivity, but in Equation (A6-5), it is used as an average effective conductivity based on the mean physical properties of the bed.

Equating Equations (A6-4) and (A6-5), we obtain

$$\sum_{n=1}^{\infty} \frac{1}{\alpha_n^2} e^{-\frac{k_a \alpha_n^2 L}{C_p G_o R^2}} = \sum_{n=1}^{\infty} \frac{1}{\alpha_n^2 (m^2 \alpha_n^2 + 1)} e^{-\frac{k_e \alpha_n^2 L}{C_p G_o R^2}} \dots\dots\dots (A6-6)$$

For a sufficiently tall column, only the first terms in the infinite series are important. Or,

$$\ln (1/\alpha_1^2) - \frac{k_a \alpha_1^2 L}{C_p G_o R^2} = \ln \frac{1}{(m^2 \alpha_1^2 + 1) \alpha_1^2} - \frac{k_e \alpha_1^2 L}{C_p G_o R^2}$$

$$\frac{k_a \alpha_1^2 L}{C_p G_o R^2} = \frac{k_e \alpha_1^2 L}{C_p G_o R^2} + \ln \frac{(m^2 \alpha_1^2 + 1) \alpha_1^2}{\alpha_1^2} \dots\dots (A6-7)$$

but $J_0(\alpha_1) = 0$
 or $\alpha_1 = 2.41$

Therefore,

$$k_a = (k_e) \frac{\alpha_1^2}{5.81} + \frac{C_p G_o R^2}{(5.81)(L)} \ln \frac{\alpha_1^2 (m^2 \alpha_1^2 + 1)}{5.81} \dots\dots\dots (A6-8)$$

If L is large, usually the second term is not important, or

$$k_a = (k_e) \left(\frac{a_1^2}{5.81} \right) \dots\dots\dots(A6-9)$$

and
$$\frac{J_0(a_1)}{a_1 J_1(a_1)} = \frac{k_e}{h_w R}$$

But, from Equation (A6-1),

$$h_w \approx \frac{1}{r_p \left[\frac{1}{k'_e} - \frac{1}{k_e} \right]}$$

Or,
$$\frac{J_0(a_1)}{a_1 J_1(a_1)} = (k_e)(d_p/D_t) \left[\frac{1}{k'_e} - \frac{1}{k_e} \right] \dots\dots(A6-10)$$

Equations (A6-9) and (A6-10) may be used to calculate k_a from k_e and k'_e as expressed by Equations (V-3) and (V-5). For an illustration, the average effective conductivity, k_a and the corresponding value of the modified Peclet number are calculated for a cylindrical bed packed with 1/8-inch-diameter alumina balls and flowed with air at an average bed temperature of 200 °F. The d_p/D_t in this case is assumed to be 0.04. Under these conditions, Equation (V-3) and (V-5) give

$$k_e = 0.23 + 0.00116 Re$$

$$k'_e = 0.19 + 0.000127 Re$$

First, the average effective conductivity under the static condition is calculated. From Equation (A6-10),

$$\frac{J_0(a_1)}{a_1 J_1(a_1)} = (0.23)(0.04) \left[\frac{1}{0.19} - \frac{1}{0.23} \right]$$

whence $a_1 = 2.37$

From Equation (A6-9),

$$k_a = (0.23) \left[\frac{(2.37)^2}{5.81} \right] = \underline{0.22} \text{ Btu/(hr)(ft)(}^\circ\text{F)}$$

Now, at $Re = 1000$, Equations (V-3) and (V-5) give

$$k_e = 1.39$$

$$k'_e = 0.317$$

Or,

$$\begin{aligned} \frac{J_0(a_1)}{a_1 J_1(a_1)} &= (1.39)(0.04) \left[\frac{1}{0.317} - \frac{1}{1.39} \right] \\ &= 0.135 \end{aligned}$$

whence $a_1 = 2.11$

$$\text{Or, } k_a = (1.39) \left[\frac{(2.11)^2}{5.81} \right] = \underline{1.06} \text{ Btu/(hr)(ft)(}^\circ\text{F)}$$

The turbulent-diffusion contribution, k_{td} is then

$$k_{td} = 1.06 - 0.22 = 0.84 \text{ Btu/(hr)(ft)(}^\circ\text{F)}$$

The modified Peclet number is then given by

$$Pe = \left(\frac{C_p \mu}{k_{td}} \right) (Re) = \left(\frac{0.0127}{0.84} \right) (1000) = \underline{15.2}$$

(3) Calculation of Mean Heat Transfer Coefficient, h_o

The average effective conductivity as calculated from Equations (A6-9) and (A6-10) may be converted to a mean heat transfer coefficient, h_o through the formula given in page 291, McAdams Heat Transmission, ⁽³⁹⁾ or

$$h_o = 5.79 \frac{k_a}{D_t} + (0.00116) \frac{Re}{\left(\frac{p}{D_t}\right)(L)} \dots\dots(A6-11)$$

The values of h_o were obtained through Equations (A6-9), (A6-10), and (A6-11) and were compared in Figure (V-4) with the values calculated from Leva's correlation. ^(32,33,34)

APPENDIX VII

PHYSICAL PROPERTIES OF PACKING MATERIALS
AND AIR

(1) Thermal Conductivities

The values of k_s and k_g used in the present work are shown graphically in Figures (A7-1) and (A7-2). Except for the alumina balls, the data given in McAdam's Heat Transmission⁽³⁹⁾ were used. k_s for soft glass was assumed to be 0.44 Btu/(hr)(ft)(°F), regardless of the temperature level. The values of k_s for the alumina balls were based on the data of Aluminum Company of America.

(2) Air Viscosity and Heat Capacity

The values of air viscosity, μ and heat capacity, C_p were obtained from McAdam's Heat Transmission.⁽³⁹⁾ The values of μ are shown in Figure (A7-3).

(3) Emissivity

The values of the total emissivity, used in the present work are shown in Figure (A7-4). These were based on the data given in McAdam's Heat Transmission,⁽³⁹⁾ but the values for the

mild steel were obtained from the data of Wilkes.⁽⁵⁸⁾

In all cases, a linear interpolation was performed, and the extrapolation for the aluminum balls was carried out according to the general rule that the total emissivity of a metallic material is approximately proportional to the absolute temperature.⁽³⁹⁾

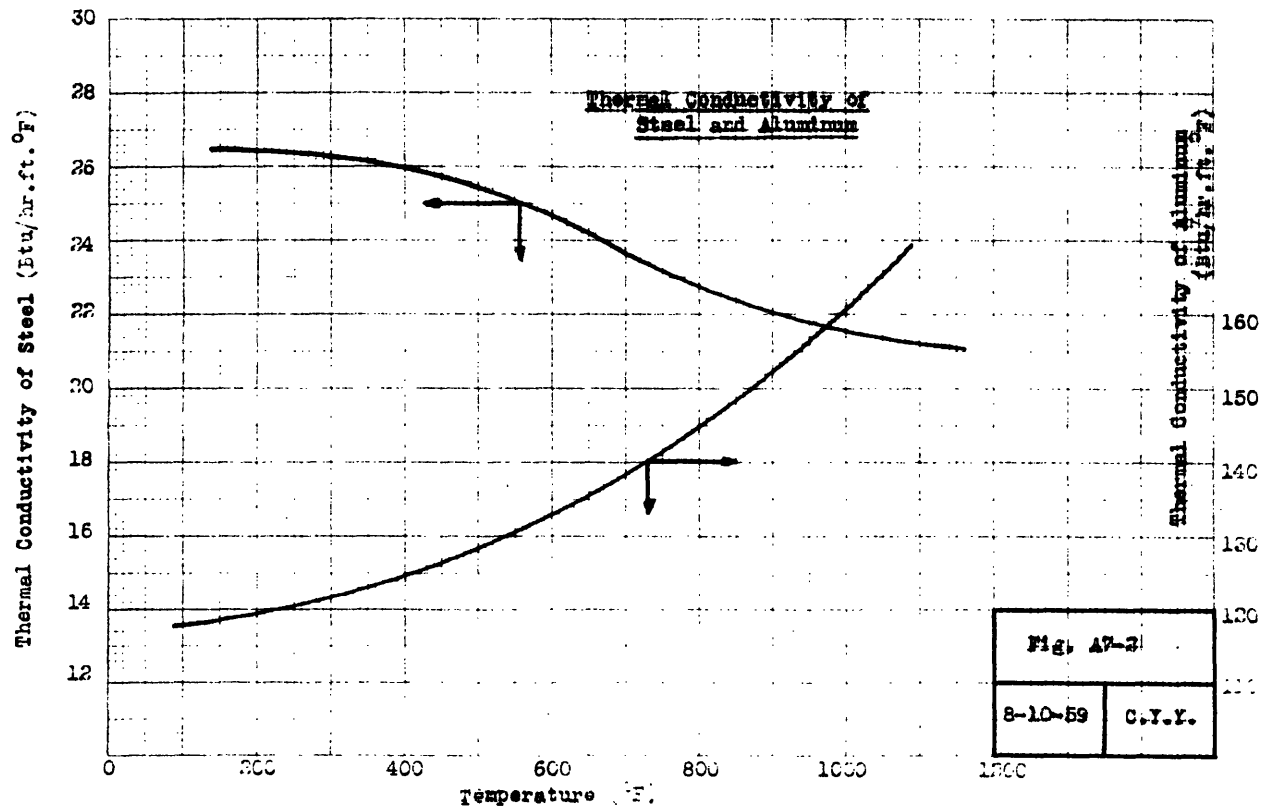
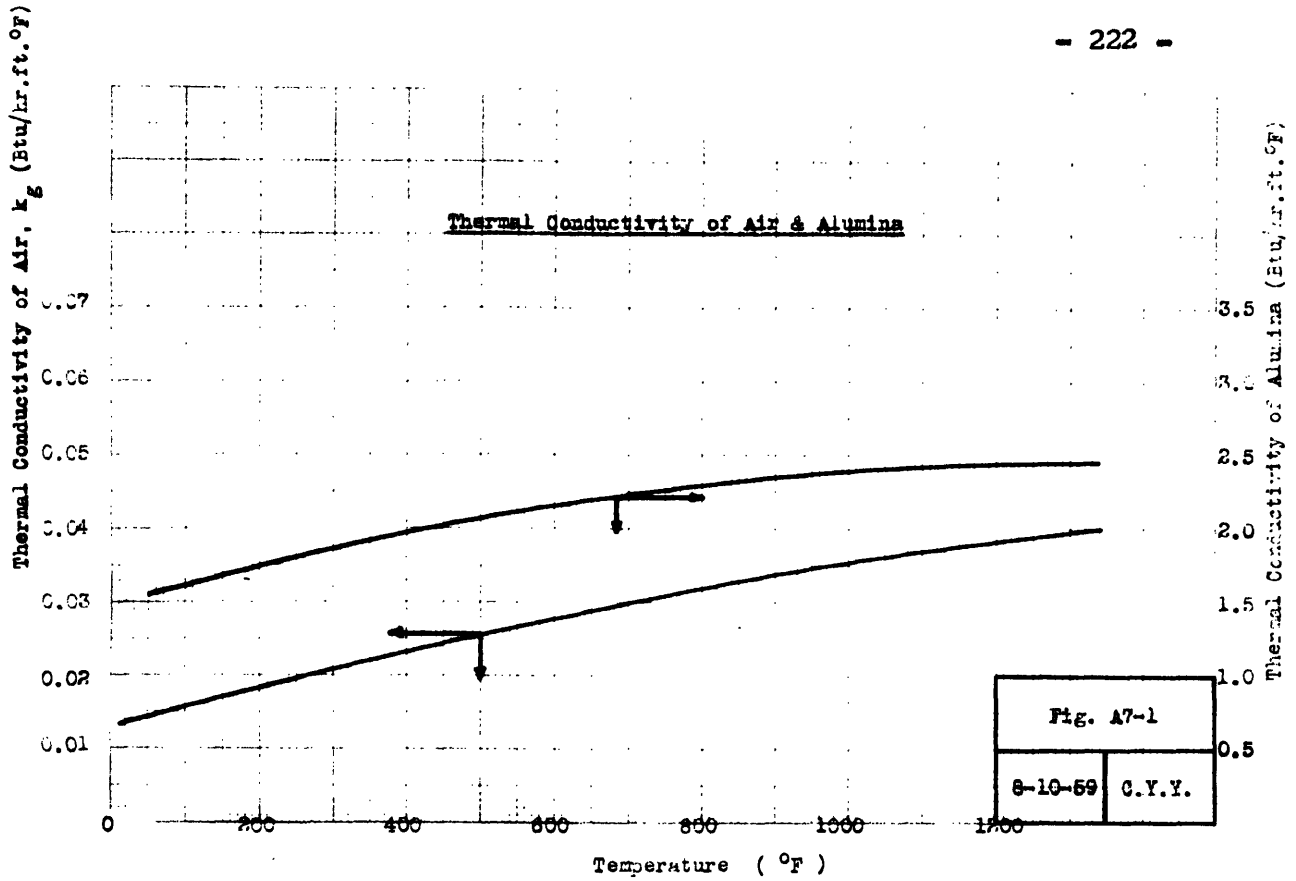
(4) Specific Gravity and Average Fraction Void of Packing Materials

The values of specific gravity were obtained from Perry's Handbook,⁽⁴²⁾ and the values of volumn fraction void, δ were obtained by actual measurement. The average values of δ for various packing materials are shown in the following:

Table (A7-1)

Specific Gravity & Average Fraction Void of Packing Materials

	<u>0.312"</u> <u>Alumina</u>	<u>0.165"</u> <u>Alumina</u>	<u>0.282"</u> <u>Steel</u>	<u>0.141"</u> <u>Steel</u>	<u>0.250"</u> <u>Aluminum</u>	<u>0.236"</u> <u>Glass</u>
Sp.Gr.	3.86	3.86	7.83	7.83	2.70	2.20
δ	0.37	0.35	0.36	0.34	0.35	0.36



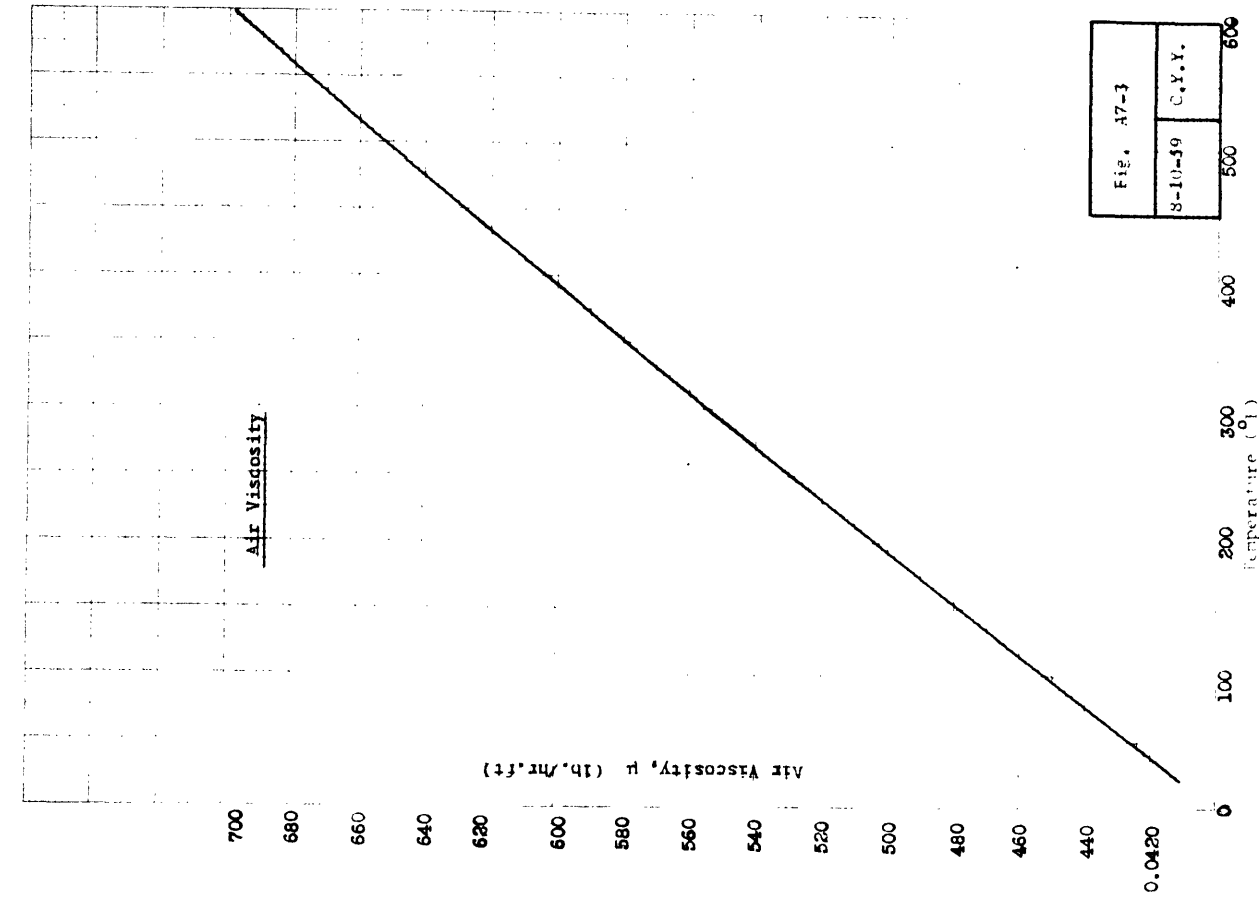


Fig. A7-3	
8-10-59	C.Y.Y.

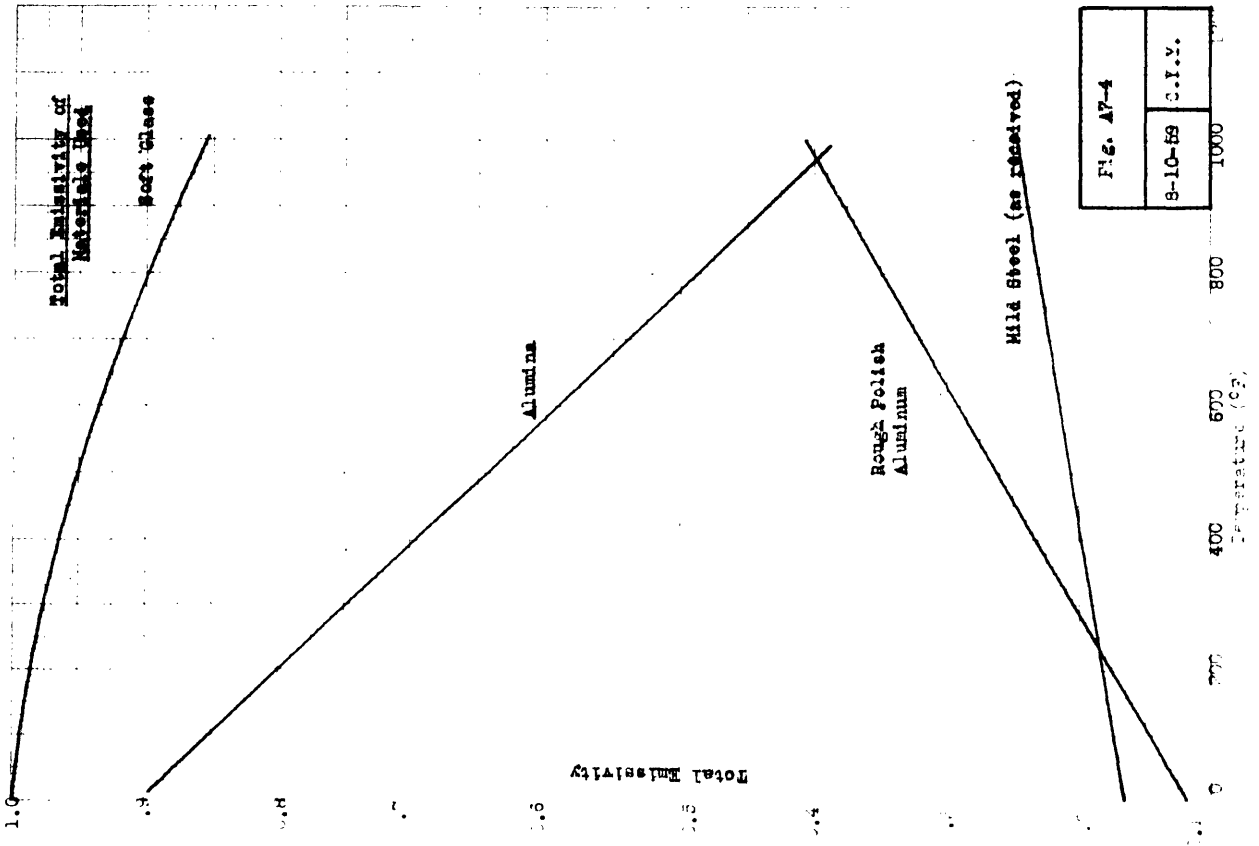


Fig. A7-4	
9-10-59	C.Y.Y.

APPENDIX VIII

FILM COEFFICIENT BETWEEN FLUID AND PACKED SOLIDS & AXIAL EFFECTIVE CONDUCTIVITY

(1) Film Coefficient between Fluid and Packed Solids

Glaser and Thodos⁽²³⁾ studied the heat transfer rate between packed solids and flowing gas. They used electrically heated 1/4-inch-diameter pellets, and heat was removed by the flowing gas. They correlated the data in terms of J-factor as follows:

$$\frac{j}{j_{h_o}} = 1 + \sqrt{\frac{A_p}{D_t}} \log \frac{4984}{(Re_h)^{0.933}} \dots\dots(A8-1)$$

where

$$j = \left(\frac{h}{C_p G_o}\right) \left(\frac{C_p \mu}{k}\right)^{2/3}, \text{ and } j_{h_o} = \frac{0.535}{Re_h^{0.30} - 1.6}$$

The Reynolds number was defined by

$$Re_h = \frac{\sqrt{A_p} G_o}{\mu(1-\delta) \phi} \dots\dots\dots(A8-2)$$

where ϕ is a shape factor which is equal to 1 for spheres.

The Reynolds number was varied between 1,000 and 10,000.

Baumeister and Bennett⁽⁵⁾ generated heat within a packed bed with induction coils, and measured the heat transfer rate between the 1/4-inch-diameter packed solids and flowing air.

They varied the Reynolds number between 200 and 10,400. The data were correlated in terms of J-factor as follows:

$$j = a Re^b \dots\dots\dots (A8-3)$$

$$a = 0.918 \left[1 + 0.0148 e^{0.565(18 - \frac{D_t}{d_p})} \right]$$

$$b = -0.267 - \frac{0.257}{\frac{D_t}{d_p} - 8.70}$$

Gamson and coworkers^(21,22) performed transient mass-transfer experiments in an adiabatic tower filled with wet porous particles. The Reynolds number was varied between 60 and 4000. They reported the results in terms of j and are correlated by

$$j = 1.06 \left(\frac{d_p G_o}{\mu} \right)^{-0.41} \dots\dots\dots (A8-4)$$

Thoenes and Kramers,⁽⁵³⁾ Wilke and Hougen,⁽⁵⁷⁾ and McCune and Wilhelm⁽³⁸⁾ similarly performed mass-transfer experiments with air and liquids, and correlated their data in terms of j_D . These results show that the Colburn analogy, $j = j_D$ applies within 25 per cent.

The film coefficient, h calculated from one of the above correlations may be used with Equations (I-2) and (I-3) to account for the inter-phase net heat transfer in a packed bed. (Mechanism No. 6).

(2) Axial Effective Conductivity

McHenry and Wilhelm⁽⁴⁰⁾ studied the axial mixing of binary gas mixtures flowing in a random bed of spheres by a technique of applying sinusoidal impulse to the fluid. Their data were correlated in terms of a modified Peclet number, which was found to be constant at about 2.

Aris and Amundson⁽¹⁾ postulated the packed bed as a series of mixing cells, and based on this model, the behavior of a tracer material injected with a certain frequency was studied statistically. As the result, they found that the axial dispersion should be expressed by a constant Peclet number of 2.

Carberry and Bretton⁽⁹⁾ studied the axial dispersion of water flowing through a fixed bed, by measuring the damping of a pulse input of dye at one or two points downstream of the injection site. As the result, they found the Peclet number was constant at about 1.

The results of the above various authors seem to agree on that the axial dispersion as measured by a frequency response technique is represented by a constant Peclet number of about 2. However, because of experimental difficulties, the above results have not been verified on a steady-state operation.

No data are available on the static bed conductivity in the axial direction, but since a static bed is considered to be

essentially isotropic, the same static-bed conductivity is believed to apply to both radial and axial directions.

In many practical applications of a packed bed, the amount of heat flux due to the bulk flow in the axial direction is much greater in comparison with the axial conduction. Therefore, it would be seldom necessary to make use of these correlations of the axial effective conductivity. If, however, a need arises to account for the axial conduction, the above correlations are recommended with the understanding that they have not been verified on a steady-state operation.

APPENDIX IX

FLUID PULSATION
TO IMPROVE THE HEAT TRANSFER RATE

(1) Axial Pulsing

In an attempt to improve the radial heat transfer rate in a packed bed, the technique of fluid pulsation was tried in the present study. This was carried out in two different ways: (1) periodic cut-off of inlet fluid, and (2) piston breazing.

In the first method, the steady flow of inlet fluid was periodically cut off by means of a solenoid valve. This caused the effective flow rate to decrease in proportion, but the actual flow velocity during each "on-period" remained more or less the same as before applying the pulsation. The effective conductivity observed under such a condition was almost identical with what the effective Reynolds number based on the net flow rate would have given under a steady flow condition. This indicated that the effective conductivity is determined only by the total flow rate and is not affected by how the total flow is injected, either in a steady flow or in a pulse flow.

In the second method, a certain quantity of fluid was forced in and out of the column by means of an 8-inch-diameter piston breazer, while a steady stream of air was simultaneously injected into the column. The stroke was varied between 1 and 4.5 inches,

and several different cycles were tried over the range of 20 to 150 cycles per minute. From the total piston displacement per unit time (not including the return stroke), the effective incremental Reynolds number was calculated. The effective conductivity observed under such a condition was somewhat larger than under a steady flow alone. The observed gain in k_e was compared with the theoretical increment which would have been obtained if the same incremental Reynolds number had been caused by an increase in the steady-flow rate instead of the piston pulsing. This ratio of the observed k_e to the theoretical value was found to be between 0.8 and 1, when the piston pulsing was applied to a static bed. The ratio, however, dropped linearly with the amount of simultaneous steady flow and reached zero when the Reynolds number based on the steady flow was around 800. This was probably because, as the Reynolds number increased, the piston pulsing did no more than merely oscillating the steady flow. In order to be significantly effective, therefore, the piston would have to be much larger requiring accordingly large power input.

The above result indicates that the axial pulsing is not a practical method of improving the heat transfer rate, unless its use is justified in a compelling situation in spite of the cost.

(2) Radial Pulsing

If the fluid flowing through a column can be forced to oscillate in the radial direction with a sufficiently large amplitude, the heat transfer rate should increase considerably. In an ordinary tubular packed bed, however, a radial pulsation is mechanically quite difficult to perform, and its effect would be at best localized within a limited region around where the pulse is injected. Furthermore, the axial momentum of the bulk fluid is normally quite large, and this would require considerable amount of energy input in order to force the fluid to move in the radial direction across a sufficient radial distance.

Therefore, the radial pulsation as performed with a piston breazer is believed to be little more practical than the axial pulsation.

APPENDIX X

TABLE OF NOMENCLATURE

<u>Symbols</u>	<u>Legend</u>
A Heat Transfer Area, (ft ²)
(A) _{lm} Logarithmic Mean Area, (ft ²)
A _p Surface Area of One Piece of Packing, (ft ²)
A _s Heat Transfer Area through the Solid Phase, (ft ²)
a Surface Area of Packing per Unit Volume of Bed, (ft ²)
a _n Eigenvalues
C ₁ , C ₂ Constants
C _p , (C _p) _g , (C _p) _s Heat Capacity; The Same of the Fluid; The Same of the Solid, (Btu/lb. °F)
D _e Effective Diffusivity, (L ² /θ)
D _f Molecular Diffusivity, (")
D _t Tube Diameter, (ft)
d _p Particle Diameter, (ft)
E Eddy Diffusivity, (L ² /θ)
f The Friction Factor
G Local Mass Flow Rate, (lbs./hr.ft ²)
G _o Overall Mass Flow Rate, (lbs./hr.ft ²)
g _c 32.2 (lb-mass.ft/lb-force.sec ²)
g(subscript) Refers to the Fluid Phase
ΔH Energy Absorbed by the Reactants in the Bed, (Btu)

TABLE OF NOMENCLATURE (Cont'd)

h	Film Coefficient between Fluid and Packed Solids, (Btu/hr.ft. ² .°F)
h _o	Mean Heat Transfer Coefficient, (Btu/hr.ft. ² . °F)
h _w	Wall Coefficient, (Btu/hr.ft. ² °F)
J ₀ , J ₁	Bessel Functions of the 1st Kind, of Order of 0, and 1
j	= (h/C _p G)(C _p μ/k) ^{2/3}
j _D	Mass-transfer Counterpart of j
K _g	Fluid-phase Effective Conductivity, (Btu/hr.ft.°F)
K _{gx} , K _{gy} , K _{gz}	K _g in the x,y, and z directions
K _s	Solid-phase Effective Conductivity, (Btu/hr.ft.°F)
K _{sx} , K _{sy} , K _{sz}	K _s in the x,y, and z directions
k _a	Average Effective Conductivity, (Btu/hr.ft.°F)
k _B	Static-bed Conductivity, (Btu/hr.ft.°F)
(k _B) _c	Conduction Contribution to k _B
(k _B) _r	Radiation Contribution to k _B
k' _B	Wall Static-bed Conductivity, (Btu/hr.ft.°F)
(k' _B) _c	Conduction Contribution to (k' _B)
(k' _B) _r	Radiation Contribution to (k' _B)
k _e	Effective Conductivity, (Btu/hr.ft.°F)
k' _e	Wall Effective Conductivity, (Btu/hr.ft.°F)

k_f	$= k_a - k_B$
k_g	Thermal Conductivity of Fluid, (Btu/hr.ft. ^o F)
k_r	Radiation Conductivity, (Btu/hr.ft. ^o F) $= (0.173)(\delta)(\epsilon)(d_p)(4T^3/10^8)$
k_s	Thermal Conductivity of Solid, (Btu/hr.ft. ^o F)
k_{td}	Turbulent Diffusion Contribution to k_e
k'_{td}	Turbulent Diffusion Contribution to k'_e
k_x, k_y, k_z	"Combined" Effective Conductivity in the x,y, and z directions
L	Bed Height, (ft)
m,n	Number of Incremental Lengths
ΔP	Pressure Drop, (psia)
Pe	Modified Peclet Number $= d_p GC_p / k_{td}$
Pr	Prandtl Number, ($C_p \mu / k$)
q	Heat Input, (Btu/hr)
q_s	Amount of Heat Flow through the Solid, (Btu/hr)
q_v	Amount of Heat Flow through the Void, (Btu/hr)
R	Radius of Column, (ft)
Re	Particle Reynolds Number $= d_p G / \mu$
r_p	Particle Radius, (ft)
s	Proportionality Constant
s(subscript)	Refers to Solid-phase

TABLE OF NOMENCLATURE (Cont'd)

T	Absolute Temperature, ($^{\circ}\text{R}$)
t	Temperature Common to Both Phases, ($^{\circ}\text{F}$)
t_{exit}	Exit Temperature, ($^{\circ}\text{F}$)
t_o	Inlet Temperature, ($^{\circ}\text{F}$)
t_g	Fluid Temperature, ($^{\circ}\text{F}$)
t_s	Solid Temperature, ($^{\circ}\text{F}$)
t_w	Wall Temperature, ($^{\circ}\text{F}$)
Δt	Incremental Temperature
U_n	Functions of x
u, u_x, u_y, u_z	Flow Velocity; The Same in the $x, y,$ and z -directions, (ft/hr)
V_n	Functions of x
x	x -axis; or Heat Transfer Distance, (ft)
Δx	Increment of x ; Total Heat Transfer Path Length, (ft)
$\Delta x_g, \Delta x_s$	Heat Transfer Path Length in the Fluid and Solid Phases, (ft)
Y_o	Weber's Form of Bessel Function of the Second Kind, of Order Zero
y, z	$y,$ and z -axis

TABLE OF NOMENCLATURE (Cont'd)

α	Thermal Diffusivity, $(k/C_p \rho)$
α_n	Eigenvalues
δ	Volume Fraction Void
ϵ	Total Emissivity
ρ	Density, (lbs/ft^3)
ρ_g, ρ_s	Density of Fluid and Solid, (lbs/ft^3)
λ	Electric Conductance, (mho)
λ_e	Effective Electric Conductance, (mho)
$\varphi_1 \varphi_2$	Functional Forms
θ	Time; The Angle in the Polar Coordinate System
μ	Viscosity, $(\text{lb}/\text{hr}\cdot\text{ft})$

APPENDIX XI

BIBLIOGRAPHY

1. Aris, R.; N.R. Amundson
A.I.Ch.E.J., 3, 280, (1957)
2. Argo, W.B.; J. M. Smith
C.E.P., 49, 443, (1953)
3. A.S.T.M., Fluid Meters, Their Theory and Applications,
4th Edition, A.S.M.E., (1937)
4. Baron, T.
C.E.P., 48, 118, (1952)
5. Baumeister, E. B.; C. O. Bennett
A.I.Ch.E.J., 4, 69, (1958)
6. Bernard, R. A.; R. H. Wilhelm
C.E.P., 46, 233, (1950)
7. Bunnell, D. G.; H. B. Irvin; Olson; Smith
I.E.C., 41, 1977, (1949)
8. Calderbank, P. H.; Pogorski
Trans. Inst. Chem. Engr., 35, 200, (1957)
9. Carberry, J. J.; R. H. Bretton
A.I.Ch.E.J., 4, 367, (1958)
10. Carman, P. C.
Trans. Inst. Chem. Engr. (London), 16, 168, (1938)
11. Coberly, C. A.; W. R. Marshall
C.E.P., 47, 141, (1951)
12. Colburn, A. P.
I.E.C., 23, 910, (1931)
13. Colburn, A. P.
Trans. Am. Inst. Chem. Engr., 29, 174, (1933)
14. Damköhler, G.
Der Chemie Ingenieur, 3, 441, (1937)
15. Deissler, R. G.; J. S. Boegli
Trans. A.S.M.E., 80, 1417-25, (1958)

BIBLIOGRAPHY (Cont'd)

16. Deissler, R. G.; C. S. Eian
NACA Research Memorandum, NACA, June 24, 1952
17. Drew, T. B.
Trans. Am. Inst. Chem. Engr., 26, 26, (1931)
18. Fahien; Smith
A.I.Ch.E.J., 1, 28, (1955)
19. Felix, J. R.; W.K. Neill
Preprints of Heat Transfer Symposium, Annual Meeting of A.I.Ch.E., 125, (1951)
20. Furnas, C. C.
Trans. A. I. Ch. E., 24, 142, (1930)
21. Gamson, B. W.
C.E.P., 47, 19, (1951)
22. Gamson, B. W.; G. Thodos; Hougen
Trans. A. I. Ch. E., 39, 1, (1943)
23. Glaser, M. B.; G. Thodos
A.I.Ch.E.J. 4, 63, (1958)
24. Hildebrand, F. B., Advanced Calculus for Engineers,
Prentice-Hall, Inc., Englewood Cliffs, N.J., 1949
25. Hill, F. B.; R. H. Wilhelm
Preprint 16, 2nd National Heat-transfer Conference,
A.I.Ch.E.-A.S.M.E., Chicago, Ill., Aug., 1958
26. Hougen, J. O.; E.L. Piret
C.E.P., 47, 295, (1951)
27. Hougen, O. A.; Wilke
Trans. A. I. Ch. E., 41, 445, (1945)
28. Irvin, H. B.; Olson; Smith
C.E.P., 47, 287, (1951)
29. Kimura; Ueda; Ofka
Chem. Engr. (Japan), 21, 2-7, (1957)
30. Kimura, M.; Ueda; T. Ofuka
Kagaku Kogaku, (Japan), 21, 472, (1957)

BIBLIOGRAPHY (Cont'd)

31. Kwong, S. S.; Smith
I.E.C., 49, 894, (1957)
32. Leva, M.
I.E.C., 39, 857, (1947)
33. Leva, M.
I.E.C., 42, 2498, (1950)
34. Leva, M.; Grummer
I.E.C., 40, 415, (1948)
35. Leva, M.; Grummer
C.E.P., 43, 713, (1947)
36. Leva, M.; Grummer
C.E.P., 48, 307, (1952)
37. Leva, M.; Weintraub; Grummer; Clark
I.E.C., 40, 747, (1948)
38. McCune, L. K.; R. H. Wilhelm
I.E.C., 41, 1124, (1949)
39. McAdams, W. H., Heat Transmission, 3rd Edition,
McGraw-Hill Co., 1954
40. McHenry, K. W.; R. H. Wilhelm
A.I.Ch.E.J., 3, 83, (1957)
41. Morale, M.; W. O. Spin; J. M. Smith
I.E.C., 43, 225, (1951)
42. Perry, J. H., Chemical Engineers' Handbook, 3rd Edition,
McGraw-Hill Co., 1950.
43. Phillips, B. D.; F. Leavitt; C. Yoon
Preprint 124, 3rd National Heat-transfer Conference,
A.S.M.E.-A.I.Ch.E., Storrs, Connecticut, Aug., 1959.
44. Plautz, D. A.; Johnstone
A.I.Ch.E.J., 1, 193, (1955)
45. Polack, J.
Sc. D. Thesis in Chem. Engr., M. I. T., 1948.

BIBLIOGRAPHY (Cont'd)

46. Ranz, W. E.
C.E.P., 48, 247, (1952)
47. Roblee, L. H. S.; R. M. Baird; J. W. Tierney
A.I.Ch.E.J., 4, 460, (1958)
48. Schuler, R. W.; Stallings; Smith
C.E.P. Symposium Series No. 4, 48, 19, (1952)
49. Schumann, T. E. W.; Voss
Fuel, 13, 249, (1934)
50. Schwartz, C. E.; J. M. Smith
I.E.C., 45, 1209, (1953)
51. Singer, E.; R. H. Wilhelm
C.E.P., 46, 343, (1950)
52. Sokolinskoff, I. S., Higher Mathematics for Engineers
and Physicists, McGraw-Hill Co., 1941.
53. Thoenes, D.; H. Kramers
Chem. Engr. Sci., 8, 271, (1958)
54. Vershoor, H.; Schuit
Appl. Scientific Research, 42, A-2, 97, (1952)
55. Wax, N., Noise and Stockastic Processes,
Dover Publication, New York, 1954.
56. Wilhelm, R. H.; Johnson; Wynkoop; Collier
C.E.P., 44, 105, (1948)
57. Wilke, C. R.; O.A. Hougen
Trans. A. I. Ch. E., 41, 445, (1945)
58. Wilkes, G. B., Final Report on Contract No. W 33-038-20486,
Air Material Command, Wright Field, Dayton, Ohio,
Division of Industrial Cooperation, M.I.T., 1950.
59. Wyllie
Trans. Am. Inst. Mining Met. Engr., 198, 103, (1953)
60. Yagi, S.; Kunii
Chem. Engr. (Japan), 18, 576-85, (1954)

BIBLIOGRAPHY (Cont'd)

61. Yagi, S.; D. Kunii; Y. Shimomura
Kagaku Kogaku (Japan), 21, 343, (1957)
62. Yagi, S.; D. Kunii
A.I.Ch.E.J., 3, 373, (1957)
63. Yagi, S.; N. Wakao
Kagaku Kogaku (Japan), 22, 82, (1958)
64. Yagi, S.; N. Wakao
A.I.Ch.E.J., 5, 79, (1959)

APPENDIX XII

BIOGRAPHICAL NOTE

The author was born in Kunsan, Korea and received his primary education there. He received a 6-year-course high school education in Chongju and Seoul between 1944 and 1948. He entered Seoul National University in September, 1948 as a freshman in the Chemical Engineering Department.

Upon the outbreak of the Korean War in June, 1950, he joined the 8th U.S. Army and served for three and half years as a Critical Military Specialist, Grade 4 until the end of 1953.

He came to the United States in 1954 to attend Oregon State College, Corvallis, Oregon, from which he graduated in June, 1956 with a B. S. degree in chemical engineering.

In September, 1956, he was admitted to the Chemical Engineering Department of M. I. T. as a graduate student. He held a teaching assistantship during the subsequent two academic years.

In the first term of 1957-58, he attended the M. I. T. School of Chemical Engineering Practice at the field stations in Bethlehem Steel Company, Buffalo, N. Y., and Hercules Powder Company, Parlin, N. J. He was awarded the degree of S. M. in chemical engineering practice from M. I. T. in February, 1958. He started on his doctorate research work in September, 1958 and is expecting to conclude it in September, 1959. During the year of 1958-59, he held a Scientific Design Fellowship.

He has been employed as a chemical engineer by Crown Zellerbach Corporation, West Linn, Oregon; Linde Company, Tonawanda, N. Y.; and Standard Oil Company (Indiana), Whiting, Indiana, during the summers of 1956, 1957, and 1958 in that order.

He has accepted a position with The Upjohn Company to start upon the completion of this thesis.